# NANOPARTICLE-MEDIATED INHIBITION OF MIR-10B AS A CLINICALLY VIABLE THERAPY FOR METASTATIC BREAST CANCER

By

Alan Surya Halim

A DISSERTATION

Submitted to
Michigan State University
in partial fulfillment of the requirements
for the degree of

Physiology – Doctor of Philosophy

2024

## ABSTRACT

Breast cancer is expected to be the most diagnosed cancer in the United States in 2024, with a predicted 310,000 new diagnoses. Hormone and targeted therapies, as well as earlier detection, have greatly improved the outlook for the majority of breast cancer patients. Unfortunately, there is still an unmet clinical need for the breast cancer subtypes that are not receptive to these therapies and, more importantly, the metastases that may arise if the cancer is allowed to progress, as their effect on vital function is reported to be the cause of up to 90% of cancer-related deaths. Current standard of care for metastatic disease includes treatments based on the subtyping of the primary tumor and chemotherapy; however, these treatments fail to appreciate the changes cancer cells undergo during the metastatic process and the differences that may exist between metastases and the primary tumor they originate from, which can include a change in subtype.

The discovery of miR-10b, a small noncoding RNA that acts as a translational repressor for select targets, as a driver of breast cancer metastasis provided a target for the design of therapeutics tailormade against the metastatic process; and with reports that metastases have greater miR-10b expression than their matched primary tumors, these therapeutics may also be effective in treating existing metastases. Our lab developed one such therapeutic by conjugating anti-miR-10b antisense oligonucleotides to a Magnetic iron oxide Nanoparticle (MN) core, collectively named MN-anti-miR10b. In previous studies using a mouse model of spontaneously metastatic breast cancer, intravenous administration of MN-anti-miR10b has already demonstrated the ability to prevent onset of metastasis and to halt the growth of existing metastases. While not able to induce regression of metastases as a monotherapy, combination therapy with doxorubicin – a chemotherapeutic commonly used in the treatment of breast cancer – reproducibly eradicated

metastases in both immunocompromised and immunocompetent mouse models of spontaneously metastatic breast cancer.

Within this work, I showcase several of the contributions I made in advancing MN-anti-miR10b toward the clinic. I begin by consolidating the literature on miR-10b in breast cancer, highlighting many of the properties it has been associated with conferring and discussing its potential applications as a clinical marker and therapeutic target. Then, I demonstrate the modalities through which MN delivery to target metastatic tissues can be monitored, which is a major advantage when working to treat widespread metastatic disease that may present in otherwise undetectable or sensitive locations. These techniques are applied to a new study in which I investigate how miR-10b expression changes in mouse metastatic tissues as a function of the number of doses of MN-anti-miR10b administered. After showing that miR-10b can be almost completely suppressed in these tissues in as little as two treatments, I use RNA sequencing to identify the transcriptional effects of miR-10b inhibition in breast cancer cell lines, producing what I believe to be the first public dataset of its kind in this type of cancer. The sequencing results indicate the activation of developmental processes in response to miR-10b inhibition, which I then use to establish a link between miR-10b and stem-like cancer cells and further validate by finding that stemness is reduced in breast cancer cells upon treatment with MN-anti-miR10b. Lastly, I summarize work I contributed to in which a companion cat with spontaneous metastatic breast cancer recapitulating human disease was treated with MN-anti-miR10b. This work is part of translational studies that the Moore Lab is conducting with the aim of bringing this therapeutic into the clinic. The findings from this study support the clinical applications of MN-anti-miR10b as a therapy for metastatic breast cancer in humans in different ways, bringing the drug one step closer toward filling this urgent need.

This dissertation is dedicated to Mom and Dad.
Thank you for your unwavering love, support, and patience throughout all these years.

## ACKNOWLEDGEMENTS

To my advisor and mentor, Dr. Anna Moore, thank you for seeking me out and encouraging me to rotate in your lab. I had never heard of a PI doing such a thing before, and it went a long way toward making me feel valued (so valued that I told the lab I was scheduled to rotate with after yours that I'm happy to do the rotation but that my mind was made). Your influence on me, from my writing to my confidence that I know my project better than anyone in the room, is obvious to anyone who witnessed my growth over the past few years. And with a career interest in clinical research, I cannot imagine a more perfect research focus for my Ph.D. training than your pioneering therapeutic. I know the project is not what either of us envisioned from the start, but I'm proud of the work we accomplished and am excited to see what the future holds for MN-anti-miR10b. To the past and present members of the Moore Lab – Jennifer, Nazanin, Beth, Anna S, Ming, Neil, Jack, Bryan, Nasreen, and Sujan – and the rest of the Precision Health Program, thank you for all the daily help, conversation, and fun you have provided. Being part of PHP feels like being part of one super lab. I'm grateful to the faculty for having their doors open for questions, to the staff for all their assistance, and to the students for reminding me daily that I'm not going through the training process alone. You are all like family to me and I am glad you were a part of my journey.

To Dr. Justin McCormick and Bethany, thank you for taking a chance on me and inviting me to join the Summer Undergraduate Physician-scientist training Education & Research (SUPER) Training Program and, later, the D.O.-Ph.D. Program. SUPER was pivotal in my decision to pursue training as a physician-scientist, and the way you made me feel truly *wanted* during the dual-degree applications process cannot be overstated. To the current D.O.-Ph.D. program leadership – especially Dr. Brian Schutte and Michelle – thank you for all the continued

support and all the work you have done and continue to do in improving the program. When I joined the program, students at each stage of training felt friendly but separate. It's thanks to your efforts the students feel closer-knit than ever before. And to my cohort: one degree down, one to go. We're almost there.

To my guidance committee – Drs. Vilma Yuzbasiyan-Gurkan, Lorenzo Sempere, Kathy Gallo, and Eran Andrechek – thank you for your insights and contributions toward making me a better scientist. I began my Ph.D. training thinking I already knew how to conduct research. You all very quickly humbled me and showed me how much I still had to learn. I hope you can all see how much of a positive effect you had on me and my research project. Additional thanks to Dr. Yuzbasiyan-Gurkan for being someone I felt comfortable turning to throughout my training and for having the perspective that graduate students are allowed to have fun during some of the best years of their lives. You're a great mentor and student-oriented leader.

To all the friends I'm so lucky to have, thank you for putting up with me and letting me be a part of your lives. To Zack, Jane, and Travis, you've done so for over a dozen years now. I look forward to continuing to celebrate each other's successes for decades to come. And to the Squirtle Squad and Neighbruhood, our weekly rituals always gave me something to look forward to and my physical and mental health would not be the same without you.

To my boys: Thank you, Louis, for being the best study buddy. Thank you, Charlie, for your inspirational redemption arc. And thank you, Winston, for your unconditional positivity. To Michelle, Jeremy ("Sir"), Noah, and the Byrges and Conners, thank you for welcoming me into your family and for all your love and support. I'm fortunate to have married into such a caring family.

To my wife, Kayla, thank you for joining me Year One of this journey and being by my side every step of the way. You supported me through the lows and we indulged in the highs. I'm so proud of the family and life we have built together. Coming home to our house to you and our boys was the reason why when people asked me "How's it going?" I could honestly answer, even at my lowest points, that things were going well. I love talking about our past and all the small things that had to happen for us to meet, enjoying the present and everything we have to be grateful for, and envisioning our future adventures, lakeside home, and speakeasy. This dissertation could not have happened without you (literally). I hear there's a bottle of Lillet Blanc waiting for us at the end of this chapter of our lives.

And lastly, to Mom, Dad, and Audrey, thank you for literally always being *there* for me. Returning to Michigan for my training was one of the best decisions I made, as I cannot imagine what it would have been like to go through this training without knowing you are all just a short drive away. To Audrey, thank you for being one of my best friends. Our decisions to pursue careers in the medical field made it feel like we were in this together, especially when studying together in the alcoves of the Chem Building in undergrad. To Mom and Dad, thank you for supporting me in my career. I will never forget you telling me how much you wished you could be more help when I decided to go into science. You have been so much more help than you realize, and I hope I'm making you proud.

## TABLE OF CONTENTS

## LIST OF ABBREVIATIONS

5’ ThioMC6.....5’-thiol-modifier C6 disulfide

AACR .....American Association of Cancer Research

AED .....animal equivalent dose

AGO.....Argonaute

ALDH .....aldehyde dehydrogenase

ALDH1L2.....aldehyde dehydrogenase 1 family member L2

AML .....acute myeloid leukemia

APC.....allophyocyanin

ASOs.....antisense oligomers

AST.....liver aspartate transaminase

β-catenin .....beta catenin

Bcl2l11.....B-cell lymphoma-2-like protein 11

BLI.....bioluminescence imaging

bp.....base pair

BPs.....biological processes

BW.....bodyweight

CAR .....Campus Animal Resources

CBC .....complete blood count

CC1 .....Cell Conditioning Solution

CD24.....cluster of differentiation 24

CD44.....cluster of differentiation 44

c-Jun.....Jun proto-oncogene

CK .....creatine kinase

CLL .....chronic lymphocytic leukemia

cRGD .....cyclic Arginine-Glycine-Aspartate peptide

CRISPR .....clustered regularly interspaced short palindromic repeats

CSCs .....cancer stem cells

CT .....computed tomography

Cy5.5 .....Cyanine5.5 fluorescent dye

DAPI .....4’,6-diamidino-2-phenylindole

DCIS .....ductal carcinoma in situ

DEGs.....differentially expressed genes

DMEM .....Dulbecco’s Modified Eagle Medium

DNA .....deoxynucleic acid

dsDNA .....double stranded DNA

DTCs .....disseminated tumor cells

dUTP .....deoxyuridine triphosphate

EMT .....epithelial-to-mesenchymal transition

EMT-TFs .....EMT transcription factors

EpCAM .....epithelial cell adhesion molecule

ER .....estrogen receptor

FBS .....fetal bovine serum

FDR .....false discovery rate

Fe.....iron

FFPE .....formalin-fixed paraffin-embedded

FLI.....fluorescence imaging

FMC .....feline mammary carcinoma

FOV .....field of view

GBM .....glioblastoma multiforme

GEO .....Gene Expression Omnibus

GFP .....green fluorescent protein

GSEA .....gene set enrichment analysis

H .....heart

H&E .....hematoxylin and eosin staining

HER2.....human epidermal growth factor receptor 2

HOXD .....homeobox D

HOXD10 .....homeobox D10

$HNO_3$.....nitric acid

HS .....high sensitivity

IACUC .....Institutional Animal Care and Use Committee

$IC_{50}$.....half-maximal inhibitory concentration

ICP-OES .....inductively coupled plasma optical emission spectroscopy

IDC .....infiltrating ductal carcinoma

IHC.....immunohistochemistry

IR.....infrared

IRB.....Institutional Review Board

ISH .....in situ hybridization

IVIS.....In vivo Imaging System

Ki-67 .....antigen Kiel 67

KLF4 .....Krüppel-like factor 4

KLF7 .....Krüppel-like factor 7

KPC.....K-ras$^{LSL.G12D/+}$; p53$^{R172H/+}$; PdxCre mouse model

KRAS.....Kirsten rat sarcoma viral oncogene homologue

let-7 .....lethal-7 miRNA

lfcSE .....standard error of the log2 fold change estimate

LGR5.....Leucine-rich repeat-containing G-protein coupled receptor 5

LN .....lymph node

LNA .....locked nucleic acid

MaSC .....mammary stem cells

miR- .....microRNA-

miRDB .....microRNA Prediction Database

miRISC .....miRNA-induced silencing complex

miRNA.....microRNA

MMTV-PyMT.....mouse mammary tumor virus-polyoma middle tumor antigen

MN/MNP .....magnetic nanoparticles

MRI.....magnetic resonance imaging

mRNA.....messenger RNA

MSU.....Michigan State University

n.....number of samples

NES.....normalized enrichment score

NHS .....N-hydroxysuccinimide

NTC.....non-treated control

OCT.....optimal cutting temperature compound

PBS .....phosphate buffered saline

PC1.....first principal component

PCA.....principal component analysis

PCR.....polymerase chain reaction

PDAC.....pancreatic ductal adenocarcinoma

PE.....phycoerythrin

PI.....propidium iodide

PLGA-b-PEG .....Poly(lactic-co-glycolic acid)-block-polyethylene glycol

pMCF-7 .....parental MCF-7 cells

PR.....progesterone receptor

pre-miRNA .....precursor microRNA

pri-miRNA .....primary microRNA

PyMT .....polyoma middle tumor-antigen

QBEAM.....Quantitative Bio-Element Analysis and Mapping

qPCR.....quantitative polymerase chain reaction

RBC .....red blood cell

RFP .....red fluorescent protein

RNA .....ribonucleic acid

ROI.....region of interest

RPKM .....Reads Per Kilobase transcript per Million mapped reads

RT.....reverse transcription

RT-qPCR .....reverse transcription quantitative polymerase chain reaction

SCID .....severe combined immunodeficiency

s.d. .....standard deviation

SEM .....standard error of the mean

siRNA .....small interfering RNA

sMCF-7 .....sorted CD44+/CD24–/low/ESA+ cells

snRNA .....small nuclear RNA

SPDP .....N-succinimidyl 3-[2-pyridyldithio]-propionate

T2* .....T2 star MRI scan

T2W .....T2-weighted MRI scan

T75 .....tissue culture flask with 75 $cm^2$ growing surface

TCEP .....tris(2-carboxyethyl)phosphine

TMZ .....temozolomide

TNBC .....triple negative breast cancer

TTX-MC138 .....TransCode Therapeutics MN-anti-miR10b therapeutic

TUNEL .....terminal deoxynucleotidyl transferase dUTP nick end labeling

U6.....RNU6-1 small nuclear RNA

VDL .....Veterinary Diagnostic Laboratory

**Units of measurement**

°C .....degrees Celsius

g.....gravity

g.....gram

G.....gauge

h.....hours

kg.....kilogram

mg .....milligrams

min .....minutes

mL .....milliliters

µg .....microgram

µL .....microliter

µm .....micrometer

nm .....nanometer

nmol .....nanomole

s .....seconds

v/v .....volume per volume

x.....times

# CHAPTER 1: MICRORNA-10B IN BREAST CANCER

## Contributions to Science

I was responsible for the conception and design of this review and contributed most of the intellectual content, the only exception being the review of nanoparticle-based approaches to miR-10b inhibition *in vivo* by Bryan Kim. Dr. Anna Moore provided guidance for notable studies to include, and Beth Kenyon assisted with editing.

## Simple Summary

Current standard of care for metastatic breast cancer is not tailored to metastatic processes, resulting in notorious side effects while often not being effective. MiR-10b is a well-characterized driver of metastasis in breast cancer, as well as several other cancers, and is a promising therapeutic target specific to metastatic disease. Here, I review what is known about miR-10b in the context of breast cancer and its potential clinical applications.

## Outlook for metastatic breast cancer

With over 310,000 estimated new cases, breast cancer is predicted to be the most diagnosed cancer in the United States in 2024 (1). Although survival rates for breast cancer have improved with advances in detection and treatment, nearly one-third of cases are expected to progress to metastatic disease (2), which carries a five-year survival rate of 30% overall (3). This grim prognosis can be largely attributed to the lack of therapeutics specifically targeting metastases, whose effects on vital function comprise the vast majority of cancer-related deaths (up to 90%) (4; 5). Instead, metastases are commonly treated with chemotherapy, which is non-specific and laden with adverse effects, or hormone or targeted therapies aimed at major signaling pathways of the primary tumor, which may or may not be maintained in metastases. As such, development of

treatments specific to metastatic disease requires a better understanding of the drivers of the metastatic process and critical pathways for metastasis survival.

Having only been discovered at the turn of the millennium, investigation of microRNAs (miRNAs) is a relatively new field that has already yielded insights into the regulatory mechanisms that govern various diseases, including cancer (6; 7). In the case of metastatic breast cancer, one miRNA that has come under immense scrutiny is miR-10b, which appears to both drive metastasis and be vital to their persistence at distant sites. Here, we review how miRNAs function and what has already been discovered about the roles of miR-10b in breast cancer, its value as a clinical marker, and its potential as a therapeutic target.

**MicroRNA biology**

MicroRNAs are small, noncoding RNAs composed of 19-25 nucleotides that function as gene silencers (8), similar to small interfering RNAs (siRNAs); however, an important distinction is that miRNAs can target hundreds of genes at a time, whereas siRNAs are typically specific to a single target (9). This enables a single miRNA to be a regulator of multiple biochemical pathways at one time, serving to fine tune processes through small effects on many genes rather than large, potentially more disruptive effects on specific target genes or proteins (10).

The production of miRNAs is a multistep process that relies on several important proteins. Briefly, beginning in the nucleus, RNA polymerase II transcribes a region of DNA that encodes a primary miRNA (pri-miRNA) (11). The resulting RNA – generally, 60-70 nucleotides in length – folds over and base pairs with itself, creating a characteristic stem loop structure (12-14). The ribonuclease Drosha then truncates the pri-miRNA into a shorter precursor miRNA, or pre-miRNA, while maintaining the stem loop (15). This is then shuttled by the protein Exportin 5 to the cytoplasm (16), where the stem loop is cleaved by the ribonuclease Dicer (17), generating the

mature miRNA in the form of two base-paired strands of RNA: the guide strand and the passenger strand. The guide strand is loaded onto an Argonaute (AGO) protein, together with other proteins forming the miRNA-induced silencing complex (miRISC) (18). This complex is what mediates the gene silencing function of the miRNA (19; 20).

The genes targeted by a miRNA are largely dictated by the seed region of the miRNA, defined as bases 2-8 when read from the 5' end (21). Canonical targets of miRNAs are mRNA transcripts containing sequences complementary to the seed region in their 3' untranslated region (22). This complementary site is bound by miRISC (23), which then inhibits translation through multiple mechanisms, including mRNA degradation and interference with ribosome activity. These mechanisms vary among target transcripts and AGO proteins and are the subject of ongoing research (19; 24-28). Notably, additional factors such as co-expression in cells (29; 30), thermodynamics (31), and the remainder of the miRNA (22; 32) also contribute to targeting. As a result, computational tools offer the most comprehensive approach to predicting targets (33-36), which should then be experimentally validated (36; 37). Importantly, not all target transcripts are degraded, explaining why miRNA activity is not always observed at the transcript level (e.g., via RT-qPCR) (38).

Since the discovery of the first miRNAs – lin-4 and let-7 – and their importance in *Caenorhabditis elegans* development (39; 40), miRNAs have been investigated in the context of human disease. The first evidence of miRNA involvement in pathogenesis came in 2002 when miR-15 and miR-16-1 were identified as tumor suppressors that are downregulated in the majority of chronic lymphocytic leukemia (CLL) cases (41) and, later, whose deletion in mice resulted in a CLL phenotype (42). Many miRNAs are now recognized as tumor suppressors or oncogenes,

positioning them as valuable therapeutic agents or targets, thus opening new avenues for treatment of cancer (6; 7).

## The roles of miR-10b in breast cancer

### *Discovery of miR-10b as a driver of breast cancer metastasis*

One of the first miRNAs to be implicated in cancer metastasis is miR-10b. Following a study that identified aberrantly expressed miRNAs in breast cancer relative to normal breast tissue (43), in 2007, Dr. Li Ma et al. from the research group of Dr. Robert Weinberg observed that miR-10b was upregulated in human breast cancer cell lines that were both tumorigenic and metastatic (MDA-MB-231, SUM1315) relative to cell lines that were either non-tumorigenic (HMEC, MCF-10A) or tumorigenic but non-metastatic (SUM149, SUM159) (38). The same group also observed the similar correlation between miR-10b and breast cancer cell line aggressiveness in murine cell lines (38) which was later confirmed by others (44). When miR-10b was inhibited in MDA-MB-231 cells by transfection with antisense oligonucleotides, the cells displayed decreased invasiveness *in vitro*. Conversely, overexpression of miR-10b in non-metastatic cell lines resulted in increased cell motility and invasion (38).

In mouse models, overexpression of miR-10b in GFP-expressing SUM149 and SUM159 human cell lines was sufficient to confer metastatic potential, with histological evidence of invasion and increased angiogenesis in early stages and, ultimately, visualization of GFP-expressing cancer cells in the lungs and peritoneum in later stages (38). Interestingly, while modulation of miR-10b did not demonstrate any effects on proliferation *in vitro*, overexpression of miR-10b resulted in increased expression of the proliferation marker Ki-67 at the primary tumor invasive front and the observation of Ki-67-positive cells in the lumen of blood vessels, indicating that miR-10b has some functions that can only be appreciated in the presence of other biological

processes (38). Importantly, these phenotypic effects appeared to be largely specific to the metastatic process. Despite increased expression of Ki-67, there was no appreciable difference in primary tumor size or growth (38). Additionally, overexpression of miR-10b in non-tumorigenic cell lines did not confer tumorigenicity (38). These observations, along with the identification and validation of downstream effectors of metastasis HOXD10 (suppressed by miR-10b) and RHOC (upregulated by miR-10b), collectively led to the conclusion that miR-10b is a driver of metastasis in breast cancer.

The same study then proceeded to identify the transcription factor and "master driver" of epithelial-to-mesenchymal transition (EMT) Twist as being an upstream inducer of miR-10b expression (38). Indeed, miR-10b has since been found to be an important mediator of Twist-driven metastasis of breast cancer cells to bone (45). This axis provides valuable insights into the role of miR-10b in normal biology. Studies in *Drosophila* and in mice have found Twist is an important regulator of embryonic development, particularly in mesoderm-derived tissues (46). In adult mice, its expression is primarily restricted to adult stem cells of the mesenchyme (47). Similarly, in human tissues, Twist is most strongly expressed in the fetal portions of the placenta, with lower levels of expression seen primarily in mesoderm-derived tissues (e.g., pancreas and skeletal muscle) and no observable expression in ectoderm- and endoderm-derived tissues (48). Collectively, these findings suggest that miR-10b plays an important role in early development, though its importance in adults outside of the contexts of cancer remains understudied.

Since the seminal 2007 study with breast cancer models, miR-10b has been implicated in at least 17 other types of cancer, and its roles across different cancers is generally conserved. Many more upstream regulators and downstream effectors have also been identified in support of these

roles, as reviewed by Sheedy et al. in 2018 (49). With a focus on metastatic breast cancer, hereafter, we review the roles of miR-10b that have been identified specifically in models of breast cancer.

***Associations of miR-10b with EMT and stemness***

Through its association with Twist and the increased migration and invasion properties miR-10b expression confers, miR-10b has been proposed to be a mediator of EMT, the process by which relatively immobile and tightly adherent "epithelial-like" cells transform into more mobile and invasive "mesenchymal-like" cells (50). Additional changes include a morphological change from polygonal to spindle-like, a loss of apical-basal polarity, and changes in the proteins comprising the cytoskeleton, namely a decrease in E-cadherin and increase in vimentin (50). In support of this relationship, another known activator of EMT, the cytokine TGF-β1, has also been found to upregulate miR-10b (44; 51). When miR-10b is inhibited or ablated completely, studies have reported decreased vimentin and increased E-cadherin expression (i.e., transition to a more epithelial-like state) (44; 52). There is, however, uncertainty about the exact role of miR-10b in EMT. Inhibition of miR-10b could not fully reverse Twist- or TGF-β1-induced EMT (38; 44), and overexpression of another key activator of EMT, Snail, decreased miR-10b expression (38). Furthermore, there are conflicting reports about whether miR-10b overexpression can induce EMT on its own (38; 53).

Another role miR-10b has been implicated in is chemotherapy resistance, a property that is also commonly associated with a mesenchymal cancer cell phenotype. A study found that tamoxifen-resistant MCF-7 breast cancer cells had over 7-fold miR-10b expression relative to the parental strain (54). Similarly, overexpression of miR-10b in the multiple cell lines increased the $IC_{50}$ of tamoxifen by up to 8-fold (54). Importantly, inhibition of miR-10b in resistant cell lines re-sensitized the cells to tamoxifen, demonstrating the potential utility of miR-10b inhibition as an

adjuvant to existing chemotherapeutics (54). Indeed, combination therapy of a systemic miR-10b inhibitor and doxorubicin has been shown to elicit a complete and stable regression of lymph node metastases in mouse models of breast cancer where neither monotherapy did (55; 56).

Closely related to EMT and drug resistance, breast cancer cell stemness, or the stem cell-like properties that are commonly conferred by genes associated with normal stem cells, is also associated with miR-10b. In addition to EMT and drug resistance, stem-like cancer cells also have features such as ability for self-renewal, potential to differentiate, and anchorage-independent growth. In multiple breast cancer cell lines, miR-10b expression was higher in cells sorted for expression of stem-associated surface markers CD44 or EpCAM than in surface marker-negative populations (53). This increase in miR-10b coincided with increases in the expression of bona fide stemness genes – SOX2 and OCT3/4 – and EMT genes – Snail, Vimentin, and Twist. Alterations in miR-10b expression levels also paralleled changes in mammosphere formation capability in anchorage-independent conditions and in percent of ALDH-positive cells, another marker associated with stemness (53). Similarly, miR-10b was reported to be upregulated in breast cancer cells grown as organoids in anchorage-independent conditions relative to monolayer culture, with many of the downregulated genes associated with miR-10b activity (57). Collectively, these findings suggest that the properties associated with miR-10b expression may be the result of a miR-10b-mediated shift toward a stem-like state.

For a mini-review on the topic of EMT and stemness in cancer metastasis, see Chapter 5.

***Interactions between miR-10b and the tumor microenvironment***

MiR-10b from breast cancer cells may also act on the tumor microenvironment. Immortalized and primary breast cancer cells have been reported to secrete miR-10b *in vitro* (58; 59). When non-malignant human mammary epithelial (HMLE) cells were treated with conditioned

medium, miR-10b targets were downregulated and the cells became more invasive (59), demonstrating the potential of breast cancer cells to transform non-malignant cells in the microenvironment. This is particularly notable as it may explain the observation of increased miR-10b in tumor endothelial cells and endothelial progenitor cells of mice implanted with breast or lung cancer cells relative to normal mice, as well as in the vasculature of patients with invasive infiltrating ductal carcinoma (IDC) grade III tumors (all with spread to lymph nodes) relative to localized ductal carcinoma *in situ* (DCIS) (60). Separately, cultured human endothelial cells were found to upregulate miR-10b in response to vascular endothelial growth factor (60), supporting a role for miR-10b in modeling tumor vasculature.

***Influence of miR-10b on cancer cell viability***

Perhaps most importantly, miR-10b has been linked to breast cancer cell survival. Inhibition of miR-10b in MDA-MB-231 cells *in vitro* with antisense oligonucleotides delivered using iron oxide nanoparticles resulted in increased cell apoptosis compared to controls, in addition to the expected decreases in migration, invasion, and proliferation (55). Furthermore, complete knockout of miR-10b induced morphological changes within 24 hours and 100% cell death by 72 hours, pointing at a dependency on miR-10b for survival (55). Interestingly, when MDA-MB-231 cells were implanted into mice and allowed to spontaneously metastasize, inhibition of miR-10b using the same construct delivered intravenously led to apoptosis specifically in lymph node metastases but not in primary tumors (61), further supporting the notion that miR-10b is linked more to metastases and the metastatic process than to tumorigenesis. Notably, the effects of miR-10b on breast cancer cell viability appear to be most prominent in mesenchymal breast cancer cell lines, demonstrating variable effectiveness of miR-10b inhibition as a therapy (55). This was confirmed in a separate study of over 600 cell lines of various types of cancer, in which inhibition

of miR-10b was found to be either very cytotoxic or ineffective even at high doses (62). Computational analysis of the susceptible cell lines revealed an enrichment in genes regulated by c-Jun, a proto-oncogene reported to be upregulated by miR-10b (63). It is sensible, then, that the mesenchymal states and enrichment in genes regulated by c-Jun are secondary to high miR-10b activity, explaining the increased sensitivity to miR-10b inhibition.

With over 350 predicted targets on miRDB (33), it is likely that new roles for miR-10b will continue to be uncovered. Importantly, since many of the functions identified in breast cancer have also been observed in other types of cancer (49), there is optimism that implementation of miR-10b-related diagnostics, prognostics, and therapeutics in the clinic may have pan-cancer utility.

## MiR-10b in the clinic

### *MiR-10b as a clinical marker in breast cancer*

In patient primary tumors, miR-10b has been correlated with greater tumor diameter, worse histological and clinical grades, and greater vascularization (64-66). Additionally, miR-10b appears to positively correlate with HER2 status (64; 67) and negatively correlate with both estrogen and progesterone receptors (64). This variability among breast cancer subtypes, as well as intratumoral heterogeneity in miR-10b expression (68), may explain why studies comparing miR-10b expression in breast primary tumors versus normal tissues have yielded inconsistent results (38; 43; 69). Nevertheless, because of these correlations and the phenotypes it confers in laboratory settings, many studies have begun investigating the potential of miR-10b as a diagnostic or prognostic indicator of breast cancer and metastatic disease. Circulating tumor cells (70) and the secretion of miR-10b by breast cancer cells (58; 59) also provide a rationale for serum-based analyses.

As a diagnostic marker, one study of 61 breast cancer patients found that miR-10b expression in patient serum could discern breast cancer patients of Stages I-III from healthy patients with a sensitivity of 83.30% and specificity of 100% (71). Another research group also noted upregulation in patient serum (72). Interestingly, unlike in studies performed with patient primary tumor tissue, serum analysis in these studies did not reveal any significant differences between the different stages of breast cancer when using the overall, Stage I-IV grading system (71; 72). For monitoring purposes, miR-10b expression in patient serum significantly decreased post-operation relative to matched pre-operation levels, and further decreased post-radiotherapy (72). Recently, one group proposed to include miR-10b among a panel of miRNAs for predicting response to treatment (73), demonstrating another possible clinical application of miR-10b as a marker of patient outcome. In support of this, elevated miR-10b in patient serum has been shown to be predictive of anemia in response to chemoradiotherapy (74), potentially relating to the increased miR-10b in hematopoietic stem cells relative to differentiated megakaryocytes (75), though this has not been confirmed. As a prognostic indicator, miR-10b expression has been correlated with disease relapse in breast cancer (69; 76), which may be a specific finding, as this correlation was not observed in a pan-cancer meta-analysis (77). Furthermore, expression has been linked to worse overall survival through meta-analysis of three breast cancer cohorts and in aggregate analysis of 21 cohorts spanning six types of cancer (77). Indeed, in one study, the tumors of patients deceased at the time of analysis were also increased relative to those of patients still living (65).

Given its association with pro-metastatic features, it is possible that miR-10b has the greatest utility as a marker in the context of metastasis. Indeed, one consistent finding is the upregulation of miR-10b in metastatic breast primary tumors, relative to non-metastatic tumors or

healthy tissue (38; 64-66). Similarly, several studies suggest that miR-10b expression in serum could be used as a marker for breast cancer spread to lymph nodes, finding significant upregulation in patients with metastatic lymph nodes relative to those without metastasis (72; 78; 79). In one study, the median miR-10b expression of 35 patients with spread to lymph nodes was 4.44-fold that of the 25 patients without spread to lymph nodes, and the odds ratio between miR-10b expression and lymph node spread was calculated to be 2.19. When used as a diagnostic test, a threshold expression value identified patients with spread to lymph nodes with a sensitivity of 71% and a specificity of 72% (78). These findings are particularly notable given that miR-10b is upregulated in lymph node metastasis samples relative to their matched primary tumors, as reported in a study that included 43 pairs of samples across four different types of cancer (80), as it implicates increased miR-10b at every stage of the metastatic process, from primary tumor to circulation to metastases. These findings also align with the expression patterns of miR-10b relative to HER2, ER, and PR status described earlier, as HER2-overexpressing tumors have increased rates of metastasis relative to hormone receptor-positive tumors.

***MiR-10b as a therapeutic target***

The use or inhibition of miRNAs in therapeutic settings have been extensively reviewed in recent publications (6; 81; 82). MiRNAs make for promising therapeutic targets due to their regulation of hundreds of genes that affect several, often-related pathways or processes (9; 10). As they are believed to have relatively minor effects on each individual gene (10), modulation of one miRNA is less likely to perturb normal biological function the way that other therapeutics do. This is evident in studies investigating therapeutic inhibition of miR-10b. Though believed to be an important contributor to early development, genetic knockout of miR-10b in mice is nonlethal, with no significant effect on body weight, overall survival, fertility, or complete blood count (52).

Moreover, the expression of miR-10b in normal tissues is low compared to primary breast tumors (44). These findings collectively suggest that inhibition of miR-10b in patients would have little or no off-target effects while still potentially having profound effects on cancers that depend on miR-10b activity. Here, we highlight the different approaches that have been used across cancer models to specifically silence miR-10b *in vivo*, their results, and their clinical promise.

At the core of most of the methods used to inhibit miR-10b is the delivery of an anti-miR-10b antisense oligonucleotide (ASO), an RNA molecule with base complementarity to miR-10b. By binding miR-10b, the ASO renders miR-10b nonfunctional and triggers its degradation. The challenges to delivery of ASOs include nucleases, a short blood half-life, and charge-charge repulsion at the cell membrane (81-83). As such, modifications to the ASO or conjugation to a vehicle are generally required. One of the more basic strategies toward therapeutic miR-10b inhibition utilized an ASO with a phosphorothioate backbone, 2'-O-methylation of ribose sugars, and a cholesterol moiety at the 3' end, all contributing toward stability and delivery (84). In mice implanted with the spontaneously metastatic 4T1 mouse breast cancer cell line, intravenous administration of the ASO (twice per week, 50mg ASO/kg bodyweight) resulted in no effect on primary tumor size while decreasing pulmonary metastases by 86%, relative to mice treated with a control oligonucleotide of a similar sequence but with mismatches or with PBS. Important for this study and other methods of therapy using ASOs, this inhibition was shown to be specific to miR-10b and the findings were reproduced when miR-10b was inhibited in the cancer cells prior to implantation, demonstrating that the effects were due to miR-10b suppression in cancer cells and not in other cells (e.g., the tumor microenvironment). Moreover, treated mice displayed no behavioral changes and blood and histologic analyses revealed minimal signs of toxicity.

Although the described modifications to the ASO appear to have overcome some of the limitations to delivery *in vivo*, a major criticism is the high dosage that was required for therapeutic effect, which the authors acknowledge may be the reason for liver and spleen enlargement in both the anti-miR-10b and oligonucleotide control treatment mice relative to PBS treatment. To further optimize the use of ASOs as therapeutics, extensive research has gone into the formulation of vehicles for ASO delivery. At the forefront of delivery methods for miR-10b ASOs are nanoparticles, which have been widely used as vehicles of various payloads, including nucleic acids, to increase delivery to the tumor. Furthermore, nanoparticles are remarkably versatile, allowing them to be engineered for unique and specific properties with precise surface modifications, tailored sizes, and targeting moieties, making them ideal platforms for drug delivery. In early studies, polylysine nanoparticles carrying anti-miR-10b ASOs demonstrated their ability to inhibit invasion and migration; however these particles were not carried forward into *in vivo* testing (85).

To date, one of the more promising treatment approaches involves the conjugation of anti-miR-10b ASOs to an iron oxide magnetic nanoparticle (MN) core. This compound, termed MN-anti-miR10b, was first administered intravenously to mice bearing implanted MDA-MB-231 breast cancer cells (61). Similar to the study using an unconjugated ASO, weekly MN-anti-miR10b (10mg Fe/kg bodyweight) had no effect on primary tumor size; however, its administration prior to the appearance of the lymph node metastases visualized by bioluminescence imaging (BLI) was sufficient to prevent metastatic spread to lymph nodes, as seen by BLI and histology. Furthermore, administration of MN-anti-miR10b after onset of lymph node metastases stopped the growth of the BLI signal of the lymph node metastasis. Histological analyses of lymph node metastases revealed a significant reduction in cell proliferation but not apoptosis. In a subsequent study, MN-

anti-miR10b was used with adjuvant doxorubicin in mice with established spontaneous metastases and the combination induced stable regression of the metastases by the fourth week of treatment (55). Treatment was stopped at the fourth week and BLI signals did not remerge over the remaining eight weeks of the study. At sacrifice at week 12, there was no evidence of metastasis in the lymph nodes by histology. Importantly, the therapeutic study was initially performed in an immunocompromised model of breast cancer metastases (MDA-MB-231 cells) and was then reproduced in an immunocompetent model (4T1 cells) (56), and its activity was demonstrated in a case report in a feline model of breast cancer (86). In all these studies, treatment with MN-anti-miR10b did not appear to cause adverse effects (55; 61; 86). Collectively, they support the translation of MN-anti-miR10b to the clinic, particularly for the prevention of metastasis or to limit their growth. In 2023, MN-anti-miR10b, under the name TTX-MC138 (TransCode Therapeutics), completed an early Phase I clinical trial for its use in "advanced solid tumors" (87), and a multicenter Phase I/II study is expected to begin in 2024 (88).

Building on the mounting evidence implicating other miRNAs in multiple cancers, especially metastatic breast cancer, recent studies have explored targeting other miRNAs in addition to miR-10b. Devulapally et al. investigated the anti-tumor efficacy of PLGA-b-PEG nanoparticles coloaded with anti-miR-10b and anti-miR-21 (another miRNA implicated in breast cancer) ASOs and decorated with uPA-peptide for tumor cell targeting (89). These PLGA-b-PEG nanoparticles decreased tumor growth in a subcutaneous, triple-negative breast cancer model after systemic administration. Interestingly, breast cancer cells treated with anti-miR-10b PLGA-b-PEG nanoparticles prior to intracardiac injection formed fewer metastatic nodules than untreated cells. In another study, mesoporous silica nanoparticles loaded with anti-miR-10b ASOs and miR-34

mimic was shown to decrease tumor growth in both *ex ovo* and orthotopic *in vivo* models of human triple-negative breast cancer (90).

Beyond ASOs, another approach to miR-10b inhibition is the repurposing of existing compounds. One group used a luciferase reporter to screen 450 small molecule inhibitors for miR-10b suppression, identifying thirteen compounds (91). Of these, the vascular endothelial and platelet derived growth factors inhibitor linifanib was determined to be the only molecule that suppressed miR-10b specifically, finding no effect on five other clinically relevant miRNAs, including miR-10a. Administration of once-daily oral linifanib to mice implanted with bioluminescent MDA-MB-231 breast cancer cells led to tumor bioluminescence, volume, and weight comparable to that of mice treated with liposome-delivered anti-miR-10b ASO, both of which showing decreases in all three parameters relative to vehicle and scrambled ASO controls (91). As it has already demonstrated therapeutic potential in clinical trials for various cancers, including colorectal (92), lung (93), and hematologic (94), linifanib has unique potential as a readily available miR-10b inhibitor; however, adverse effects may ultimately limit its use (91). Another non-ASO-based approach toward miR-10b inhibition is the use of anti-miR-10b CRISPR plasmid constructs via lipid-polymer nanoparticles, with increased payload delivery to the tumor by destruction of the nanoparticle after administration by focused ultrasound (95). Consistent with other approaches, these nanoparticles failed to reduce primary tumor volume but reduced the number of metastatic lung nodules, further demonstrating the cruciality of miR-10b in breast cancer metastasis development.

With its implications in the tumorigenesis of other cancers, including colorectal cancer and glioblastoma, nanoparticle-based delivery methods for anti-miR-10b ASOs have been tested in those models as well and may have potential applications in breast cancer. Wang et al. investigated

the therapeutic efficacy of a novel EGFR-targeted quantum dot nanoparticle to codeliver the chemotherapy 5-fluorouracil and anti-miR-10b ASO in human colorectal cancer xenografts (96). Systemic administration of this nanoparticle construct significantly decreased the growth of primary tumors and reduced the development of metastases in established human cell line xenograft models. Furthermore, tumor growth was also suppressed in patient-derived xenograft models. Multiple nanoparticle constructs have been developed to target miR-10b in glioblastoma. In 2016, Teplyuk et al. reported on a novel lipid nanoparticle loaded with anti-miR-10b ASOs which was continuously delivered intracranially into the tumor via osmotic pump (97). This therapeutic strategy reduced orthotopic glioblastoma growth; however, it was insufficient for complete elimination of the tumor. Other groups have explored the co-delivery of anti-miR-10b and anti-miR-21 ASOs as a therapeutic strategy against glioblastoma using a similar PLGA nanoparticle as reported above targeting breast cancer. cRGD targeted formulations of this PLGA nanoparticle sensitized glioblastoma to temozolomide (TMZ), the standard of care chemotherapeutic for glioblastoma, in subcutaneous tumor models (98; 99). Chen et al. demonstrated the therapeutic potential of MN-anti-miR10b and cytotoxic synergy with TMZ in glioblastoma cell lines *in vitro* (100), resembling the apparent synergistic effect seen with MN-anti-miR10b and doxorubicin. Notably, some of these and previously described studies included contributions from Regulus Therapeutics Inc. (84; 97), who have developed a novel anti-miR-10b oligonucleotide that exhibited therapeutic efficacy as a monotherapy and synergistic effects in combination with TMZ (101). Although this oligonucleotide therapy demonstrated pre-clinical efficacy and completed preliminary safety screening in 2019, clinical trials have not yet commenced.

## Conclusions and Future Directions

MiR-10b is a well-established driver of metastasis and has been shown to confer several properties associated with aggressive cases of breast cancer. As a result, it has the potential to be a valuable diagnostic and prognostic marker for breast cancer patients. And with two separate therapeutics that have entered clinical trials, miR-10b also shows tremendous promise as a novel drug target for the treatment of breast cancer, metastatic disease, and likely other cancers. However, these therapeutics are among the first miRNA-based therapeutics in a field of research that is still in its infancy. Techniques such as RNA sequencing, cell or tissue staining, and cell sorting have only recently been adapted to miRNAs and are not yet prevalent or cost-effective enough to be accessible to all scientists. As they develop and become more commonplace, it is expected that the roles of other miRNAs, as well as new roles for miR-10b, will be uncovered, in addition to insights into how these miRNAs can be exploited in medicine. Concurrently, miRNA targeting presents its own unique challenges as a separate but intimately connected research focus. While several approaches to targeting miR-10b have been described, it is important to reiterate that other miRNAs are being studied as therapeutic agents or targets, and with them, innovative methods for delivery of oligonucleotides. Collectively, the considerable room for growth in miRNA research positions miRNAs as a new frontier for the management of cancers, with inhibition of miR-10b as a pioneering therapeutic.

# CHAPTER 2: MONITORING OF NANODRUG ACCUMULATION IN MURINE BREAST CANCER METASTASES

## Preface

This chapter has been previously published as

> **Halim, A.**, Mondal, S. K., Al-Qadi, N., Kenyon, E., MacRenaris, K., O'Halloran, T. V., Medarova, Z., Moore, A. Monitoring of Nanodrug Accumulation in Murine Breast Cancer Metastases. *J. Vis. Exp.* (210), e66961, doi:10.3791/66961 (2024).

on which I am lead author. In the publication, I describe step-by-step how the magnetic nanoparticle vehicle component of MN-anti-miR10b can be used to monitor drug delivery to target tissues. In this chapter, I have omitted the "Protocol" section of the publication and associated discussion to focus on the insights to the vehicle that were gained and had not previously been presented to the scientific community.

## Contributions to Science

Dr. Anna Moore and I were responsible for the conception and design of this technical publication. Beth Kenyon and I contributed equally to conducting the experiments, using drug ("MN-anti-miR10b") conceptualized by Dr. Zdravka Medarova and synthesized by Dr. Sujan Kumar Mondal. Protocols were established by me and Beth Kenyon, with the help of Nasreen Al-Qadi. Drs. Keith MacRenaris and Thomas V. O'Halloran of the Quantitative Bio-Element Analysis and Mapping (QBEAM) Center at Michigan State University assisted with inductively coupled plasma optical emission spectroscopy (ICP-OES). Final figure generation was performed by me.

I contributed most of the intellectual content, the only exception being the procedural steps directly involving living mice by Beth Kenyon. Beth Kenyon also assisted with editing.

**Simple Summary**

For the treatment of metastatic breast cancer, it is critical that systemically administered therapeutics can reliably accumulate in widespread cancer tissues. The Cy5.5-conjugated magnetic nanoparticle vehicle that MN-anti-miR10b is built upon has several features that allow for *in vivo* and *ex vivo* confirmation of drug delivery. Here, I demonstrate how drug delivery to metastatic lungs can be confirmed via *ex vivo* fluorescence imaging, fluorescence microscopy, and inductively coupled plasma optical emission spectroscopy (ICP-OES).

**Acknowledgments**

This work was supported in part by the NIH R01CA221771 grant to A.M. and by the P41GM135018 grant to T.O. supporting the Quantitative Bio-Element Analysis and Mapping (QBEAM) Center at Michigan State University. We would like to thank Danielle Ferguson, DVM, MS, of the Department of Campus Animal Resources (CAR) at Michigan State University for supervising animal procedures and ensuring compliance with IACUC protocols and Nazanin Talebloo, PhD, for assistance with ICP-OES.

**Disclosures**

Z.M and A.M. are co-founders and shareholders of TransCode Therapeutics Inc.

**Abstract**

Metastatic breast cancer is a devastating disease with very limited therapeutic options, calling for new therapeutic strategies. Oncogenic miRNAs have been shown to be associated with the metastatic potential of breast cancer and are implicated in tumor cell migration, invasion, and viability. However, it can be difficult to deliver an inhibitory RNA molecule to the tissue of interest.

To overcome this challenge and deliver active antisense oligonucleotides to tumors, we utilized magnetic iron oxide nanoparticles as a delivery platform. These nanoparticles target tissues with increased vascular permeability, such as sites of inflammation or cancer. Delivery of these nanoparticles can be monitored *in vivo* by magnetic resonance imaging (MRI) due to their magnetic properties. Translation of this therapeutic approach into the clinic will be more accessible because of its compatibility with this relevant imaging modality. They can also be labeled with other imaging reporters such as a Cy5.5 near-infrared optical dye for correlative optical imaging and fluorescence microscopy. Here, we demonstrate that nanoparticles labeled with Cy5.5 and conjugated to therapeutic oligomers targeting oncogenic miRNA-10b (termed MN-anti-miR10b, or "nanodrug") administered intravenously accumulate in metastatic sites, opening a possibility for therapeutic intervention of metastatic breast cancer.

**Introduction**

Despite many advances in the treatment of breast cancer, clinical options for metastatic disease remain limited. Patients commonly receive therapies targeted against drivers identified in the primary tumor, such as estrogen or HER2, but these drivers are not always conserved in metastases, rendering therapy ineffective (102). Other systemic therapies, such as chemotherapy, are non-specific and known for their side effects. To develop effective options for the treatment of metastatic breast cancer, it is important to consider the biological drivers that allow cancer cells to spread and colonize distant sites. One of these drivers is miR-10b, an oncogenic microRNA, implicated in breast cancer cell viability, invasion, and migration, which has been shown to be sufficient to confer metastatic potential in otherwise-nonmetastatic breast cancer cells (38; 55). Importantly, miR-10b is also expressed at higher levels in metastases compared to matched primary tumors (80), making it a promising target for the treatment of existing metastases.

Although miRNAs such as miR-10b have great potential as therapeutic targets for metastatic disease, the design of therapeutically viable methods for miRNA silencing presents unique challenges. Antisense oligonucleotides (ASOs) that bind their complementary miRNA sequence are commonly transferred to the cells *in vitro* using lipofection but cannot easily reach tumor cells *in vivo* due to inherent instability, risk of destruction by nucleases, short blood half-life, and the inability to enter cells due to charge-charge repulsion (83). To combat these challenges, we developed a clinically applicable carrier for biomolecules using dextran-coated magnetic iron oxide nanoparticles (MNP) (103). Amine groups on the nanoparticle allow for the conjugation of oligonucleotides, fluorescent dyes (e.g., Cy5.5), and targeting moieties. Additionally, the iron oxide core allows for *in vivo* monitoring of vehicle delivery using magnetic resonance imaging (MRI). We conjugated anti-miR-10b locked nucleic acid ASO and Cy5.5 to MNP to create a "nanodrug" referred to as MN-anti-miR10b, depicted in **Figure 1.1** (61).

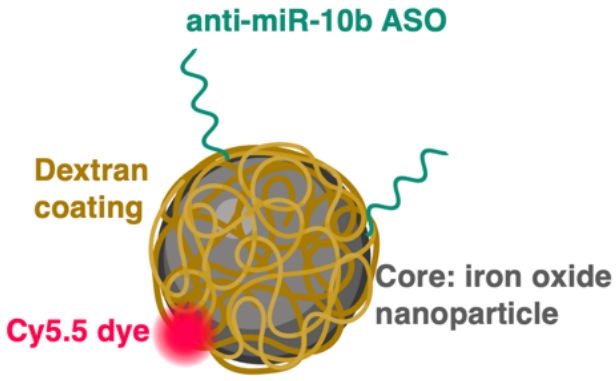


**Figure 1.1: Schematic design of the MN-anti-miR10b "nanodrug."** The nanodrug components include the iron oxide core covered with dextran, conjugated to Cy5.5 dye and single stranded anti-miR10b oligonucleotide molecules. Abbreviation: ASO = antisense oligonucleotide. Created with BioRender.com.

In our previous studies, we showed that the nanodrug efficiently causes downregulation of miR-10b and inhibits the migration and invasion of triple-negative breast cancer cells *in vitro* (61). In murine models of metastatic breast cancer, intravenous delivery of the nanodrug prevented the

development of lymph node metastases or, if administered after lymph node metastasis formation, halted their growth (61). Notably, the nanodrug was observed to readily accumulate in cancer tissues. While the nanodrug did not eradicate metastases on its own, in subsequent studies, we showed that combination treatment with adjuvant doxorubicin was curative in both immunocompromised and immunocompetent mouse models (55; 56). The effects of miR-10b inhibition by the nanodrug have also been seen in feline mammary carcinoma (86).

To effectively treat breast cancer, it is imperative to demonstrate that the drug accumulates in tissues of interest. Here, we present a protocol for demonstrating the accumulation of the magnetic nanoparticle carrier used to deliver therapeutic anti-miR-10b ASOs to cancer tissues using multiple modalities in murine models of metastatic breast cancer.

**Representative Results**

In our previous therapeutic *in vivo* studies, we treated mice with one dose of nanodrug (10 mg Fe nanodrug/kg mouse bodyweight) weekly for several weeks (55; 56; 61). For this demonstration, we sought to determine whether accumulation of nanodrug could be observed in lung metastases after one dose, 1 week later. The results of this study would guide the timeline for monitoring the nanodrug accumulation in future longitudinal studies. Ultimately, it can also serve as an indication of the nanodrug persistence in the tissue of interest.

We followed the protocol described above and induced orthotopic breast primary tumors. Mice were regularly imaged for the development of metastases. At 5–6 weeks, primary tumors were resected due to excessive size. Resection allowed mice to survive and metastases to continue to grow. Lymph node and/or lung metastases were observed in mice after 6–7 weeks post induction, and signal persistence and growth were monitored regularly using BLI. After visualization of persistent and widespread signals at metastatic sites (**Figure 1.2A, B**), one dose of

nanodrug or PBS control was administered via the tail vein. After 7 days, mice were imaged one final time using BLI and sacrificed for sample collection. For mice with lung metastases, the lungs and heart were collected and imaged using BLI *ex vivo* to confirm that the lungs were the site of metastasis (**Figure 1.3, top row**).

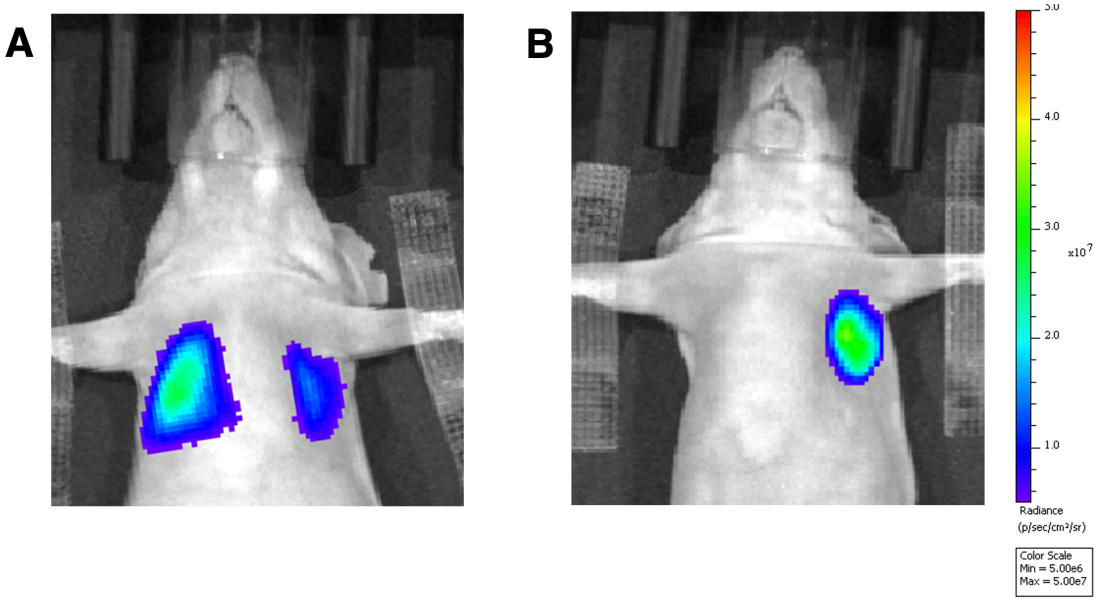


**Figure 1.2: Representative *in vivo* BLI.** Constitutive luciferase expression by the MDA-MB-231 cell line allows for BLI monitoring of metastasis formation *in vivo*. In this model, metastases are commonly seen at (**A**) the lungs or (**B**) lymph nodes. A minimum threshold of $5 \times 10^3$ radiance was used for a positive signal during monitoring. Abbreviation: BLI = bioluminescence imaging.

Samples were then imaged using fluorescence imaging using the excitation/emission wavelengths for Cy5.5, confirming that Cy5.5 from the nanodrug accumulated only in tissues harboring metastases (**Figure 1.3, bottom row**). A mouse with lung metastases that did not receive nanodrug treatment was used as a negative control (marked Control in **Figure 1.3**), showing bioluminescence but not Cy5.5 fluorescence in the lung tissue, demonstrating that Cy5.5 signal was independent from bioluminescence signal. Lung tissue was divided, and one part was embedded in OCT for sectioning and fluorescence microscopy and the other part was weighed and frozen for ICP-OES.

Fluorescence microscopy confirmed Cy5.5 signal in the lung metastases of nanodrug-treated mice but not in control mice (**Figure 1.4**), supporting the FLI results. ICP-OES revealed an increase of iron of more than 187 µg Fe/g tissue in lung metastases of nanodrug-treated mice (n = 2) compared to control mice (n = 2) with greater than 2.3-fold Fe concentration, indicating nanoparticle accumulation in the metastases of nanodrug-treated mice but not in control mice (**Figure 1.5**). Together, these results demonstrate that the nanodrug accumulated in the intended tissues, validating our methods as a means to monitor the delivery of nanotherapeutics.

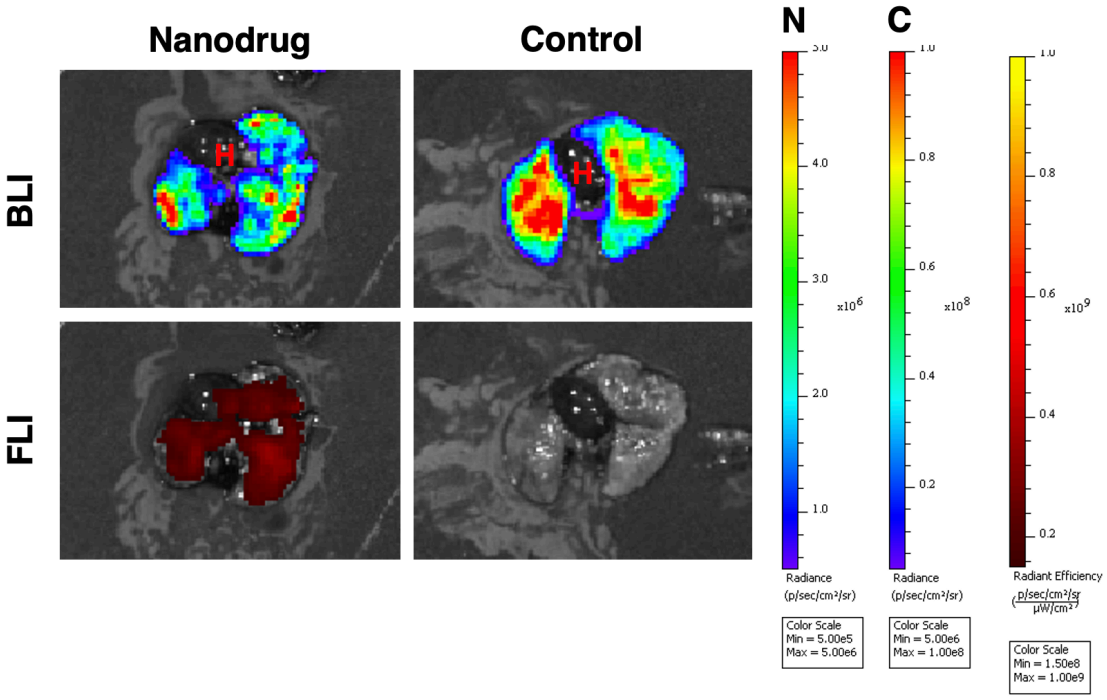


**Figure 1.3: *Ex vivo* BLI and FLI.** BLI (top row) and Cy5.5 FLI (bottom row) of heart and metastatic lungs from mice that received one dose of the nanodrug and control mice treated with PBS, collected after 1 week of treatment. Cy5.5 fluorescence in lung metastasis is only seen in animals injected with the nanodrug and not in control animals. N = BLI scale for nanodrug injected mice; C = BLI scale for control mice. Abbreviation: H = heart.

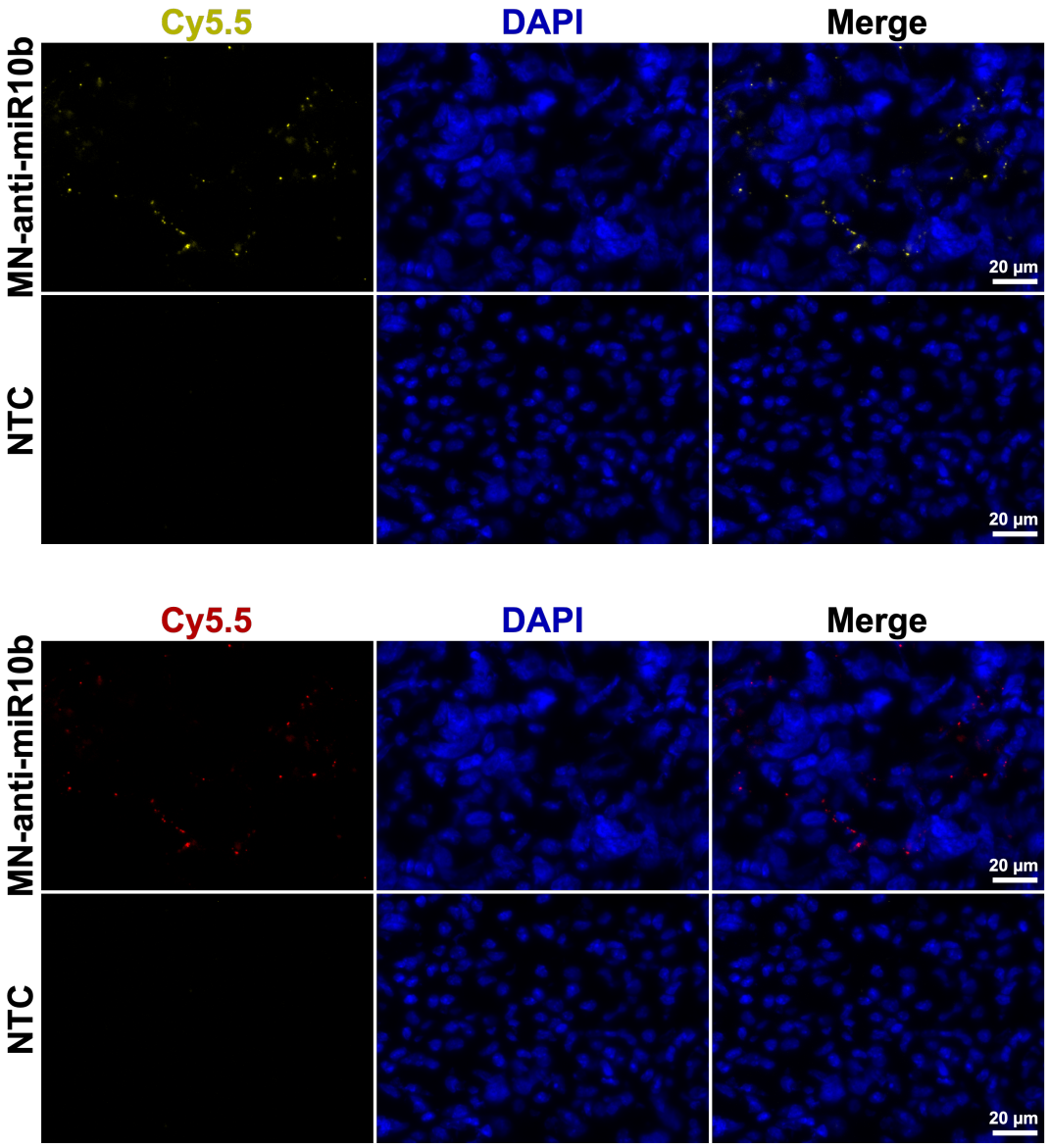


*Figure presented here is an adaptation of the published figure, magnified for better visualization of Cy5.5 signal and recolored to include a colorblind-friendly palette (top set) and conventional pseudocoloring (bottom set).*

**Figure 1.4: Correlative fluorescence microscopy.** Fluorescence microscopy of metastatic lung sections from mice that received one dose of the nanodrug (top row) and control mice treated with PBS (bottom row), collected after 1 week of treatment. Cy5.5 fluorescence is only seen in metastatic tissues of mice injected with the nanodrug. Scale bar = 20 µm. Abbreviation: DAPI = 4',6-diamidino-2-phenylindole.

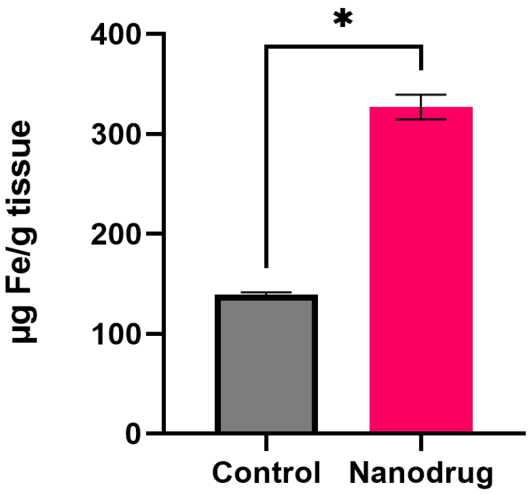


**Figure 1.5: Inductively coupled plasma optical emission spectroscopy results.** Iron concentrations in metastatic lungs from mice receiving one dose of nanodrug and control mice, collected after 1 week of treatment. Shown are mean ± SEM, statistical analysis performed using Welch's *t*-test, n = 2 per condition.

**Discussion**

Nanoparticles have great potential for cancer treatment. Here, we showed that a Cy5.5-conjugated MNP carrier can reach cancer tissues to deliver therapeutic oligonucleotides in a murine model of metastatic breast cancer. The ability to administer the nanodrug systemically while still achieving considerable accumulation in cancer tissues offers tremendous advantages over many existing ASO delivery methods, which commonly require local and often invasive administration. As target specificity is imperative to patient safety and drug efficacy, these methods are valuable for establishing the feasibility of translation to the clinic. Additionally, the iron oxide core and Cy5.5 offer monitoring capabilities that other carriers or conventional therapeutics cannot.

Nanoparticles offer unprecedented customizability compared to traditional therapeutics. Although our studies utilize the platform for inhibition of a microRNA using an antisense oligomer, the methods shown here apply to the delivery of other therapeutic moieties using the platform,

such as small interfering RNAs (siRNA). By adding functional components such as Cy5.5, drug delivery in preclinical models can be monitored in ways previously not possible. These insights can be used to optimize drug delivery and efficacy, advancing these experimental therapeutics toward translation to the clinic.

# CHAPTER 3: INHIBITION OF MIR-10B TREATS METASTATIC BREAST CANCER BY TARGETING STEM CELL-LIKE PROPERTIES

## Preface

This chapter is adapted, with additional data, from a manuscript previously published as

> **Halim A**, Al-Qadi N, Kenyon E, Conner KN, Mondal SK, Medarova Z, Moore A. Inhibition of miR-10b treats metastatic breast cancer by targeting stem cell-like properties. Oncotarget. 2024 Aug 26;15:591-606. doi: 10.18632/oncotarget.28641. PMID: 39189967; PMCID: PMC11348941.

on which I am lead author. It represents my most novel contributions to the scientific community and offers insights into the pharmacodynamics and therapeutic mechanisms of MN-anti-miR10b that will help in its advancement to clinical use.

## Contributions to Science

I was responsible for the conception and design of this research project. Experiments were performed using drug ("MN-anti-miR10b") conceptualized by Dr. Zdravka Medarova and synthesized by Dr. Sujan Kumar Mondal. Beth Kenyon and I contributed equally to conducting animal experiments. All other experiments were led by me. Nasreen Al-Qadi assisted with generation of cultured cell samples for RNA sequencing, the Michigan State University Genomics Core performed RNA sequencing, and Dr. Kayla Conner assisted with file management, mapping, and annotating of raw sequencing files. Nasreen Al-Qadi assisted with conducting and analyzing mammosphere experiments. All other experiments were performed independently by me, and final

figure generation for all experiments was performed by me. I contributed all intellectual content. Beth Kenyon assisted with editing.

**Simple Summary**

MN-anti-miR10b is an inhibitor of miR-10b that has reproducibly induced regression of breast cancer metastases, but its downstream actions after miR-10b inhibition are not well understood. Here, we learn from RNA sequencing that inhibition of miR-10b activates developmental processes in breast cancer cells. We then establish a connection between miR-10b and stem-like cancer cells and show that MN-anti-miR10b inhibits breast cancer cell stemness.

**Ethical Statement**

All procedures involving animal subjects have been approved by the Michigan State University Institutional Animal Care and Use Committee (IACUC) and conformed to all regulatory standards (PROTO202300364).

**Acknowledgments**

The authors would like to thank Anna Savan, B.S. for her help with performing *in vitro* experiments.

**Conflicts of Interest**

Z.M. and A.M. are scientific founders and shareholders at TransCode Therapeutics Inc. The remaining authors declare that the research was conducted in the absence of any commercial or financial relationships that could be construed as a potential conflict of interest.

**Funding**

This work was supported in part by R01CA221771 and R01CA261691 to AM.

**Abstract**

Despite advances in breast cancer screening and treatment, prognosis for metastatic disease remains dismal at 30% five-year survival. This is due, in large, to the failure of current therapeutics to target properties unique to metastatic cells. One of the drivers of metastasis is miR-10b, a small noncoding RNA implicated in cancer cell invasion, migration, viability, and proliferation. We have developed a nanodrug, termed MN-anti-miR10b, that delivers anti-miR-10b antisense oligomers to cancer cells. In mouse models of metastatic triple-negative breast cancer, MN-anti-miR10b has been shown to prevent onset of metastasis and eliminate existing metastases in combination with chemotherapy, even after treatment has been stopped. Recent studies have implicated miR-10b in conferring stem cell-like properties onto cancer cells, such as chemoresistance. In this study, we show transcriptional evidence that inhibition of miR-10b with MN-anti-miR10b activates developmental processes in cancer cells and that stem-like cancer cells have increased miR-10b expression. We then demonstrate that treatment of breast cancer cells with MN-anti-miR10b reduces their stemness, confirming that these properties make metastatic cells susceptible to the nanodrug actions. Collectively, these findings indicate that inhibition of miR-10b functions to impair breast cancer cell stemness, positioning MN-anti-miR10b as an effective treatment option for stem-like breast cancer subtypes.

**Introduction**

Breast cancer is estimated to be the most diagnosed cancer overall and second-most lethal cancer among women in 2024 (1). Changes to screening guidelines and advances in medicine have greatly increased survival rates; however, the most favorable prognoses are reserved for breast cancer detected when still localized, with a five-year survival rate of 99% (3). Five-year survival rates for breast cancer that has metastasized to distant sites remain dismal at 30% overall (3). A

major contributor to this disparity in survival between localized and metastatic disease is the lack of therapeutics designed specifically for targeting metastases. Indeed, the breast cancer subtypes with the best survival rates – hormone receptor-positive or HER2-enriched – are those that are less likely to metastasize and with dependencies on signaling pathways that can be targeted therapeutically (3). In contrast, metastatic disease is commonly of the triple-negative subtype, lacking a clear target and making treatment particularly difficult. While there is a need to identify treatments for triple-negative breast cancer in general, it is metastases that cause most patient deaths (4; 5; 104). As such, the development of therapeutics aimed specifically at metastases or the metastatic process is of great clinical urgency. These therapeutics would serve as effective treatments for the most common cause of death not only for triple-negative breast cancer but for all aggressive breast cancers.

To fill this gap and develop effective options for treatment of metastatic breast cancer, it is important to understand the drivers of metastasis. MicroRNA-10b (miR-10b) is a small noncoding RNA molecule overexpressed in metastases compared to their primary tumors (80). It has been implicated in breast cancer cell invasion and migration (38; 55; 61), and its overexpression is sufficient to confer onto breast cancer cells the ability to spontaneously metastasize (38). Importantly, we found that miR-10b also serves as a critical driver of metastatic cell viability and proliferation (55). This discovery led us to the notion that inhibition of miR-10b is a feasible mechanism to treat metastatic breast cancer. To accomplish this, we synthesized the nanodrug consisting of anti-miR-10b antisense oligomers (ASOs) conjugated to iron oxide-based magnetic nanoparticles (MN) that serve as delivery vehicles for oligonucleotides to tumor cells *in vivo.* The magnetic properties of these nanoparticles allowed for their detection by magnetic resonance imaging (MRI) so the delivery of the nanodrug can be monitored non-invasively (61). Our previous

studies in metastatic breast cancer models showed that systemic delivery of this therapeutic, termed MN-anti-miR10b, in mice bearing aggressive primary tumors prevented the onset of metastatic spread with high reproducibility, and if metastases were already present, their growth was halted (61). Subsequent studies found that combination therapy with doxorubicin elicited regression and elimination of metastases in metastatic breast cancer models corresponding to Stage II and IV of human disease even after treatment was stopped (55; 56).

While MN-anti-miR10b shows tremendous clinical potential, a limitation of our previous studies is their focus on therapeutic outcomes. MiR-10b has over 350 predicted targets (33), many of which regulate gene transcription and translation themselves. Currently it is not known which genes and processes are governed by miR-10b inhibition by the nanodrug, but most importantly, it is not clear which properties make metastatic cells susceptible to the nanodrug actions. Thus, in this work we analyzed differentially expressed genes in response to miR-10b inhibition by the nanodrug to determine which biological processes are affected and how these processes are involved in the therapeutic response. Answering these questions and understanding the consequences and the mechanism of miR-10b inhibition in cancer cells may yield insights toward better therapy optimization for individual patient candidates and/or more effective adjuvant drug combinations.

Previously, we have observed various MN-anti-miR10b effects on cancer cells *in vitro*, including decreased migration, invasion, and proliferation (55; 61) and a direct effect on viability (55; 62). Phenotypic effects were observed in as little as 24-48 hours treatment, with miR-10b expression decreased almost 90% relative to controls (55; 61). In this study, we first determined the persistence of miR-10b inhibition after repeated treatments in mouse models of metastatic breast cancer. We observed an average of 99% downregulation within two weekly treatments,

demonstrating the ability of MN-anti-miR10b to overcome physiological barriers and effectively downregulate its primary target. To identify mechanisms of therapy, we next performed RNA sequencing of breast cancer cells treated with MN-anti-miR10b *in vitro*. This revealed that inhibition of miR-10b affected many genes associated with developmental processes, suggesting that MN-anti-miR10b acts on the properties of cancer cells conferred by their dedifferentiation into a more stem cell-like state. We also found that this relationship was not limited to breast cancer and has a potential to be extended to other cancers. Lastly, we show that miR-10b expression is tightly connected to stem-like cancer cell subpopulations and demonstrate that inhibition of miR-10b decreases phenotypes associated with stemness. These data provide an explanation for the efficacy of MN-anti-miR10b in mouse models of metastatic breast cancer and support its use in high grade, poorly differentiated breast cancer cases.

**Results**

***Systemic administration of MN-anti-miR10b efficiently downregulates miR-10b in metastases***

We have previously demonstrated that miR-10b expression was significantly inhibited in metastatic lymph nodes 24-48 hours after treatment with MN-anti-miR10b (55; 61). Here we extended these studies to investigate the time course of the inhibition after repeated treatments in local and distant metastases. To that end, we first confirmed accumulation of the nanodrug in various metastatic sites 72 hours after injection (**Figure 2.1A**).

Bioluminescence imaging (BLI) and fluorescence imaging (FLI) of excised lung and lymph node metastases showed excellent co-localization of the nanodrug accumulation with metastatic tissues (**Figure 2.1A**) similar to our previous findings [10], which was confirmed by fluorescence microscopy (**Figure 2.1B**). Consequentially, RT-qPCR of cryosectioned samples showed that miR-10b was inhibited by over 93% (**Figure 2.1C**).

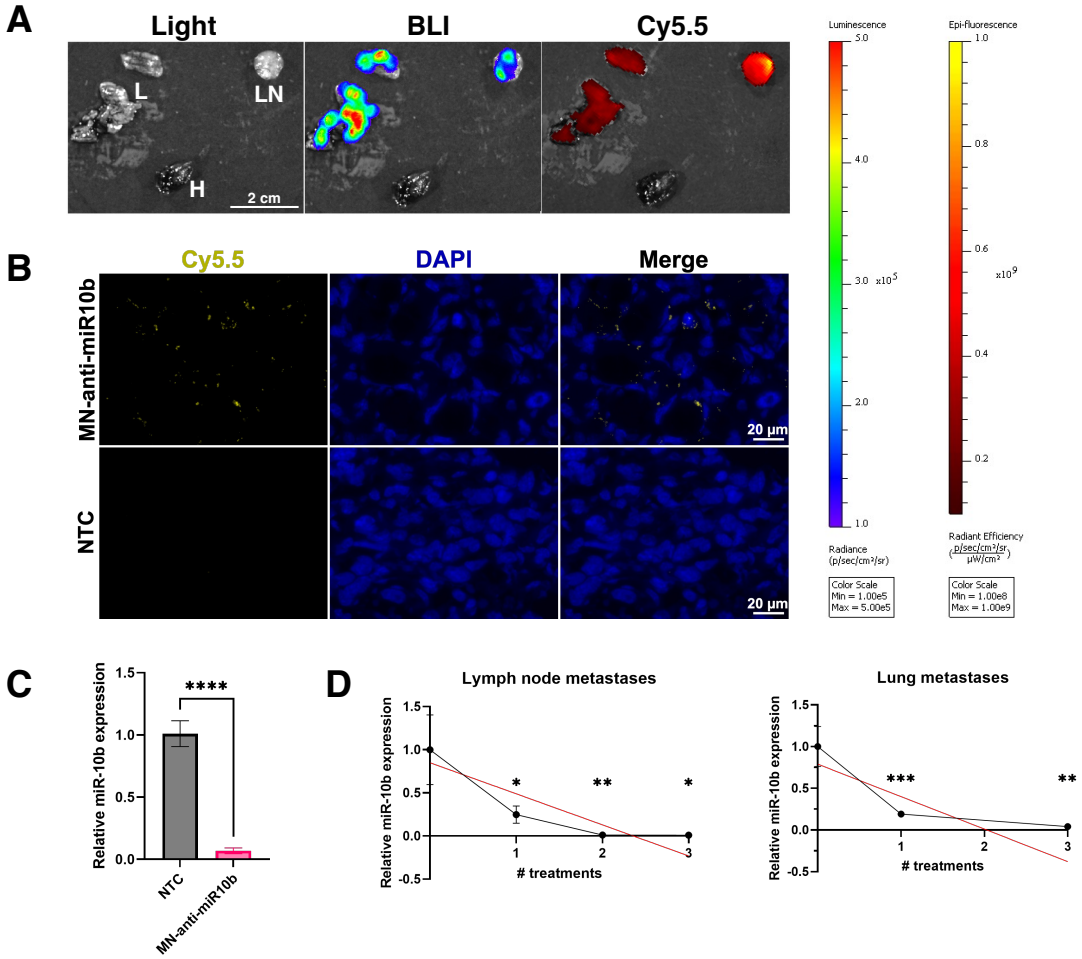


**Figure 2.1. MN-anti-miR10b accumulates in breast cancer metastases within 72 hours and downregulates miR-10b significantly following systemic administration *in vivo*.**
(A) *Ex vivo* imaging of representative metastatic tissues of a mouse treated with MN-anti-miR10b 72 hours prior. L = lung, LN = lymph node, H = heart.
(B) Fluorescence microscopy of representative metastatic lymph node tissue treated with MN-anti-miR10b 72 hours prior or non-treated control (NTC). *Recolored from publication to a colorblind-friendly palette.* Blue = DAPI. Yellow = Cy5.5, conjugated to MN-anti-miR10b.
(C) qPCR of metastatic tissues treated with MN-anti-miR10b 72 hours prior vs. non-treated control (NTC).
(D) qPCR of metastatic tissues treated with MN-anti-miR10b at weekly intervals, collected 1 week after last treatment. Plots represent mean ± SEM. *p < 0.05, **p < 0.01, ***p < 0.001, ****p < 0.0001.

To determine whether miR-10b inhibition remained stable over the course of the repeated treatment, we performed weekly dosing as we did in our previous therapeutic studies [7, 9, 10]. At

each treatment point, we tested miR-10b expression in lymph node (LN) and lung metastases. In this study, we found that for each number of treatments and in both lymph node and lung metastases, miR-10b was significantly decreased relative to untreated mice, with downregulation of 99% or greater in lymph node metastases after 2 and 3 treatments and downregulation of over 80% in lung metastasis already after one treatment (Figure 2.1D). When looking at changes over the course of three treatments, linear regression indicates that miR-10b is gradually decreasing (LNs $p < 0.021$, lung $p < 0.022$). This suggests that the rapid downregulation seen at 72 hours here or in our previous work at 24-48 hours (55; 61) could be transient and that repeated treatments are necessary for stable inhibition of miR-10b.

***MN-anti-miR10b upregulates genes associated with developmental processes***

To understand what mechanisms may underlie the therapeutic effects of MN-anti-miR10b, we performed RNA sequencing and differential gene expression analysis on the two triple-negative breast cancer cell lines used in our previous therapeutic studies – human MDA-MB-231 and murine 4T1. Cells were treated with MN-anti-miR10b, vehicle control (MN), or left untreated (non-treated control, NTC) for 48 hours. As both MN-anti-miR10b and MN are routinely synthesized in small batches, successful inhibition of miR-10b by MN-anti-miR10b and not by MN was confirmed prior to sequencing (**Figure 2.2A**; n = 3 biological replicates). Principal component analysis (PCA) revealed that, in both cell lines, the anti-miR-10b ASO was the largest contributor to variance, as the MN and NTC samples clustered together and apart from MN-anti-miR10b along the first principal component (PC1; **Figure 2.2B**). In addition to demonstrating the largest perturbance caused by the nanodrug, importantly, this finding supported MN as a transcriptionally innocuous platform for delivery of therapeutic biomolecules.

With consideration to the differences in human and mouse genomes, we first analyzed the MDA-MB-231 and 4T1 samples independent of each other for differentially expressed genes (DEGs). To identify changes induced by the anti-miR-10b ASO specifically, we compared the transcriptomes of MN-anti-miR10b-treated samples to MN-treated samples. In the MDA-MB-231 samples, we found 144 genes upregulated and 67 genes downregulated by MN-anti-miR10b (**Figure 2.2C**). As microRNAs inhibit translation of their target genes (105), upregulation of targets is the most immediate consequence of miR-10b inhibition. Of the upregulated genes, 7 are predicted to be targets on microRNA Target Prediction Database (miRDB) (33) – ATP6V0D2, EPHB2, KLF4, KLF7, NCOR2, TMEM268, and VDR – positioning them as genes whose relationship with miR-10b should be further investigated in the context of miR-10b inhibition-based therapy for metastatic breast cancer. Notable downregulated genes include members of the aldo-keto reductase family 1 (AKR1B1P7, AKR1C1, AKR1C2, AKR1C3), chemokine ligands (CXCL1, CXCL8, CXCL10), and the intestinal stem cell marker LGR5. In the 4T1 samples, more predicted targets were observed among the upregulated genes: Anxa7, Arg2, Bcl2l11, Btbd11, Csgalnact1, Lss, Sdc1, Tiam1, Tnrc6b, Vdr, and Wdr26. Notably, of 10 genes upregulated in both cell lines, VDR/Vdr is the only predicted target.

For a broader approach to understanding the therapeutic mechanisms of miR-10b inhibition, we next sought to identify and compare the biological processes affected by MN-anti-miR10b in the two cell lines. Functional enrichment analysis was performed on upregulated and downregulated genes to determine overrepresented biological processes. Of 72 biological processes overrepresented in genes upregulated by the nanodrug in MDA-MB-231 cells, 60 were also observed in the 4T1 cells (**Supplemental File 2**), with many of them relating to developmental processes, including “cell differentiation” and “tissue development.” While this is not surprising

given the importance of miRNAs in early development, the persistence of this relationship in the MDA-MB-231 and 4T1 cells suggests that the cells have de-differentiated into a more stem cell-like state and that MN-anti-miR10b may serve to decrease the stem cell-like features commonly associated with cancer cells, such as chemoresistance (106). In contrast, there was low overlap in the biological processes overrepresented by downregulated genes, all of them being nonspecific (e.g., "biological regulation" and "response to stimulus"; **Supplemental File 2**).

For a more global approach to understanding the therapeutic mechanisms of miR-10b inhibition, we analyzed samples from both cell lines together, correcting for cell line as a covariate. Again, we first isolated differences due to the anti-miR-10b ASO by comparing MN-anti-miR10b-treated samples to MN-treated samples, identifying 162 upregulated genes and 98 downregulated genes (**Figure 2.6A**). When performing unsupervised hierarchical clustering of all samples (including NTC) using the DEGs, MN-treated and NTC samples clustered together and separate from MN-anti-miR10b-treated samples and subsequently clustered by cell line (**Figure 2.2D**), supporting the PCAs and indicating that MN has relatively little effect on the cancer cells as a vehicle. As expected, functional enrichment analysis found that developmental processes were significantly overrepresented by the upregulated genes (**Figure 2.2E**). Biological processes overrepresented by the downregulated genes include those associated with stress or immune response, possibly indicating that MN-anti-miR10b functions to decrease tumorigenic inflammation (**Figure 2.6B**).

To show applicability of our findings to other cancers, we sought to determine whether the DEGs and overrepresented biological processes seen with MN-anti-miR10b in breast cancer can be extended to publicly available data. To that end, we compared our dataset to a published microarray dataset in which miR-10b was inhibited in a glioblastoma multiforme (GBM) cell line,

U87, by transducing miR-10b binding sites (107). In the associated study, inhibition of miR-10b resulted in decreased invasion *in vitro* and smaller tumors *in vivo* compared to controls, as seen with our nanodrug (61) and other miR-10b inhibition studies (84).

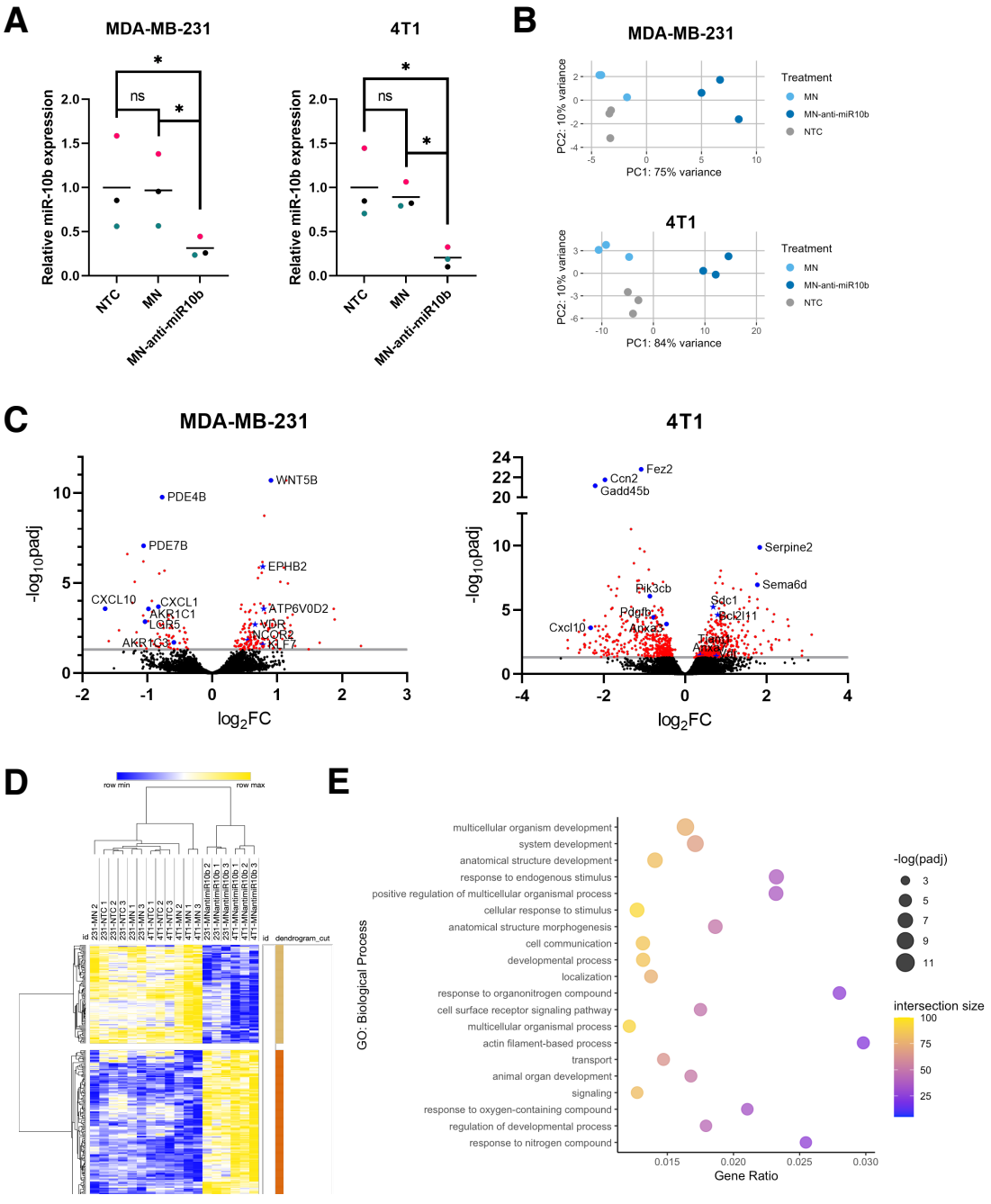


**Figure 2.2. Differential gene expression and functional enrichment analysis of breast cancer cells with miR-10b inhibited by MN-anti-miR10b.**

**Figure 2.2 (cont'd)**
(A) qPCR of MDA-MB-231 and 4T1 cells treated with MN-anti-miR10b or MN for 48 hours or non-treated control (NTC). Colors represent matched replicates. Line represents mean. *$p < 0.05$.
(B) Principal component analysis of transcriptomes of MDA-MB-231 and 4T1 cells treated with MN-anti-miR10b, MN for 48 hours or non-treated control (NTC).
(C) Volcano plots of MDA-MB-231 and 4T1 cells representing differential gene expression between MN-anti-miR10b and MN treatment for 48 hours. Line indicates $p_{adj} = 0.05$. Red points indicate $p_{adj} < 0.05$. Blue points are notable genes, with titles. Blue stars are predicted targets of miR-10b, with titles.
(D) Unsupervised hierarchical clustering of normalized, batch-corrected MDA-MB-231 and 4T1 transcriptomes. Rows represent differentially expressed genes between MN-anti-miR10b and MN.
(E) Top 20 most significant biological processes overrepresented by genes upregulated in MN-anti-miR10b-treated samples vs. MN-treated.

Comparison of the genes upregulated by miR-10b inhibition identified only one overlapping gene: VDR (**Figure 2.3A**). The consistency with which VDR is upregulated in response to inhibition of miR-10b regardless of species, cancer type, or method and its status as a predicted target of miR-10b makes the gene particularly interesting for future studies in miR-10b-based therapies. In contrast, no genes were consistently downregulated in all three cell lines. With consideration to differences between human (MDA-MB-231 and U87) and mouse (4T1) genomes and biology, we further investigated the overlapping DEGs between MDA-MB-231 and U87 cells. In addition to VDR, there were 10 shared upregulated genes (**Figure 2.3A**), including the predicted target ATP6V0D2 and two genes within the same family as predicted targets, LRRC8E and WNT5B (LRRC8B and WNT9B are predicted targets), suggesting that these genes may be human-specific effectors of miR-10b inhibition.

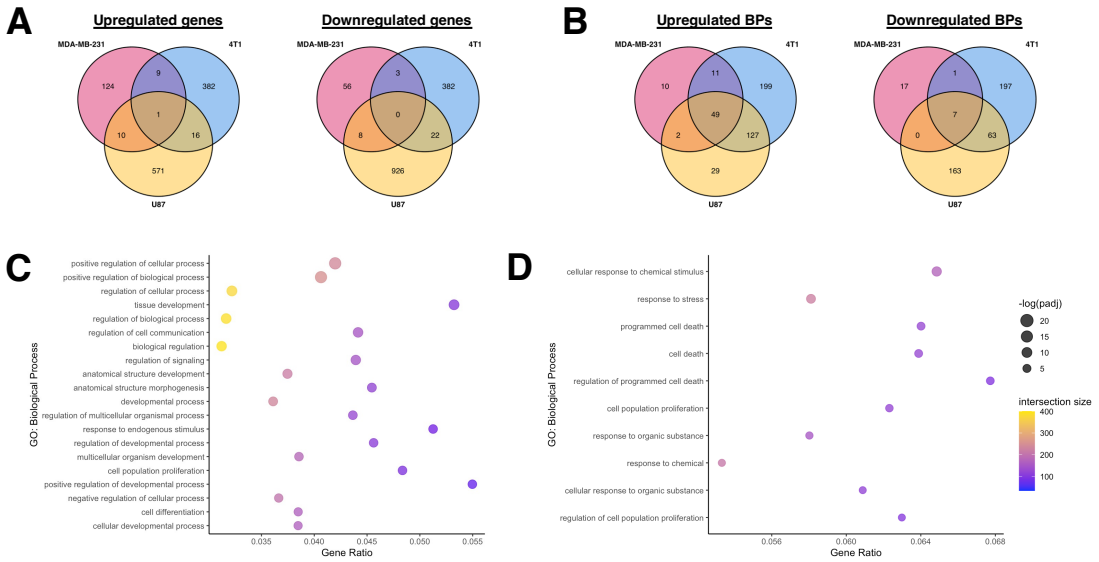


**Figure 2.3. Comparison of transcriptomic effects of miR-10b inhibition in breast cancer cells and glioblastoma.**
(A) Comparison of overlapping genes between MDA-MB-231, 4T1, and U87 datasets, miR-10b inhibited vs. control.
(B) Comparison of overlapping biological processes overrepresented by upregulated and downregulated genes between MDA-MB-231, 4T1, and U87 datasets, miR-10b inhibited vs. control.
(C) Top 20 most significant biological processes overrepresented by genes upregulated in U87 dataset, miR-10b inhibited vs. control, also found in MN-anti-miR10b-treated samples.
(D) All biological processes overrepresented by genes downregulated in U87 dataset, miR-10b inhibited vs. control, also found in MN-anti-miR10b-treated samples.

Functional enrichment analysis of the upregulated and downregulated genes in the U87 dataset was also performed, and the overrepresented biological processes of each gene set were compared to the ones identified in MDA-MB-231 and 4T1 cells (**Figure 2.3B**) and combined analysis (**Figure 2.3C, D**). Interestingly, despite the low similarity in DEGs, 47 of the 125 biological processes overrepresented by the genes upregulated by MN-anti-miR10b were also overrepresented by the genes upregulated in the U87 dataset (**Figure 2.3C**, **Supplemental File 2**), again with many of them related to development. From the downregulated genes, despite zero

shared genes, 10 overrepresented biological processes are shared (**Figure 2.3D**), including processes relating to both cell death and proliferation.

Together, these datasets provide insights into the effects of miR-10b inhibition on cancer cells across delivery methods, tissue types, and species. The relatively large overlap in biological processes relative to the overlap in DEGs suggest that the mechanism of therapeutic efficacy of MN-anti-miR10b may be better explained by its functional effect on cancer cells rather than its effects on any one target or pathway. Specifically, the numerous developmental processes implicated by the upregulated genes continue to support a connection between miR-10b inhibition and induction of differentiation in cancer cells.

DESeq2 output for significantly differentially expressed genes ($p_{adj} < 0.05$) between MDA-MB-231 and 4T1 cells treated with MN-anti-miR10b versus MN can be found in **Supplemental File 1**.

g:Profiler functional enrichment analysis results of significantly upregulated or significantly downregulated genes between MDA-MB-231, 4T1, or U87 cells with miR-10b inhibited versus control can be found in Supplemental File 2.

***MiR-10b is upregulated in cancer cells with increased stemness***

Recent studies have described a link between miR-10b and stem-like properties in cancer cells (53; 108), supporting inhibition of these properties as a possible mechanism for the therapeutic effects of MN-anti-miR10b. To further investigate this relationship, we analyzed publicly available microRNA profiles of MCF-7 breast cancer cells sorted for a surface marker phenotype commonly associated with increased stemness, $CD44^{+}/CD24^{-/low}/ESA^{+}$ (109-112). The sorted cells in the dataset were found to have increased tumor initiation capability relative to parental MCF-7 cells and the capacity to differentiate into both epithelial and myoepithelial

subpopulations in a tumor (109). Despite our a priori hypothesis that the sorted cells would have greater miR-10b expression, we utilized an unbiased approach to our analysis and applied the Benjamini-Hochberg procedure to the results, finding that sorted $CD44^+/CD24^{-/low}/ESA^+$ cells (sMCF-7) have increased miR-10b expression relative to parental MCF-7 cells (pMCF-7) (**Figure 2.4A**; $p_{adj} < 0.022$). These results support a study in which MCF-7 cells sorted for only $CD44^+$ had increased miR-10b relative to $CD44^-$ cells (53). Additionally, rno-miR-10b is upregulated in the sorted MCF-7 cells ($p_{adj} < 0.007$). In the human genome, the sequence corresponding to rno-miR-10b aligns with the precursor to miR-10b (pre-miR-10b). When comparing these microRNA profiles to the microRNA profile of mammary stem cells (MaSC) (113), although MaSCs have greater miR-10b and pre-miR-10b expression than parental MCF-7 cells ($p_{adj} < 0.035$ and $< 0.014$, respectively), there are no significant differences between sorted MCF-7 cells and MaSCs, demonstrating the utility of the $CD44^+/CD24^{-/low}/ESA^+$ phenotype in selecting for a more stem-like population in breast cancer cells. Indeed, sorted MCF-7 cells and MaSCs cluster together and apart from parental MCF-7 cells when the complete profiles are analyzed by principal component and unsupervised hierarchical clustering (**Figure 2.7A**).

To translate the relationship between miR-10b and stem-associated properties to our previous studies, we sought to test these findings in MDA-MB-231 cells. Cells were sorted into $CD44^+/CD24^-$ and $CD44^-/CD24^-$ populations, with $CD24^+$ cells not analyzed due to consistently low yields. RT-qPCR analysis of the two populations indicate that sorting for CD44 was effective (**Figure 2.7B**), and subsequent analysis for miR-10b shows that cells with the more stem cell-like $CD44^+/CD24^-$ surface marker phenotype have greater than 2-fold miR-10b expression compared to $CD44^-/CD24^-$ (**Figure 2.4B**; $p < 0.027$, $n = 4$ independent sorting events). Notably, of other assorted miRNAs that were tested, none showed significant differences. We then used RT-qPCR

to measure relative mRNA expression levels of two targets of miR-10b, HOXD10 (38) and PTEN (52), and observed decreased expression of both genes in the stem cell-like population compared to the non-stem-like population (**Figure 2.4C**; $p < 0.010$ and $< 0.004$, respectively), as would be expected with increased miR-10b expression.

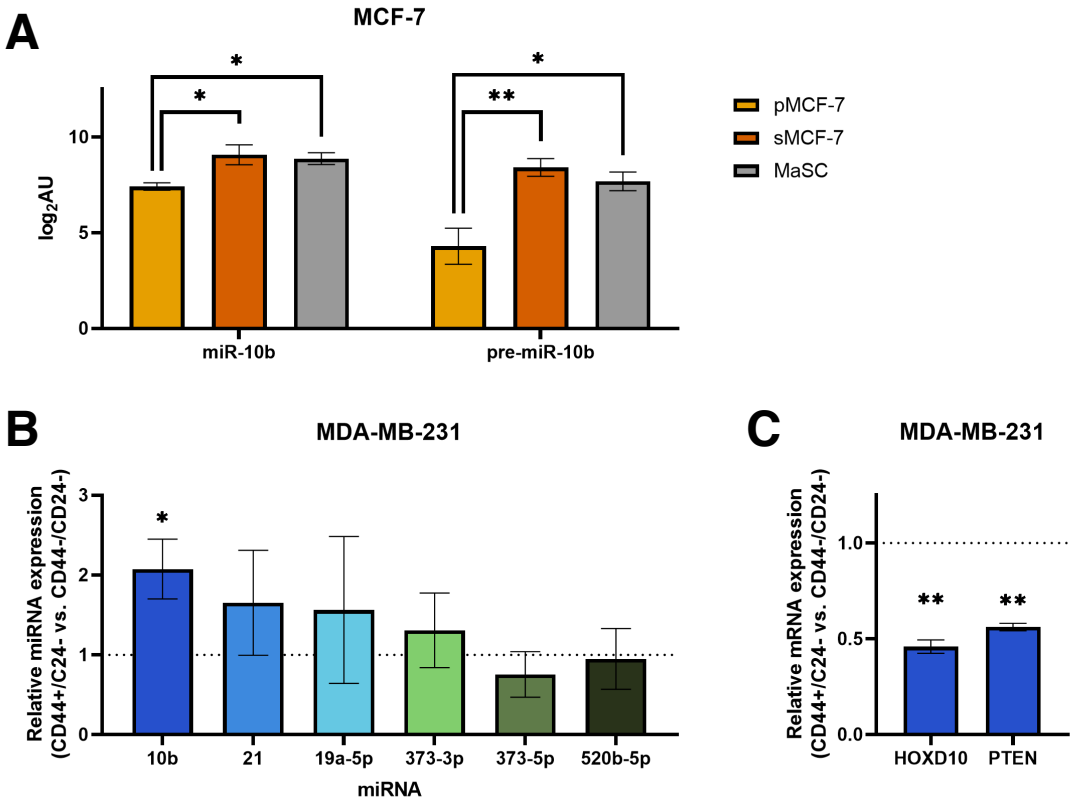


**Figure 2.4. Breast cancer cells sorted for stemness-associated surface markers have upregulated miR-10b expression.**
(A) Log2-transformed arbitrary units of miR-10b and pre-miR10b microarray data in MCF-7 cells. pMCF-7 = parental MCF-7; sMCF-7 = sorted ($CD44^+/CD24^{-/low}/ESA^+$) MCF-7; MaSC = mammary stem cell. *$p_{adj} < 0.05$, **$p_{adj} < 0.01$.
(B) qPCR of miRNAs representing fold change of $CD44^+/CD24^-$ MDA-MB-231 cells relative to $CD44^-/CD24^-$ (dashed line).
(C) qPCR of mRNAs representing fold change of $CD44^+/CD24^-$ MDA-MB-231 cells relative to $CD44^-/CD24^-$ (dashed line).
(B and C) Plots represent mean ± SEM.
*$p < 0.05$, **$p < 0.01$.

Together, these data support recent claims that miR-10b is associated with cancer cell stemness, importantly demonstrating this relationship in the MDA-MB-231 cell line used in previous studies with the MN-anti-miR10b nanodrug.

***MN-anti-miR10b decreases breast cancer cell stemness***

Having identified a correlation between miR-10b expression and a stem-associated surface marker phenotype in both MCF-7 and MDA-MB-231 cells, we next sought to test whether inhibition of miR-10b using MN-anti-miR10b can inhibit properties associated with stem-like cancer cells. *In vitro* methods for studying these properties were reviewed in 2018 by Samanta and Semenza (114).

The Aldefluor assay is commonly used to identify cancer cells with increased stemness (115). It reports on the activity of aldehyde dehydrogenase (ALDH), an enzyme known to be overexpressed by stem-like cancer cells and one whose expression selects for subpopulations with increased self-renewal, differentiation, and tumor initiation (116; 117). The Aldefluor assay of the cells treated with MN-anti-miR10b or MN (vehicle control) for 48 hours revealed that both MDA-MB-231 (**Figure 2.5A**) and MCF-7 (**Figure 2.5B**) cells treated with MN-anti-miR10b have decreased ALDH activity compared to cells treated with MN ($p < 0.0001$ in both cell lines), suggesting that inhibition of miR-10b reduced stemness. Notably, stemness associated with ALDH activity is reported to be distinct from stemness associated with the $CD44^+/CD24^-$ surface marker phenotype, demonstrating generalizability of the link between miR-10b and different markers of stemness (112).

We further tested our hypothesis by assessing spheroid formation of MCF-7 cells in tumorsphere medium. Tumorsphere formation is indicative of self-renewal capability (118; 119), a characteristic of stem-like cancer cells, and decreased or impaired spheroid formation would

support the previous conclusion that inhibition of miR-10b reduces cancer cell stemness. Cells were treated with MN-anti-miR10b or MN for 48 hours under standard, adherent cell culture conditions before being transferred as a single-cell suspension into treated tumorsphere medium in 6-well and 96-well formats for microscopy and a viability assay, respectively. This pre-treatment was done to ensure nanodrug distribution to all cells prior to spheroid formation, as the three-dimensional spheroid structure is known to create a nutrient, oxygen, and drug penetrance gradient (120). Once transferred to tumorsphere medium, cells were monitored for spheroid formation daily for 7 days. By Day 7, cells treated with MN formed large, clustering spheroids as untreated MCF-7 cells are known to do (119; 121; 122) (**Figure 2.5C**). In contrast, cells treated with MN-anti-miR10b form significantly smaller spheroids (less than 38% average surface area as MN, $p < 0.007$), albeit at greater numbers ($p < 0.007$) (**Figure 2.5D**). A viability assay performed on Day 7 found that cells treated with MN-anti-miR10b have decreased viability (**Figure 2.5E**; less than 14% decrease, $p < 0.034$) relative to cells treated with MN. Notably, staining for dead cells using propidium iodide found no dead cells among cells treated with MN-anti-miR10b (Supplementary **Figure 2.3A**), suggesting that the decrease in viability in cells treated with MN-anti-miR10b may be due to reduced proliferation or self-renewal rather than induced apoptotic processes. These experiments were also performed with MDA-MB-231 cells; however, these cells are known to form spheroids poorly (119), aggregating into a loosely-packed structure (123). As with MCF-7 cells, treatment with MN produced the typical structure of MDA-MB-231 spheroids and treatment with MN-anti-miR10b disrupted this organization (**Figure 2.8B**), though with no significant effect on cell viability (**Figure 2.8C**). Thus, these findings were consistent across two cell lines and two characterization methods and indicate that MN-anti-miR10b reduces breast cancer cell stemness.

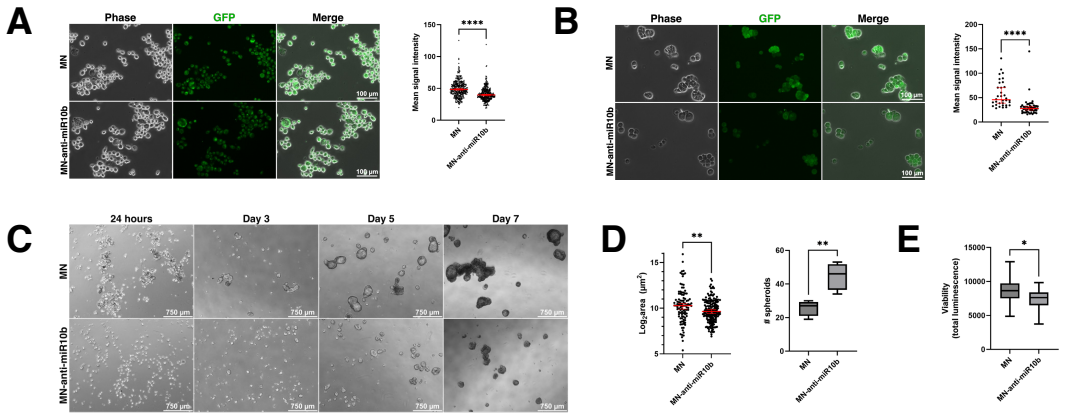


**Figure 2.5: MiR-10b inhibition by MN-anti-miR10b decreases Aldefluor accumulation and impairs spheroid formation.**
(A) Fluorescence microscopy of representative MDA-MB-231 cells after incubation with Aldefluor reagent.
(B) Fluorescence microscopy of representative MCF-7 cells after incubation with Aldefluor reagent.
(A and B) Mean signal intensity = mean gray value in ImageJ.
(C) Mammosphere formation over time of MCF-7 cells treated with MN-anti-miR10b or MN 48 hours prior to (adherent conditions) and during culture in mammosphere medium.
(D) Spheroid size (left) and quantity in a field of view (right) of MCF-7 spheroids at Day 7 in treated medium. Plots represent mean ± SEM (left) and mean ± max/min (right).
(E) Viability assay of MCF-7 spheroids at Day 7 in treated medium. Plot represents mean ± max/min.
(A-E) *$p < 0.05$, **$p < 0.01$. ****$p < 0.0001$.

## Discussion

Inhibition of miR-10b has been shown to be a viable strategy for treatment of metastatic breast cancer (55; 56; 61). Previously, we have shown that MN-anti-miR10b affects cell migration, invasion, proliferation, and viability with 80-90% downregulation (55; 61). To understand the effects of the nanodrug and its therapeutic effects over the course of therapy, we first assessed the efficacy with which MN-anti-miR10b downregulates miR-10b *in vivo* and found that the nanodrug decreases expression by 99% after two rounds of weekly treatment, demonstrating comparable if not superior inhibition of miR-10b *in vivo* as is seen *in vitro*. Importantly, we confirmed that this

effect was similar in regional (lymph node) and distant (lung) metastases. To investigate secondary effects of miR-10b inhibition by MN-anti-miR10b and to understand the affected pathways, we used RNA sequencing to identify differentially expressed genes and observed an overrepresentation of upregulated genes associated with developmental processes, suggesting an effect on the stem cell-like properties of cancer cells. We then confirmed that miR-10b is associated with cancer cell stemness and that phenotypes associated with stemness could be mitigated by MN-anti-miR10b. Together, these data indicate that MN-anti-miR10b has a differentiation effect on cancer cells and implicate dedifferentiated, stem cell-like cancer cells as most vulnerable to its action. This could also explain why in our earlier studies treatment of the primary MDA-MB-231 tumors with the nanodrug completely abrogated metastasis formation [7], as these metastasis-forming stem cell-like cancer cells lost their ability to invade and migrate and most likely died within the primary tumor.

The upregulation of genes associated with developmental processes by MN-anti-miR10b is not unexpected. While details of the role of miR-10b beyond cancer are sparse, miRNAs are collectively associated with regulation of growth and development (124). Furthermore, the effects of miRNAs are influenced in part by their location in the genome and miR-10b is coded among the HOXD cluster of genes (125). Indeed, HOXD10 was one of the first genes found to be regulated by miR-10b (38) and is a computationally predicted target (33). The finding is notable, though, as it suggests that the cancer cells overexpressing miR-10b are in a less-developed, more stem cell-like state. This is supported by previous findings that more mesenchymal cancer cell lines have higher susceptibility to MN-anti-miR10b than more epithelial cell lines (55), as mesenchymal cancer cells share many of the same properties as stem-like cancer cells and the epithelial-mesenchymal spectrum is commonly associated with the spectrum of stemness (126;

127). Additionally, higher susceptibility to MN-anti-miR10b has been seen in cancer cell lines with increased expression of genes associated with the proto-oncogene transcription factor c-Jun (62). As c-Jun has been implicated in conferring stemness in cancer cells (128; 129), this further supports the notion that cancer cells with increased stemness are most sensitive to the nanodrug. Indeed, there are no indications of toxicity from MN-anti-miR10b in developed tissues (55; 61).

Evidence for stem-like states in cancer cells date back to 1994, when a subpopulation of acute myeloid leukemia (AML) cells was found capable of inducing AML in mice when other subpopulations could not (130). A stem cell-like state in cancer cells is thought to be achieved through either transformation of an adult stem cell or through dedifferentiation of a malignant cell (131). In this state, the cancer cells have numerous properties that allow them to evade complete eradication. For example, their capacity to self-renew allows for increased tumor initiation capability, whether in the form of primary tumors or metastases, and their ability to differentiate confers tumor heterogeneity (132). Furthermore, the cells reside in a metabolically quiescent state (106), allowing them to resist therapeutics aimed at rapidly dividing cells. Differentiation therapy to decrease these properties is a focus of many modern research efforts, buoyed by the successful use of all-trans retinoic acid in treating acute promyelocytic leukemia (133). In solid tumors, differentiation therapy has also resulted in increased cure rates in neuroblastoma patients (134). While similar successes have not yet been seen in breast cancer, research is ongoing. Several studies have produced promising results in preclinical experiments (135) (including miRNA-based approaches (136)) and early-stage clinical trials (137), and recent efforts aimed at computationally modeling stemness in breast cancer may uncover novel insights into how to best implement differentiation therapy (138).

Surface markers have been used to identify cells with increased stemness since the aforementioned AML study, in which AML-inducing cells were identified by their $CD34^{+}/CD38^{-}$ phenotype (130). While markers vary across cell lines (139; 140), they are generally validated by testing for similar phenotypic properties, such as increased tumor initiation capacity (139). The $CD44^{+}/CD24^{-}$ phenotype was reported to be a marker of increased stemness in breast cancer in 2003 by Al-Hajj et al. (110). Many groups have since validated this finding in their research and it continues to be commonly used for the isolation of breast cancer cells with increased stemness (111; 112) and studies into prognostic indicators (reviewed in (141)). In this study, we showed that in two breast cancer cell lines – MDA-MB-231 and MCF-7 – subpopulations with the $CD44^{+}/CD24^{-}$ surface marker phenotype have increased miR-10b expression relative to their parental cell line or other subpopulations. The stem-like properties of the $CD44^{+}/CD24^{-}$ in these cell lines have been described previously (53; 111; 112; 142). These findings support previous studies that report that miR-10b drives a stem cell-like phenotype in both cancer cells (53; 108; 143) and progenitor cells (144).

The two most common methods for characterizing stemness in cancer cells *in vitro* are the Aldefluor assay and mammosphere formation (114). The Aldefluor assay has been used to identify cells with increased stemness in both healthy and cancerous contexts, hematopoietic and solid, and increased ALDH activity in cancer cells is associated with properties such as drug resistance, tumorigenicity, and invasiveness (116; 117). We observed decreased ALDH activity in the cells after treatment with MN-anti-miR10b for 48 hours. Notably, our RNA sequencing studies did not show any significant changes in the gene expression of any ALDH family genes; however, ALDH family member L2 (ALDH1L2) was significantly downregulated in the U87 dataset (probe 231202_at; padj $< 0.029$). Though these results are incongruent, the sequencing results are only

indicative of transcript expression and are not necessarily indicative of the activity of ALDH protein. Indeed, ALDH enzymes are reported to have low turnover rates (145), and thus, changes in transcript expression should not be expected in a 48-hour treatment period. In contrast to the Aldefluor assay, mammosphere assays characterize stemness using the ability of cells to self-renew and form three-dimensional spheroids in anchorage-independent conditions (118). Cells grown in these conditions display increased drug resistance, proliferation, and migration properties (119). Notably, patient-derived metastatic cells are more effective at forming mammospheres than cells isolated from primary tumors (146). In our mammosphere assays, we found that treatment with MN-anti-miR10b prevented MCF-7 cells from forming large spheroids, supporting similar studies that inhibited miR-10b by other means (53; 108). Of note, the reverse relationship wherein miR-10b increases spheroid size has also been observed (53). Phenotypic effects were also seen in MDA-MB-231 cells, though their analysis is limited by their poor mammosphere formation. This is believed to be only structural and not functional, as MDA-MB-231 cells grown in mammosphere medium display the same enhanced stem cell-like properties as other cancer cell lines when grown in mammosphere medium (119). Collectively, our results demonstrate that inhibition of miR-10b using MN-anti-miR10b decreases the stemness of breast cancer cells, supporting dedifferentiation as a mechanism through which the nanodrug may function as a therapy. In addition, these findings may be significant for synergizing anti-miR10b nanodrug with a standard of care in first-in-human clinical trials where testing it as a monotherapy is not likely. Finally, given the proven role played by miRNA-10b in other cancers beyond breast cancer, including lung, colorectal, gastric, bladder, pancreatic, ovarian, hepatocellular and brain cancer (147-149), these findings could have broad implications for the treatment of metastatic carcinoma in general.

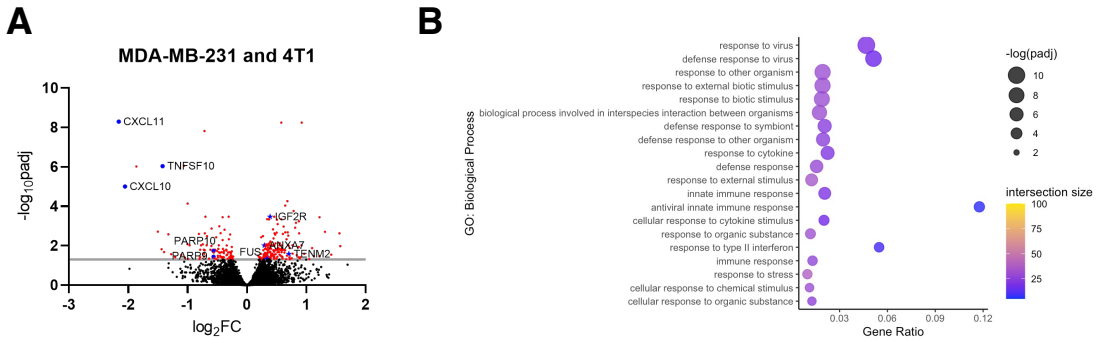


**Figure 2.6. Supplemental analyses of combined MDA-MB-231 and 4T1 datasets.**
(A) Volcano plot representing differential gene expression between MN-anti-miR10b and MN treatment for 48 hours, combined MDA-MB-231 and 4T1 datasets. Line indicates $p_{adj} = 0.05$. Red points indicate $p_{adj} < 0.05$. Blue points are notable genes, with titles. Blue stars are predicted targets of miR-10b, with titles.
(B) Top 20 most significant biological processes overrepresented by genes downregulated in MN-anti-miR10b-treated samples vs. MN-treated.

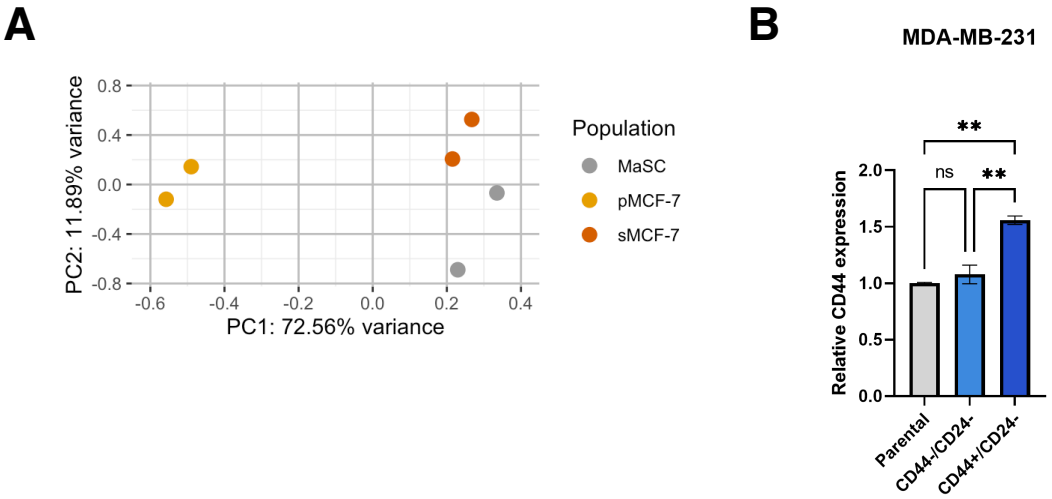


**Figure 2.7. Supplemental analyses of stem-like cell populations.**
(A) Principal component analysis of miRnomes of parental (p) and sorted (s) MCF-7 cells and mammary stem cells (MaSC).
(B) qPCR of CD44 for $CD44^{+}/CD24^{-}$,$CD44^{-}/CD24^{-}$, and parental MDA-MB-231 cells. Plot represents mean ± SEM. *$p < 0.05$, **$p < 0.01$.

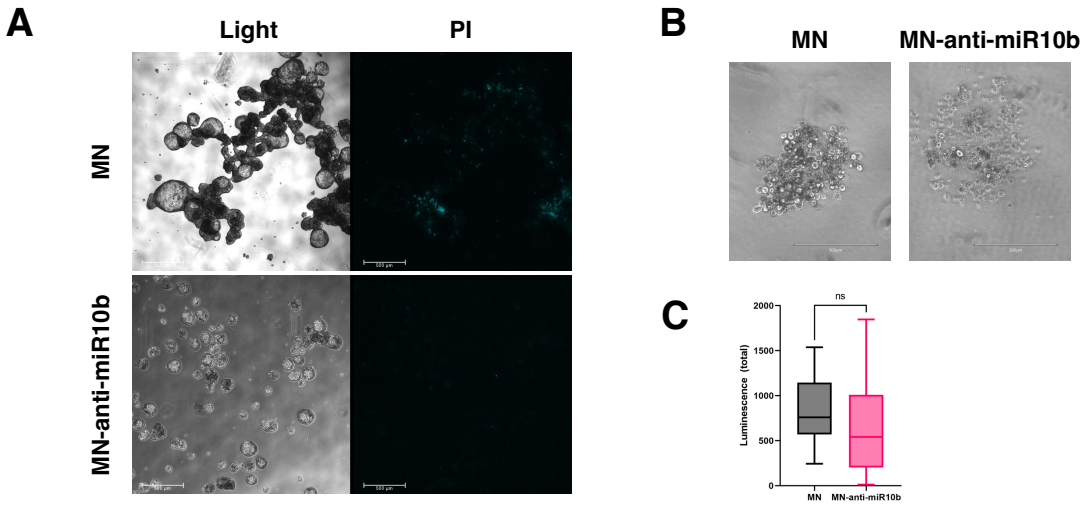


**Figure 2.8. Supplemental findings on the effects of MN-anti-miR10b on spheroid formation of breast cancer cells.**
(A) Light and fluorescence microscopy for PI (cyan) of MCF-7 cells treated with MN-anti-miR10b or MN 48 hours prior to (adherent conditions) and during culture in mammosphere medium.
(B) Mammosphere formation at Day 11 of MDA-MB-231 cells treated with MN-anti-miR10b or MN 48 hours prior to (adherent conditions) and during culture in mammosphere medium.
(C) Viability assay of MDA-MB-231 spheroids at Day 11 in treated medium. Plot represents mean ± max/min. ns = not significant.

## Methods

### *MN-anti-miR10b (nanodrug) synthesis and characterization*

The MN-anti-miR-10b was prepared following previously established protocol (55). Briefly, first the magnetic nanoparticle (MN) core was prepared by co-precipitation method and then it was aminated. The aminated MN have hydrodynamic diameter of 24.3 nm with 90 amines per MN particle. The aminated MN was then labeled with Cy5.5 near infrared optical dye by reacting with Cy5.5-NHS ester (Lumiprobe). For conjugation of MN-Cy5.5 with anti-miR-10b locked nucleic acid (LNA, Integrated DNA Technologies), MN-Cy5.5 was activated with heterobifunctional linker N-succinimidyl 3-[2-pyridyldithio]-propionate (SPDP; Thermo Fisher Scientific) and 5'-ThioMC6 end of the LNA was activated by treating with 3% TCEP. Finally,

SPDP conjugated MN-Cy5.5 was incubated with activated LNA to yield the MN-anti-miR-10b. The conjugation resulted in ~9 LNA oligo per MN particle.

***Cell culture***

MDA-MB-231 cells expressing luciferase (MDA-MB-231-luc-D3H2LN; Perkin Elmer) and MCF-7 cells (ATCC) were grown in DMEM supplemented with 10% FBS and antibiotics (100units/mL penicillin, 100mg/mL streptomycin). 4T1 cells expressing luciferase (4T1 Red F-luc; Perkin Elmer) were grown in DMEM supplemented with 5% FBS and antibiotics.

***Animal model, treatment, and in vivo and ex vivo imaging***

All procedures involving animal subjects have been approved by the Michigan State University Institutional Animal Care and Use Committee (IACUC) and conformed to all regulatory standards. Eight-week-old female nude mice (nu/nu; Jackson Laboratory, n=24) were orthotopically implanted with $2x10^6$ MDA-MB-231 human triple-negative breast cancer cells (50% PBS, 50% Matrigel) under the third mammary fat pad and monitored for metastasis formation using bioluminescence imaging (BLI), as described previously (55). With a focus on metastatic disease, primary tumors were resected when they began to compromise mouse mobility or became at risk of infection due to severe ulceration, as advised by veterinary staff.

Treatment with MN-anti-miR10b (10mg Fe/kg bodyweight) via tail vein injection was initiated when metastasis signal reached $1x10^5$ radiance (2cm x 2cm ROI). Mice were treated a single time with collection after 72 hours, or once per week for up to three weeks and collection one week after each last treatment (i.e., collected one week after one treatment, one week after two treatments and one week after three treatments). Metastatic tissue collection was guided by BLI and nanodrug delivery to the tissue was confirmed using fluorescence imaging in Cy5.5 channel. Tissues were then cryopreserved in OCT for processing.

***Fluorescence microscopy of metastatic tissue sections***

Tissues were cryosectioned at 10μm, fixed in 4% paraformaldehyde for 15 minutes, and mounted using DAPI Fluoromount-G (SouthernBiotech). Slides were imaged using channels for DAPI and Cy5.5 using a Nikon Eclipse 50i fluorescence microscope charge coupled device camera with near-IR sensitivity (SPOT 7.4 Slider RTKE), and SPOT 4.0 Advance version software (Diagnostic Instruments).

***RNA extraction and RT-qPCR***

RNA of tissues was extracted from ten 10μm sections by phenol-chloroform extraction (Qiagen) and further purified using the Zymo Quick-RNA 96 Kit. For *in vitro* samples, RNA was extracted and purified using only the Zymo Quick-RNA 96 kit. Reverse transcription and qPCR were performed using the mir-X miRNA First Strand Synthesis and RT-qPCR TB Green Kits (Takara Bio) for the analysis of miR-10b (TAC CCT GTA GAA CCG AAT TTG TG), U6 (reference gene for miRNAs, included in kit), PTEN (forward TCCTGGATGACCTTTGACATAC, reverse CCAACTTTGGTTTAATGCACAAC), HOXD10 (forward CGATTTATGCCTTGTAGCCTTTC, reverse GCATTATACATGCGACCAGAAC), and 18S (reference gene for mRNAs; forward CCAGTAAGTGCGGGTCATAAG, reverse GGCCTCACTAAACCATCCAA).

***Cell treatment***

Human triple-negative breast cancer cells MDA-MB-231, murine triple-negative breast cancer cells 4T1, and ER and PR-positive human breast cancer cells MCF-7 cells were plated in 6-well plates at an initial plating density of $1 \times 10^5$ cells/well and treated 24 hours later using MN-anti-miR10b or MN at 50μg Fe/mL (approximately 2.4nmol total oligomer), as used in previous *in vitro* studies (61). Cells were analyzed after 48 hours treatment.

***RNA sequencing and raw data processing***

RNA sequencing was performed by the Michigan State University Genomics Core. Sequencing libraries were prepared using the Illumina stranded mRNA library prep kit (Illumina) with IDT for Illumina RNA Unique Dual Index adapters following the manufacturer's recommendations, except that half-volume reactions were performed. Libraries were assessed for quantity and quality using a combination of Qubit dsDNA HS (Thermo Fisher Scientific) and Agilent 4200 TapeStation HS DNA1000 assays (Agilent). Libraries were pooled in equimolar amounts, and the pool was quantified using an Invitrogen Collibri quantification quantitative PCR kit (Invitrogen). The pooled library was loaded onto two lanes of a NovaSeq SP flow cell, and sequencing was performed in a 1 × 100-bp single-read format using a NovaSeq 6,000 v1.5 100-cycle reagent kit (Illumina). Base calling was performed with Illumina real-time analysis (version 3.4.4), and the output of real-time analysis was demultiplexed and converted to the FastQ format with Illumina Bcl2fastq (version 2.20.0).

RNA sequencing data analysis was supported through computational resources provided by the Institute for Cyber-Enabled Research at Michigan State University. FastQC (version 0.11.7) was used for pre-processing read quality assessment. Read mapping was performed against the GRCm39/mm39 mouse reference genome or the GRCh38 human reference genome, as appropriate, using Bowtie2 (version 2.4.1) with default settings. Read counts were quantified using the FeatureCounts function from the Subread package (version 2.0.0).

These data are publicly available in the Gene Expression Omnibus (GEO), Accession: GSE270229.

***Analysis of RNA sequencing counts files and figure generation***

Differential gene expression analysis was performed in R using the DESeq2 package (version 1.42.1) (150). Principal component analysis and visualization were performed in R using the ggplot2 package (version 3.5.1) (151). Volcano plots of the differentially expressed genes (DEGs) were produced using GraphPad Prism (version 9.5.0). Unsupervised hierarchical clustering was performed in the web-based Morpheus software interface by the Broad Institute (https://software.broadinstitute.org/morpheus/), using one minus Pearson correlation and average linkage. Functional enrichment analysis for overrepresented biological processes was performed using the web-based g:Profiler interface (https://biit.cs.ut.ee/gprofiler/gost) (152). Dot plots of overrepresented biological processes were produced using ggplot2. Venn diagrams of DEGs and overrepresented biological processes were produced using the VennDiagram package (version 1.7.3) (153).

***Public microarray datasets and analysis***

Gene expression profiles of U87 cells transduced with miR-10b binding sites are publicly available in the GEO under the accession number GSE35170 (107), and miRNA profiles of sorted MCF-7 and mammary stem cell populations are publicly available under the accession number GSE68271 (109; 113). Analysis of the datasets was performed in R using the limma package (version 3.58.1) (154). For the MCF-7 dataset, units were log2-transformed prior to analysis.

***Surface marker-based live cell sorting***

MDA-MB-231 cells were sorted using the MojoSort system, PE anti-human CD44 and APC anti-human CD24 antibodies, and MojoSort Human anti-PE and anti-APC nanobeads (BioLegend). Cells were first sorted for CD24, yielding $CD24^+$ and $CD24^-$ populations. This yielded relatively low numbers of $CD24^+$ cells; thus, they were not further processed or analyzed.

The $CD24^-$ population was subsequently sorted for CD44, yielding the $CD44^+/CD24^-$ and $CD44^-/CD24^-$ populations used in RT-qPCR analysis.

***Aldefluor assay***

Aldefluor assay was performed using the ALDEFLUOR kit (STEMCELL Technologies), with modifications to allow for microscopic analysis, as has been demonstrated previously (155). Cells were initially prepared according to manufacturer instructions, with cell concentrations of $1.5x10^6$ cells/mL for MDA-MB-231 cells and $5x10^5$ cells/mL for MCF-7 cells, using activated reagent at a concentration of 5µL reagent/1mL cells, and incubating for 30 minutes. Cells were then pelleted at 300xG for 5 minutes. The supernatant was aspirated, and the pellet was resuspended in 50µL of Aldefluor buffer. Ten microliters of cell suspension was transferred onto a microscope slide, coverslipped, and imaged using Phase contrast and the GFP light cube on the EVOS M5000 microscope. Fluorescence intensity of cells was analyzed using Fiji/ImageJ. Briefly, the Phase image was converted into regions of interest (ROI) approximating individual cells using the Hough Circle Transform plugin (UCB Vision Sciences). These ROIs were then applied to the corresponding GFP images and measured for mean gray value.

***Spheroid formation, viability, and propidium iodide staining***

MDA-MB-231 and MCF-7 cells were treated with MN-anti-miR10b or MN for 48 hours under standard, adherent conditions before being transferred to treated 3D Tumorsphere Medium XF (PromoCell) and ultra-low attachment plates (Corning). Spheroid growth over time was imaged using the EVOS M5000 microscope. Spheroid surface areas and number of spheroids were measured using ImageJ. Viability assays were performed using CellTiter-Glo (Promega), as it is lytic and best suited for analysis of spheroids (156), measuring total luminescence. Propidium iodide (PI; Thermo Fisher Scientific) staining was performed by adding PI at a final concentration

of 5ng/mL directly to the spheroids in tumorsphere medium 24 hours prior to imaging. Images were taken using the Leica Thunder Imager.

***Statistical analysis***

RNA sequencing and microarray data differential gene expression analyses were performed using DESeq2 and limma, as described in the corresponding sections. A simple linear regression was used to analyze time-course data. For all other applications, analysis between experimental and control groups were analyzed using a two-tailed t-test. $p < 0.05$ was interpreted as statistically significant.

**Supplementary results and discussion (not published)**

***Effects of miR-10b inhibition by MN-anti-miR10b are not reflected in predicted targets***

Here, I sought to evaluate how effectively miRNA target prediction tools could determine the transcription-level effects of miR-10b inhibition using MN-anti-miR10b. With consideration of the variability in target transcript expression level between different cell lines, I performed hierarchical clustering of the normalized, batch-corrected counts in the MDA-MB-231 dataset and included only predicted targets expressed with a Reads Per Kilobase transcript per Million mapped reads (RPKM) > 1 in the cell line, per miRDB. (miRDB does not have expression levels for 4T1 cells.) As seen in previous analyses, MN-anti-miR10b-treated samples clustered together and separate from control samples (NTC and MN); however, the trends in expression among predicted targets was not consistent, with only 47 of 223 predicted targets showing the expected upregulation in samples treated with MN-anti-miR10b relative to control samples (**Figure 2.9**, top-most dendrogram). While the exact reasons for this are unclear, it is not unsurprising for several reasons.

First, miRNAs function as inhibitors of translation more so than transcription. As such, the effects of miRNAs are believed to be best seen at the protein level. HOXD10 was one of the first

reported targets of miR-10b. It was experimentally validated as a target using a luciferase reporter on its 3' untranslated region and continues to be one of the most used indicators of successful miR-10b modulation; however, the effects of miR-10b overexpression on HOXD10 cannot be observed at the transcriptional level (38). The determinants of whether target mRNAs are degraded or only prevented from being translated are the subject of ongoing research (19; 24-28), but it is plausible that transcriptional analyses are not the best way to gauge successful miRNA modulation.

Second, with reports that individual miRNAs exert only "relatively mild" but potentially hundreds of effects at the protein level (10), it is difficult to predict the extent of target mRNA upregulation that should be expected upon miR-10b inhibition. Indeed, in the MDA-MB-231 dataset, the greatest degree of significant upregulation was a 4.89-fold increase in the PDGFB gene, and only 20 other genes were significantly upregulated more than 2-fold. This is further compounded by the role of miRNAs as quick responders to cellular changes (157), with recent findings that miRNAs function in as little as 30 minutes after export into the cytoplasm (158). As the cells in our dataset were treated for 48 hours prior to analysis, it is almost certain that the transcriptomic state of the cells includes compensatory changes to miR-10b inhibition.

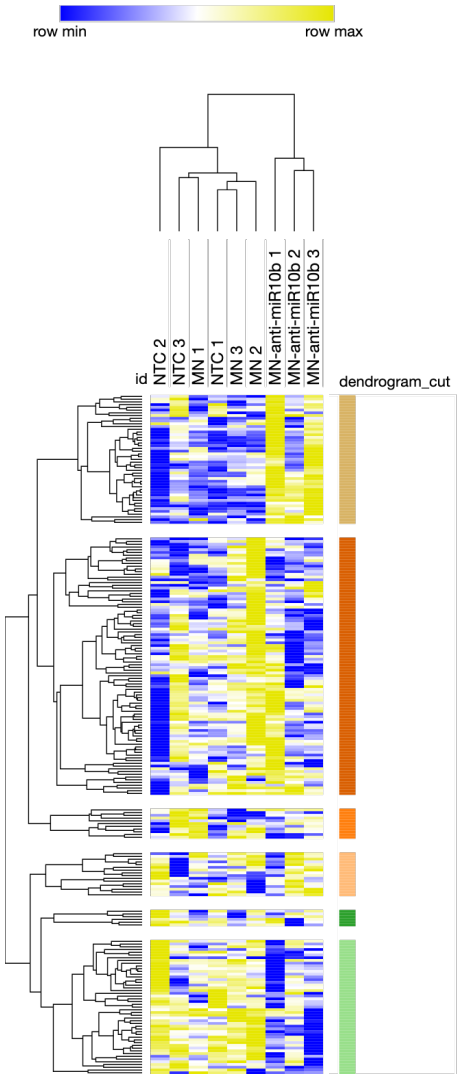


**Figure 2.9. Heatmap of predicted miR-10b targets in MDA-MB-231 dataset.** Included targets are those reported to be expressed in MDA-MB-231 cells, per miRDB.

Lastly, miRNA target prediction includes numerous factors beyond base complementarity in the 3' untranslated region, including thermodynamics (31) and whether predicted targets are expressed at the same time as the miRNA(30). miRDB functions as a tool for target prediction, but tools of this nature are meant to guide hypotheses and necessitate experimental validation. For

these reasons, predicted targets are an imperfect measure of efficacy in evaluating miR-10b inhibition by MN-anti-miR10b.

***MiR-10b inhibition upregulates genes associated with the p53 pathway***

A limitation of our published results is the use of gene ontology to identify biological processes affected by MN-anti-miR10b, or more specifically the anti-miR-10b ASO, since comparisons were performed against MN (vehicle)-treated controls. While this level of analysis led to our secondary hypothesis that inhibition of miR-10b inhibits the stem-like properties of breast cancer cells, which was supported by subsequent experiments, it did not establish the signaling pathway(s) affected to elicit this response. Determining these may further establish clinical indications for the use of MN-anti-miR10b, synergistic therapeutics, or adverse effects to be wary of.

To begin to address this limitation, I reanalyzed the RNA sequencing datasets using gene set enrichment analysis (GSEA) (159; 160) for hallmark gene sets. For consistency with the previous analyses, I used preranked GSEA using the differential gene expression results generated with DESeq2, sorted by "stat" (Wald statistic) as a metric that factors fold change, direction of change, and standard error. I began with the DESeq2 output from analyzing the MDA-MB-231 and 4T1 datasets together and found that 26 of 49 gene sets were enriched in the MN-anti-miR10b-treated cells (relative to MN-treated cells) with a false discovery rate (FDR) < 25% (the recommended parameters for discovery purposes), including gene sets associated with the Wnt/β-catenin, TGF-β, KRAS, Hedgehog, mTOR, and p53 pathways, all of which were also enriched with FDR < 25% when performing preranked GSEA on the DESeq2 output from analysis of MDA-MB-231 datasets alone (**Figure 2.10**, **Table 1**).

**A.**

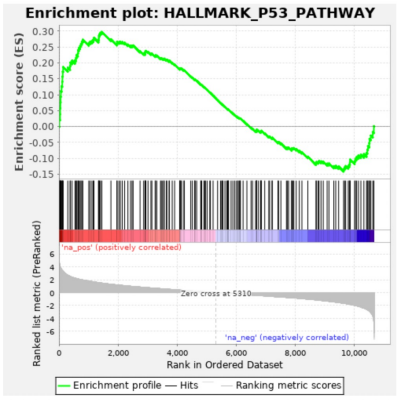


*Table: GSEA Results Summary*

| | |
|---|---|
| Dataset | ranked stat |
| Phenotype | NoPhenotypeAvailable |
| Upregulated in class | na_pos |
| GeneSet | HALLMARK_P53_PATHWAY |
| Enrichment Score (ES) | 0.2974599 |
| Normalized Enrichment Score (NES) | 1.4037728 |
| Nominal p-value | 0.019704433 |
| FDR q-value | 0.05181292 |
| FWER p-Value | 0.588 |

**B.**

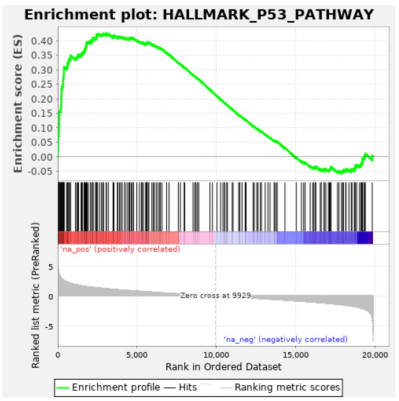


*Table: GSEA Results Summary*

| | |
|---|---|
| Dataset | ranked stat |
| Phenotype | NoPhenotypeAvailable |
| Upregulated in class | na_pos |
| GeneSet | HALLMARK_P53_PATHWAY |
| Enrichment Score (ES) | 0.42510188 |
| Normalized Enrichment Score (NES) | 2.0675392 |
| Nominal p-value | 0.0 |
| FDR q-value | 2.009804E-4 |
| FWER p-Value | 0.001 |

**Figure 2.10. Genes associated with the p53 pathway are significantly enriched upon miR-10b inhibition by MN-anti-miR10b.** Gene set enrichment plots for the p53 pathway gene set following treatment with MN-anti-miR10b relative to treatment with MN in (A) combined MDA-MB-231 and 4T1 analysis and (B) analysis of MDA-MB-231 cells alone.

Of the enriched pathways, I chose to validate enrichment of genes associated with the p53 pathway due to it having the greatest normalized enrichment score (NES) in the MDA-MB-231 analysis. Several recent reports implicate p53 in cell differentiation, both in the contexts of normal stem cells (161; 162) and stem-like cancer cells (163-165). A p53 response element has been reported in the miR-10b promoter (166), providing a direct link between p53 and miR-10b. Furthermore, an antagonistic relationship between miR-10b and p53 has been reported in the setting of drug resistance in lung cancer, supporting the enrichment of p53-associated genes by miR-10b inhibition (167).

I generated new samples of MDA-MB-231 cells treated with MN-anti-miR10b or MN (50μg Fe/mL) for 48 hours and analyzed them using RT-qPCR, as described in the publication, for

miR-10b and four core enrichment genes: KLF4, VDR, JUN, and TGFB1. (Notably, the batches of MN-anti-miR10b and MN were different from the batches used to generate the samples that were sequenced.) As seen with the RNA sequencing results, treatment with MN-anti-miR10b led to upregulation of all four p53-associated genes relative to treatment with MN (**Figure 2.11A, B**), further supporting activation of the p53 signaling pathway as a possible driver of the reduced stemness seen following miR-10b suppression.

Across all subtypes of breast cancer, mutant p53 is associated with the worst prognoses (168). Notably, the frequency of mutation increases with tumor progression and metastasis (169), and a staggering 80% of triple-negative breast cancer cases have inactive p53 (170). Going forward, it will be important to further investigate the suppression of miR-10b as a method for therapeutic reactivation of p53 signaling in breast cancer, with the high likelihood of applicability to other cancers given the prevalence of p53 mutations pan-cancer.

***MiR-10b inhibition downregulates LGR5***

Another gene of interest from our RNA sequencing results is LGR5. LGR5 is a bona fide marker of adult stem cells in the gut. LGR5-positive cells reside in intestinal crypts and lose LGR5 expression as they differentiate into goblet, Paneth, and enteroendocrine cells (171). Since this discovery, LGR5 has been implicated in oncogenesis in several cancers, particularly colorectal, and its utility as a stem cell marker has led to several connections between it and stem-like cancer cells (172; 173).

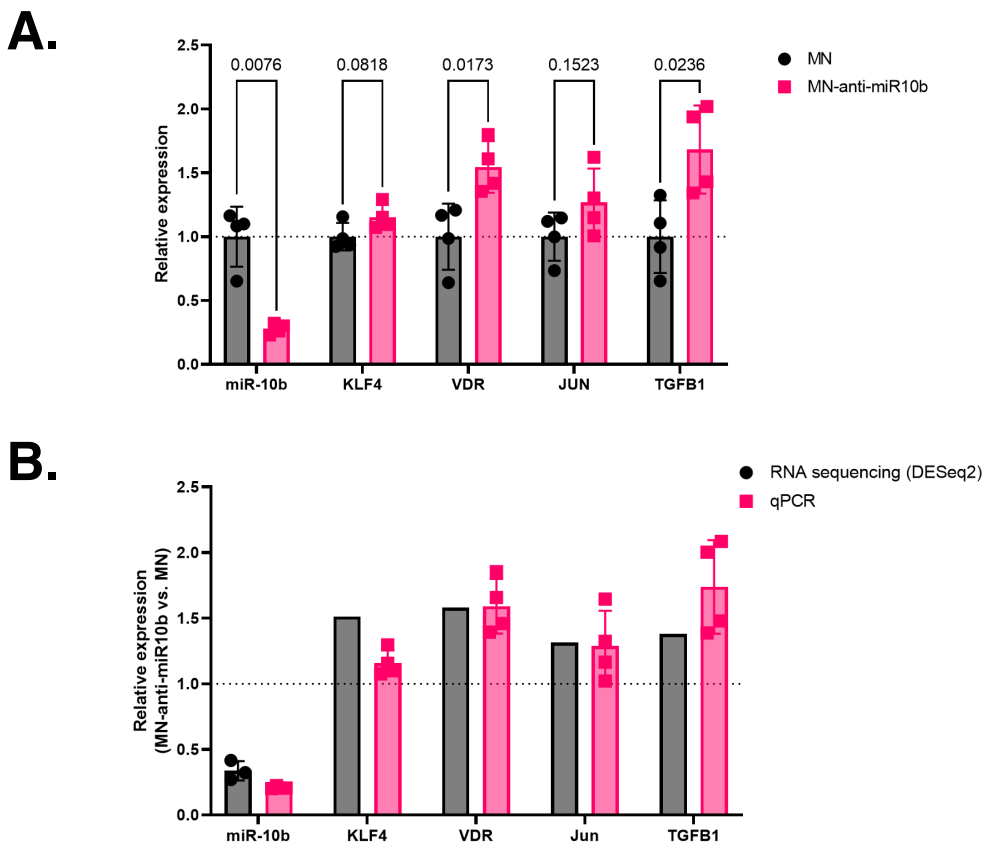


**Figure 2.11. RT-qPCR validates upregulation of p53-associated genes upon miR-10b inhibition by MN-anti-miR10b.**
(A) Normalized RT-qPCR results for miR-10b and p53 pathway-associated genes in MDA-MB-231 cells treated with MN-anti-miR10b or MN. (B) Comparison of fold change (MN-anti-miR10b versus MN) seen with RT-qPCR versus RNA sequencing, where the dashed line represents expression in MN-treated samples from the respective experiments. RT-qPCR data are represented as mean ± SEM. Error bars are not shown for RNA sequencing results because the makers of DESeq2 advise against un-transforming the lfcSE error output (https://support.bioconductor.org/p/93559/).

| NAME | SIZE | ES | NES | NOM p-val | FDR q-val | FWER p-val | RANK AT MAX | LEADING EDGE |
|---|---|---|---|---|---|---|---|---|
| HALLMARK_EPITHELIAL_MESENCHYMAL_TRANSITION | 174 | 0.500 | 2.386 | 0.000 | 0.000 | 0.000 | 2047 | tags=36%, list=10%, signal=40% |
| HALLMARK_APICAL_JUNCTION | 170 | 0.490 | 2.338 | 0.000 | 0.000 | 0.000 | 4896 | tags=53%, list=25%, signal=70% |
| HALLMARK_MYOGENESIS | 151 | 0.499 | 2.320 | 0.000 | 0.000 | 0.000 | 4328 | tags=47%, list=22%, signal=60% |
| HALLMARK_CHOLESTEROL_HOMEOSTASIS | 69 | 0.530 | 2.194 | 0.000 | 0.000 | 0.000 | 3391 | tags=48%, list=17%, signal=57% |
| HALLMARK_ESTROGEN_RESPONSE_EARLY | 187 | 0.435 | 2.113 | 0.000 | 0.000 | 0.000 | 3652 | tags=39%, list=18%, signal=47% |
| HALLMARK_P53_PATHWAY | 187 | 0.425 | 2.068 | 0.000 | 0.000 | 0.001 | 3067 | tags=34%, list=15%, signal=40% |
| HALLMARK_WNT_BETA_CATENIN_SIGNALING | 39 | 0.563 | 2.054 | 0.000 | 0.000 | 0.001 | 4139 | tags=51%, list=21%, signal=65% |
| HALLMARK_TGF_BETA_SIGNALING | 53 | 0.519 | 2.027 | 0.000 | 0.000 | 0.001 | 3187 | tags=43%, list=16%, signal=52% |
| HALLMARK_HYPOXIA | 182 | 0.386 | 1.853 | 0.000 | 0.002 | 0.011 | 3534 | tags=38%, list=18%, signal=46% |
| HALLMARK_COAGULATION | 98 | 0.422 | 1.839 | 0.000 | 0.002 | 0.011 | 3411 | tags=37%, list=17%, signal=44% |
| HALLMARK_MTORC1_SIGNALING | 197 | 0.372 | 1.813 | 0.000 | 0.002 | 0.012 | 3360 | tags=32%, list=17%, signal=38% |
| HALLMARK_MYC_TARGETS_V2 | 58 | 0.454 | 1.811 | 0.002 | 0.001 | 0.012 | 5971 | tags=59%, list=30%, signal=84% |
| HALLMARK_HEDGEHOG_SIGNALING | 32 | 0.510 | 1.792 | 0.002 | 0.002 | 0.016 | 3523 | tags=50%, list=18%, signal=61% |
| HALLMARK_ANDROGEN_RESPONSE | 97 | 0.388 | 1.670 | 0.002 | 0.006 | 0.055 | 3860 | tags=41%, list=19%, signal=51% |
| HALLMARK_UNFOLDED_PROTEIN_RESPONSE | 109 | 0.370 | 1.648 | 0.000 | 0.007 | 0.071 | 3050 | tags=31%, list=15%, signal=37% |
| HALLMARK_ESTROGEN_RESPONSE_LATE | 180 | 0.344 | 1.635 | 0.000 | 0.007 | 0.076 | 3765 | tags=33%, list=19%, signal=40% |
| HALLMARK_KRAS_SIGNALING_UP | 166 | 0.339 | 1.610 | 0.000 | 0.008 | 0.095 | 3841 | tags=36%, list=19%, signal=44% |
| HALLMARK_UV_RESPONSE_DN | 142 | 0.351 | 1.608 | 0.003 | 0.008 | 0.095 | 3587 | tags=32%, list=18%, signal=38% |
| HALLMARK_APOPTOSIS | 145 | 0.341 | 1.567 | 0.000 | 0.011 | 0.142 | 3549 | tags=33%, list=18%, signal=40% |
| HALLMARK_TNFA_SIGNALING_VIA_NFKB | 188 | 0.321 | 1.539 | 0.003 | 0.015 | 0.200 | 2066 | tags=24%, list=10%, signal=26% |

**Table 1.** Top 20 enriched hallmarks in MDA-MB-231 cells treated with MN-anti-miR10b, relative to cells treated with MN, as ranked by normalized enrichment score (NES)

In the context of the breast and breast cancer, LGR5 expression has been observed in fetal mammary stem cells, adult regenerative tissues post-injury, and in rare cases of triple-negative breast cancer (174; 175). In the rare cases of breast cancer, LGR5 is associated with worse histological and tumor grades. These reports make the downregulation of LGR5 in our RNA sequencing experiments particularly interesting, as it positions LGR5 as a possible mediator of the stem-like features characterized in our *in vitro* experiments. Transcriptomic analysis of MDA-MB-231 cells treated with MN-anti-miR10b showed over 51% downregulation in LGR5 expression relative to cells treated with MN ($p_{adj} = 0.0014$), and this downregulation was validated by RT-qPCR in both sequenced and newly generated samples. Notably, MDA-MB-231 cells are a model for triple-negative breast cancer. In the U87 glioblastoma dataset, a probe corresponding to LGR5 also indicated greater than 84% downregulation in the cell line in response to miR-10b inhibition ($p = 0.042$). Interestingly, although LGR5 is encoded in the mouse genome, no transcripts were detected in our 4T1 dataset, making the applicability of these findings to mouse models unclear.

As a translational repressor, inhibition of miR-10b is expected to result in the upregulation of miR-10b targets. The finding that LGR5 is downregulated in response to miR-10b inhibition indicates that there are intermediate processes that result in LGR5 downregulation. In the future, it will be useful to investigate upregulated genes or pathways in our datasets that are known to induce or may result in LGR5 downregulation to establish a miR-10b-LGR5 axis that could explain the downstream effects of MN-anti-miR10b.

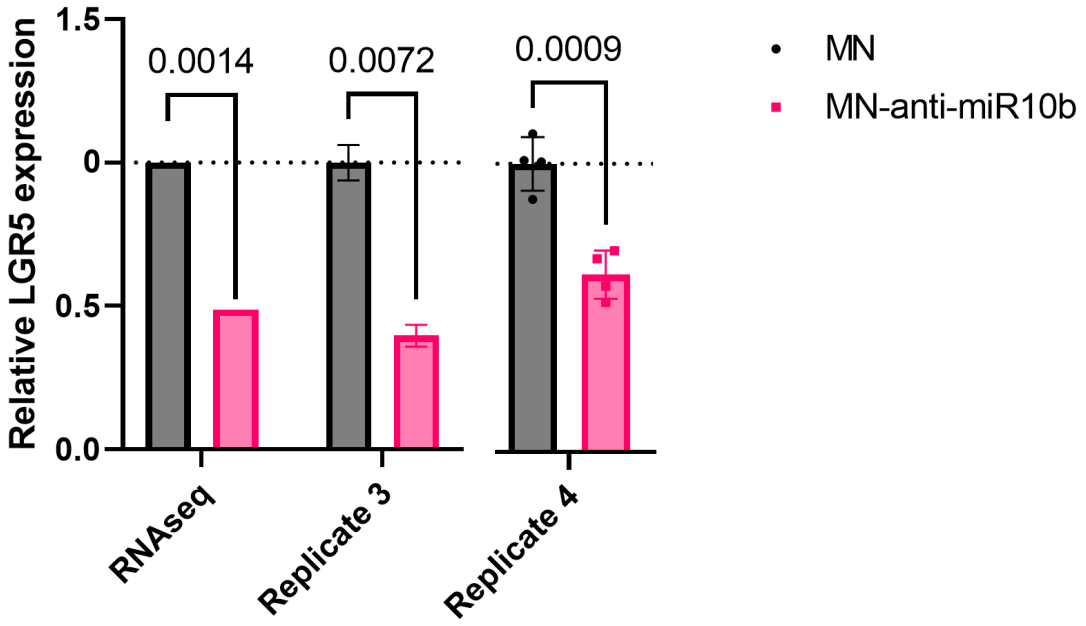


**Figure 2.12. LGR5 is significantly downregulated upon miR-10b inhibition by MN-anti-miR10b.**
Relative LGR5 expression in MDA-MB-231 cells treated with MN-anti-miR10b or MN.
Left: Fold change results per RNA sequencing of 3 biological replicates (Replicates 1-3). p-value is from DESeq2 analysis. Error bars are not shown for RNA sequencing results because the makers of DESeq2 advise against un-transforming the lfcSE error output (https://support.bioconductor.org/p/93559/).
Middle: Validation of RNA sequencing results using RT-qPCR of samples from Replicate 3. Error bars represent Expression SEM of technical replicates, per CFX Maestro software (Bio-Rad). p-value is from analysis of RT-qPCR technical replicates. Replicates 1 and 2 were not analyzed due to lack of RNA availability. MiR-10b expression can be seen in Figure 2.2A.
Right: Validation of RNA sequencing results using RT-qPCR of 4 newly generated samples. MiR-10b expression can be seen in Figure 2.11. Error bars represent SEM across samples. p-value is from analysis across samples.

***MiR-10b inhibition does not affect CD44 expression over time***

Having observed that MDA-MB-231 cells sorted for the stem-associated $CD44^+/CD24^-$ surface marker phenotype have over 2-fold increased miR-10b expression than $CD44^-/CD24^-$ cells, we sought to determine whether miR-10b inhibition decreases CD44 protein expression. We treated MDA-MB-231 cells with MN-anti-miR10b or MN conjugated to scrambled control oligonucleotides (50μg Fe/mL), or PBS and analyzed total CD44 fluorescence intensity relative to number of cell nuclei (DAPI stain) following incubation with anti-CD44 antibodies conjugated to AlexaFluor-488 fluorophore. Representative results from one of three repeats of the experiment are shown in **Figure 2.13**. We find that neither CD44 expression per cell nor change in expression over time is significantly different in cells treated with MN-anti-miR10b than with MN-scr.

A limitation of our experiment is the use of immunocytochemistry and, as a result, the use of average fluorescence intensity as a metric to answer our research question. This was done due to a limitation of resources. For the purposes of identifying stem-like populations, CD44 is generally used in sorting-based experiments. Performing analyses on average CD44 expression does not capture the heterogeneity between stem-like and non-stem-like populations, and it is possible that analysis using sorting methods to quantitate percent of stem-like vs. non-stem-like cells would reveal more striking differences between the treatment groups. Indeed, Ahir et al. (2020) performed a similar experiment and treated MDA-MB-231 cells with nanoparticle-delivered anti-miR10b ASOs and found approximately 30% $CD44^+/CD24^-$ cells in the population, down from 54.1% in control samples (90). Another consideration with these studies is the biochemical relationship between miR-10b and CD44. Bourgignon et al. (2012) performed several experiments to elucidate the signaling pathways that connect the two. Using matrix hyaluronan to activate CD44 signaling, they established that CD44 is an upstream activator of Twist, and thus,

of miR-10b (176). These results suggest that miR-10b inhibition may not have a direct effect on CD44 expression, barring feedback mechanisms, supporting the use of other methods to characterize induced effects on stemness.

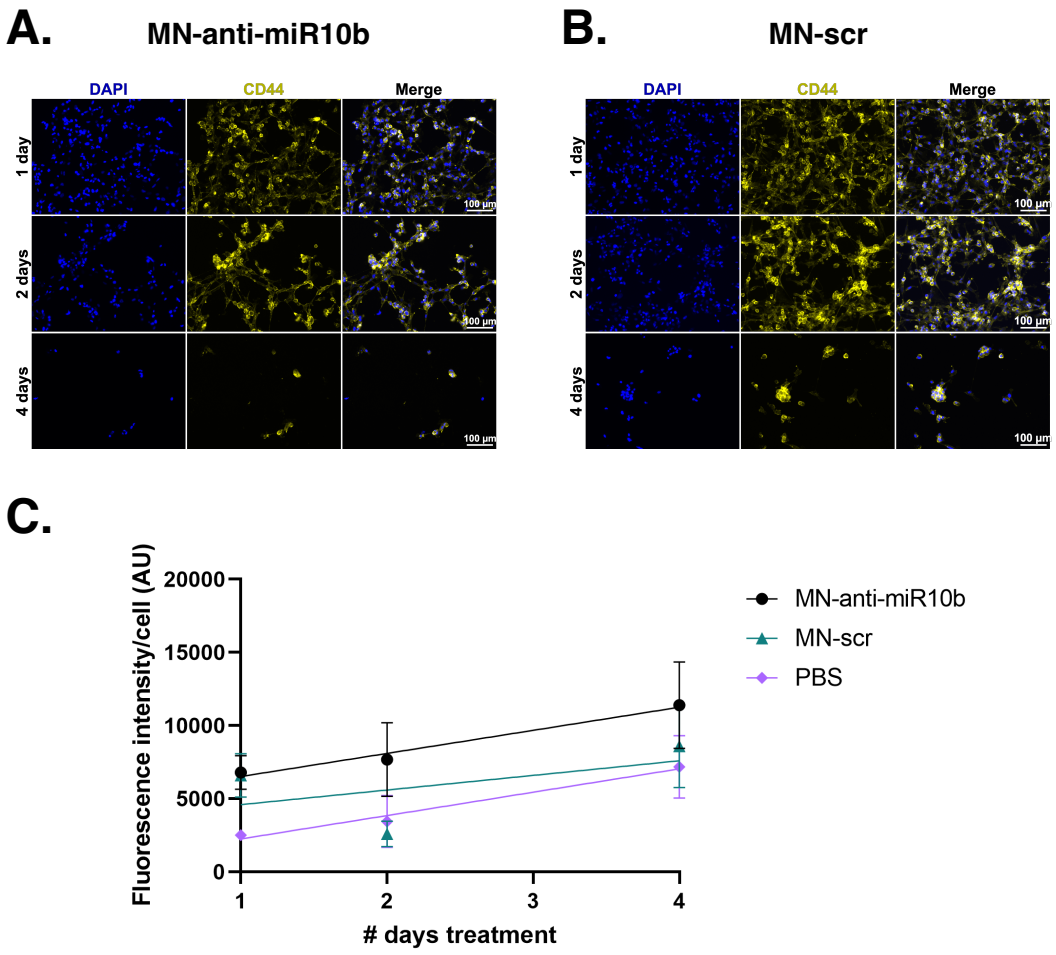


**Figure 2.13. Inhibition of miR-10b by MN-anti-miR10b does not affect average CD44 expression.** Representative immunocytochemistry of MDA-MB-231 cells treated with (A) MN-anti-miR10b or (B) MN conjugated to a scrambled control oligonucleotide (MN-scr). (C) Quantitation of total CD44 fluorescence (yellow) relative to number of cell nuclei (DAPI, blue). Error bars represent SEM across four random fields of view.

# CHAPTER 4: MICRORNA-10B AS A THERAPEUTIC TARGET IN FELINE METASTATIC MAMMARY CARCINOMA AND ITS IMPLICATIONS FOR HUMAN CLINICAL TRIALS

## Preface

This chapter is adapted from a manuscript previously published as

> Savan NA, Saavedra PV, **Halim A**, Yuzbasiyan-Gurkan V, Wang P, Yoo B, Kiupel M, Sempere L, Medarova Z, Moore A. Case report: MicroRNA-10b as a therapeutic target in feline metastatic mammary carcinoma and its implications for human clinical trials. Front Oncol. 2022 Oct 26;12:959630. doi: 10.3389/fonc.2022.959630. PMID: 36387245; PMCID: PMC9643803.

on which I am a co-author. The extension of MN-anti-miR10b to a large animal model of metastatic breast cancer offers the potential of gaining new insights into the efficacy of the therapeutic that may apply to its use in humans, bringing the therapeutic one step closer to its translation to the clinic. Here, I summarize the findings of the publication with a focus on and excerpts related to my specific contributions to the study, with additional discussion.

## Contributions to Science

Within the publication, my primary contribution was providing instruction and guidance to N. Anna Savan in performing and analyzing RT-qPCR and generation of the associated final figures. I also contributed to writing and editing.

The publication describes the first of several companion cats to be treated with the therapeutic described in the previous chapters, MN-anti-miR10b. Candidate companion cats with

metastatic disease continue to be recruited for MN-anti-miR10b efficacy studies. I am actively involved in screening potential candidates for eligibility (i.e., sufficient miR-10b expression in their lesions). When these ongoing studies are completed, I will contribute to writing and be credited as an author on the manuscript.

**Simple Summary**

Companion cats are considered by many to be the best large animal model for human breast cancer. With the goal of translation of MN-anti-miR10b to the clinic, it is valuable to demonstrate therapeutic efficacy in companion cats with metastatic breast cancer. Here, I present excerpts from our publication showing evidence of miR-10b inhibition in the first of many companion cats that will be receiving MN-anti-miR10b, and I discuss the implications and ongoing work with the project.

**Ethics Statement**

The animal study was reviewed and approved by Institutional Animal Care and Use Committee of Michigan State University. Written informed consent was obtained from the owners for the participation of their animals in this study.

**Acknowledgments**

This work was supported in part by R21CA226579 and R01CA258314 to LS and 1R01CA261691 to AM.

**Disclosures**

ZM and AM are scientific founders and shareholders at TransCode Therapeutics Inc.

**Companion cats as candidates for treatment with MN-anti-miR10b**

Support for the use of spontaneous breast cancer in domestic cats as a large animal model for human breast cancer has only grown since its proposal in 1994 (177-179). In addition to

offering many of the benefits of small animal models, such as an immune system and shorter time to maturation, companion cats are exposed to similar environmental risk factors as humans, prompting them to be described by some as "sentinels" of human health (180). At the microscopic level, feline mammary carcinomas (FMC) can be classified similarly to human breast cancer into luminal A and B, HER2-overexpressing, and triple-negative subtypes based on the expression of hormone receptors and HER2; and as with human breast cancer, HER2-overexpressing and triple-negative, basal-like cases demonstrate the greatest aggression and carry the worst prognoses (181; 182). FMC have also been reported to undergo changes characteristic of an epithelial-mesenchymal transition (EMT), such as decreases in E-cadherin and increases in vimentin and N-cadherin (183; 184), and the vast majority (80-90%) of FMC ultimately become aggressive, with signs of invasion and metastasis (184), all of which have strong ties to miR-10b. Altogether, with the objective of translation to the clinic, these features made companion cats with metastatic breast cancer a compelling large animal candidate for treatment with MN-anti-miR10b.

Prior to embarking on feline studies, it was important to establish that FMC are a good model for human breast cancer in the context of miR-10b expression and function. The following excerpt from Savan et al. (2022) (86), with adapted figures, describes some of the findings I helped make toward this end:

> We found that in 55.5% of the tumors, miR-10b expression in lymph node metastases was significantly higher than that in primary tumors with 60% of them being HER2+ (**Figure 3.1A**). In these tumors miR-10b expression was on average 37.7 ± 7.4% of that in lymph node metastases, which was in agreement with our results in murine metastatic breast cancer models (55).

To further investigate miR-10b expression, we performed qRT-PCR for HOXD10 [mRNA], an established miR-10b direct target, in those paired samples where miR-10b was overexpressed in metastases compared to primary tumors. As shown in **Figure 3.1B**, the expression of HOXD10 mRNA was significantly lower in lymph node metastases than in primary tumors.

Additionally, immunohistochemistry revealed decreased HOXD10 protein expression in lymph node metastases relative to primary tumors, and *in situ* hybridization revealed increased miR-10b expression at the invasive front and vasculature of primary tumors. These trends in miR-10b and HOXD10 expression mirrored those observed in human breast cancer patients and our previous studies in murine models of breast cancer, supporting the use of MN-anti-miR10b in the treatment of FMC. (86)

**Investigation of MN-anti-miR10b in a patient with feline mammary carcinoma**

The first feline to receive treatment with MN-anti-miR10b was a companion cat, deidentified as Cat 0, with advanced stage HER2+ breast cancer, as seen in both the primary tumor and abdominal metastases. Cat 0 was determined to be an excellent candidate for MN-anti-miR10b due to both the severity of her disease and her marked upregulation of miR-10b in her primary tumor and lymph node metastases relative to other cats (**Figure 3.1A**). As the first study of its kind, Cat 0 was evaluated for drug accumulation in metastatic tissues, drug tolerability and safety, and evidence of drug activity. This occurred over the course of two doses (2.5mg Fe/kg bodyweight; 1.4mg oligo/kg bodyweight) spaced 51 days apart, with final assessment and sample collection taking place 91 days after the second dose. Briefly, MN-anti-miR10b was observed in metastatic tissues 24 hours after the administration of the first dose. No changes in behavior were

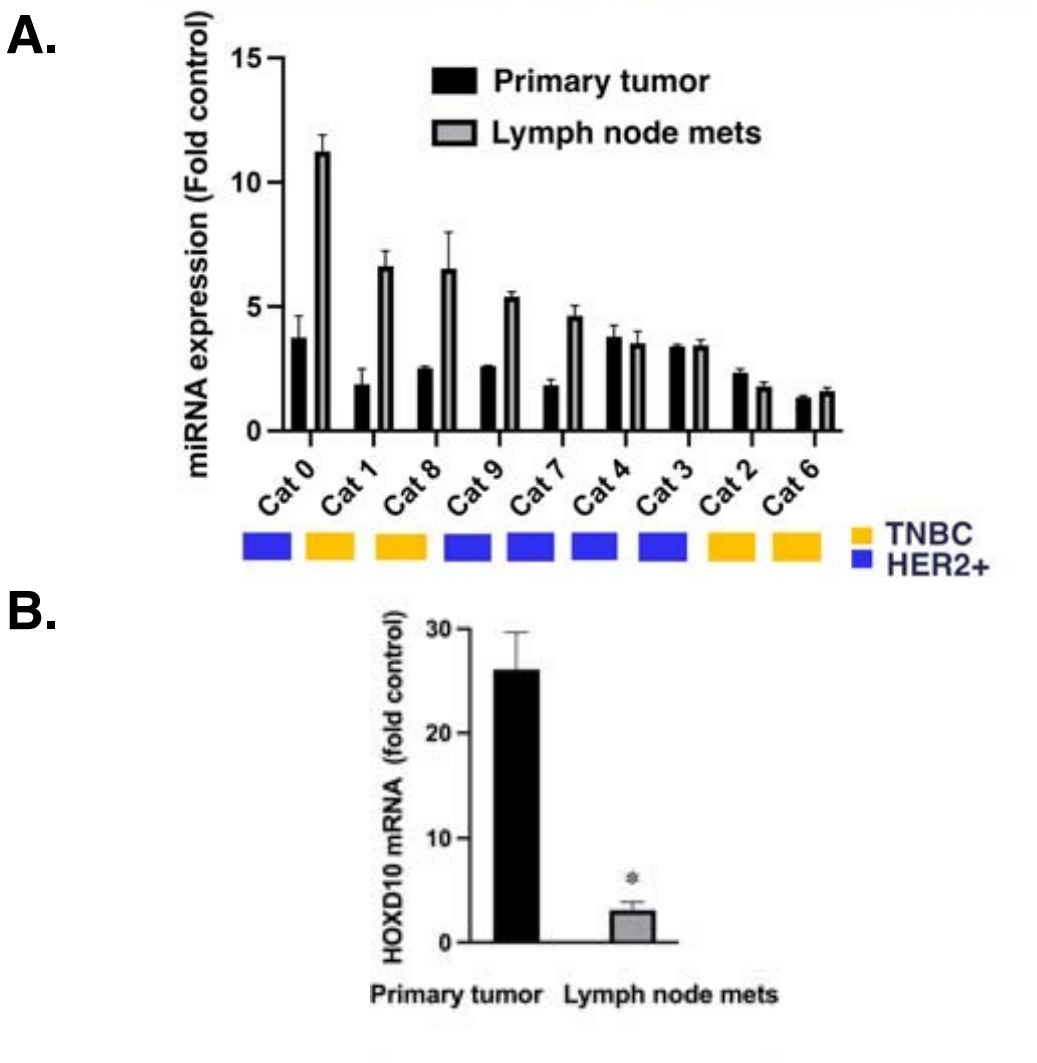


**Figure 3.1. MiR-10b expression patterns in feline mammary carcinomas resemble those in human breast cancer.**
(A) MiR-10b expression in primary tumors and lymph node metastases in feline patients. Molecular subtypes are indicated by the color legend. In 55.5% of the tumors miR-10b expression in lymph node metastases was significantly higher than in primary tumors with 60% of them being HER2+ ($n = 3$, $p < 0.05$). (B) qRT-PCR analysis of HOXD10 expression in primary tumors and lymph node metastases in spontaneous mammary carcinoma in cats. Data from cats 0, 1, 8, 9 and 7 are shown. HOXD10 expression was significantly higher in the primary tumors than in the metastases ($n = 3$, $p < 0.01$). Data are represented as mean ± s.d.

observed, and complete blood count (CBC) and serum chemistry profiles revealed only mild or transient changes over the course of the study until two weeks prior to euthanasia. Notably, Cat 0 had gained weight when measured seven weeks after the first dose and weight was stable for two months after the second dose. The conclusion of the study and the effects on miR-10b are described in this excerpt from Savan et al. (2022):

> This case of FMC was at an advanced clinical stage. Three months (13 weeks) after the second dose of MN-anti-miR10b, the animal was euthanized due to continuing metastatic growth, renal failure based on urinalysis (high RBC count, not shown), and decreased quality of life. We performed qRT-PCR of multiple metastatic lesions collected at necropsy and found that miR-10b expression was significantly decreased in lung metastases (by ~86.6%) and metastases in the abdominal area (by ~81.6%) compared to that in the lymph node metastases removed during the original surgery (**Figure 3.2**).

Furthermore, in the final collected metastatic tissues, HOXD10 protein expression was significantly increased relative to samples pre-treatment, and MN-anti-miR10b in the tissues was seen on fluorescence imaging three months after the last dose.

**Discussion**

The implications of the findings in Cat 0 are described in this excerpt from Savan et al. (2022):

> The case study with our first-in-class miRNA targeted therapeutic presented here demonstrated its delivery to metastatic lesions using MRI, which is an important step in

preclinical development of our approach. Initial safety studies demonstrated good tolerability and the general lack of toxicity of the therapeutic, which serves as another important milestone in its translation. Furthermore, we obtained proof of target engagement by MN-anti-miR10b, manifested as a significant decrease in miR-10b expression after two injections 7 weeks apart. It is important to note that efficacy studies were not part of this investigation, and the dose of the therapeutic used here was lower than the animal equivalent dose (AED) calculated based on the effective dose determined in our previous rodent studies. However, even at this reduced dose and suboptimal schedule, we achieved a significant inhibition of the miR-10b target with no toxicity. Although euthanasia was performed due to disease progression and deteriorated health, the patient survived for five additional months compared to the animal's life expectancy prior to dosing.

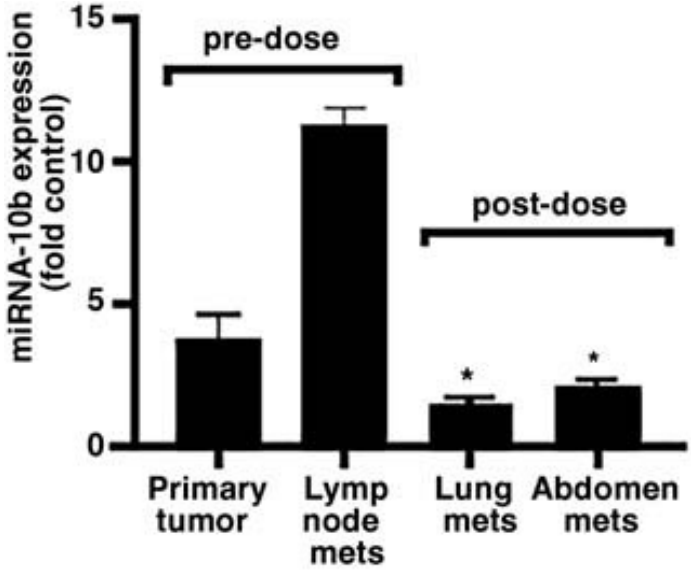


**Figure 3.2. Systemic MN-anti-miR10b decreases miR-10b expression in feline metastatic tissues.** qRT-PCR of miR-10b expression in primary tumor and lymph node metastases before dosing, and lung metastases and abdominal metastases three months after second. The expression of miR-10b was significantly reduced post-dosing relative to pre-dosing, indicating successful target engagement ($n = 3$, $p < 0.05$). Data are represented as mean ± s.d.

A limitation of our study in Cat 0 is that the pre-treatment sample was of lymph node metastases excised at initial evaluation for candidacy and the post-treatment samples were of lung and abdominal metastases. To address whether this affected our results, we orthotopically implanted 4T1 murine breast cancer cells into BALB/c mice. We used this cell line because *in vivo* it is an allograft model for Stage IV breast cancer and can spontaneously metastasize, making it more representative of Cat 0 than other models. Over the course of several weeks, lymph node and lung metastases were collected and analyzed for miR-10b expression to determine whether metastases at different sites have different levels of miR-10b expression. While there was variability in miR-10b expression across samples, there was no significant difference between lymph node (n = 7) and lung (n = 8) metastases (**Figure 3.3**), suggesting that the reduction in miR-10b in metastasis samples in Cat 0 after treatment was the result of MN-anti-miR10b administration.

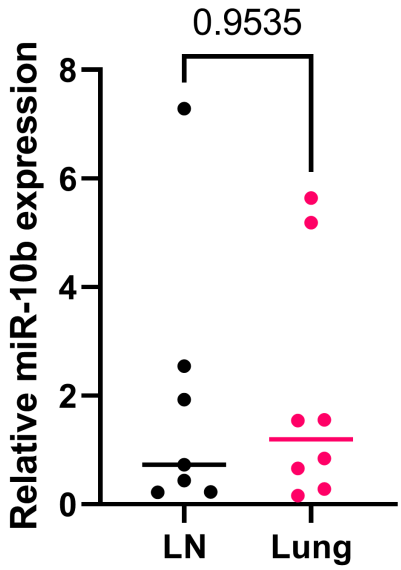


**Figure 3.3. MiR-10b expression does not significantly differ between metastatic sites.** qRT-PCR of miR-10b expression in lymph node (LN; n = 7) and lung (n = 8) metastases of BALB/c mice orthotopically implanted with 4T1 cells. Each point represents one unique sample, line represents mean.

Since the publication of the case report, the Moore Lab has continued to work with the Medical Oncology Service of the College of Veterinary Medicine at Michigan State University to recruit new candidate companion cats for treatment with MN-anti-miR10. When a prospective candidate is identified, metastasis samples and normal control tissues are collected by the veterinarians for analysis by me or my colleagues. Samples are analyzed for miR-10b expression to determine if the prospective candidate has metastases with miR-10b overexpression relative to normal tissue. If so, they are offered to enroll in our ongoing study in MN-anti-miR10b as a therapeutic for metastatic breast cancer in feline mammary carcinoma. Importantly, the narrow enrollment criteria for the study – companion cats with spontaneous, miR-10b overexpressing metastatic disease – means it will take an indeterminate amount of time to acquire enough patient cats for meaningful statistical analyses. The study will continue well beyond my training, though I hope to remain as involved as possible as it is well-aligned with my career goals of conducting clinical trials.

**Methods and Materials**

***RNA expression analysis (excerpt from Savan et al. (2022))***

RNA was isolated using the RecoverAll™ Total Nucleic Acid Isolation Kit for FFPE (Invitrogen, AM1975), and reverse transcription was performed using the miScript II RT Kit (Qiagen, 218161) according to the manufacturer's instructions. The miScript SYBR Green PCR Kit (Qiagen, 218076) was used for qPCR reaction with the appropriate specific forward primer for miR-10b: 5'-TACCCTGTAGAACCGAATTTGTG-3' and snRNAU6: 5'-GCAAGGATGACACGCAAATTC-3' in combination with the universal reverse primer provided in the kit. Forward and reverse primer set for HOXD10 was F1 5'-ATTGTCCTTGGTGAGATGGAAT-3' and R1 5'-GGACAGGTTGCTGTTGTACT - 3'.

MicroRNA expression levels were detected on a CFX96 Touch Real-Time PCR Detection System and data were analyzed using CFX Maestro software (Bio-Rad Laboratories, Hercules, CA).

Other methods and materials from Savan et al. (2022) have been omitted because I was not involved in them. They can be found in the publication. The following methods relate to **Figure 3.3** and are not published.

***Cell culture***

4T1-Red-Fluc breast cancer cells (Perkin Elmer) were cultured in high-glucose DMEM supplemented with 5% FBS and antibiotics (100units/mL penicillin, 100mg/mL streptomycin), as performed in our previous studies using 4T1 cells *in vivo* (56).

***Animal model***

Eight-week-old female BALB/c mice (The Jackson Laboratory) were orthotopically implanted with 4T1 cells (0.5 x $10^6$ cells total) under mammary gland #8. Primary tumor growth and metastasis was monitored using bioluminescence imaging (BLI), described below. This model of Stage IV breast cancer produces metastases at approximately two weeks post-implantation. With the goal of collecting appreciable metastasis samples, primary tumors were resected once metastases were observed to allow for growth of metastases prior to dissection. Upon dissection, metastasis samples were immediately snap-frozen using liquid nitrogen. These procedures were approved by the Michigan State University Institutional Animal Care and Use Committee (IACUC) and conformed to all regulatory standards.

***Bioluminescence imaging (BLI)***

Imaging was performed every two days using the IVIS Spectrum CT (Perkin Elmer) to monitor for development of metastases. Mice were injected intraperitoneally with D-luciferin

potassium salt in PBS (150mg/kg bodyweight). After eight minutes, mice were anesthetized using 2% isoflurane for imaging at approximately 10 minutes post-injection.

***Analysis of miR-10b expression in metastases***

Frozen metastasis samples were pulverized using a liquid nitrogen-cooled mortar and pestle prior to RNA extraction using the NucleoSpin miRNA extraction kit (Macherey-Nagel). Reverse transcription and qRT-PCR for miR-10b and U6 (reference gene) were performed using the miScript II RT and SYBR Green PCR kits (Qiagen), as described above.

# CHAPTER 5: GENERAL DISCUSSION

## Conclusions

The chapters in this dissertation all contribute to the development of MN-anti-miR10b as a clinical viable therapeutic for metastatic breast cancer. As the first model where the pro-metastatic properties of miR-10b was described, breast cancer constitutes a large proportion of the current literature on miR-10b. Chapter 1 provides a much-needed review of miR-10b with a focus on breast cancer. Chapter 2 relates to the vehicle component of MN-anti-miR10b, MN (magnetic nanoparticle). Nanoparticle vehicles are commonplace for delivery of RNA molecules, including miRNA mimics or antagonists, and MN has many advantages that support its use not just in MN-anti-miR10b but in other therapeutics. Synthesis of MN has been described previously in other publications. Presenting the methods used to monitor MN delivery *in vivo* – including, for the first time, through inductively coupled plasma optical emission spectroscopy – supports its use in our studies in MN-anti-miR10b and encourages its use in future therapeutics. Furthermore, the publication demonstrates accumulation of MN in metastatic lung tissues, which was previously inferred but not presented due to a focus on treatment of lymph node metastases. Chapter 3 begins by investigating how miR-10b expression in mouse metastatic tissues changes over time in response to weekly MN-anti-miR10b treatment, offering valuable pharmacodynamic insights into the therapeutic in mouse models that may apply to large animal models and, ultimately, clinical trials in humans. It then demonstrates the transcriptomic effects of miR-10b inhibition in breast cancer cell lines. Similar studies have only previously been performed in glioblastoma cell lines. Our datasets, which are deposited in public repositories, will allow us and other scientists to develop and test new hypotheses comparing and contrasting the effects of miR-10b inhibition in different types of cancer and also offers a cancer type-matched transcriptional foundation for

studies in breast cancer models. We used the datasets to generate a hypothesis for the functional mechanism for the previously described therapeutic effects of MN-anti-miR10b in mouse models of breast cancer and show evidence that MN-anti-miR10b acts on the stem cell-like properties of cancer cells. Importantly, these findings may relate to existing associations between miR-10b and the epithelial-mesenchymal transition (EMT) of cancer cells. Both characteristics are believed to exist on a spectrum of phenotypes, and stem-like cancer cells share many features of mesenchymal-like cancer cells. The two are compared and contrasted below. Our findings add to the body of evidence implicating miR-10b in the two spectra and suggest that poorly-differentiated, stem-like cancer cases may be the best candidates for therapy with MN-anti-miR10b. Lastly, Chapter 4 summarizes the findings of a study that supports the use of cats as a large animal model for miR-10b studies and a case report of the first cat with metastatic breast cancer to receive treatment with MN-anti-miR10b. The former findings back decades of evidence that cats are an excellent model for human breast cancer and provide a foundation for their use in studies specifically into miR-10b in breast cancer; the latter findings build upon this foundation and represent a major milestone in the translation of MN-anti-miR10b to the clinic, demonstrating for the first time the ability of MN-anti-miR10b to downregulate miR-10b in a large animal model of breast cancer. Candidate companion cats are actively being recruited for a follow-up study to demonstrate reproducibility of these findings and, next, show therapeutic efficacy.

**On the epithelial-mesenchymal transition (EMT) and stemness in cancer metastasis**

Most deaths due to cancer are attributable to metastasis, with some estimates as high as 90% (4). In hopes of reducing mortality, immense research has gone into understanding how cancer cells metastasize and, ultimately, how to prevent or limit the process. The current conception of the steps in the metastatic process is summarized by cancer.gov and further reviewed by Fares et al. (185) as (1) invasion of nearby normal tissue; (2) intravasation through the walls of nearby lymph nodes or blood vessels; (3) circulation to other parts of the body; (4) cessation of travel, invasion of blood vessel walls, and extravasation into the surrounding tissue; (5) growth into a small tumor; and (6) angiogenesis, allowing for continued tumor growth. While these steps are generally agreed upon by the cancer research community, the finer details that go into each of them and how the process is initiated are still being studied and are often the subject of controversy. In this brief review, I describe what is currently understood about the epithelial-mesenchymal transition (EMT) and cancer stem cells (CSCs), how they may be involved in the metastatic cascade, and the ongoing debates that surround them.

***The Epithelial-Mesenchymal Transition***

The EMT is a developmental process through which cohesive, polarized, and proliferative epithelial cells transition into more migratory and invasive mesenchymal cells (186; 187). It is most associated with the loss of E-cadherin expression, a protein involved in the formation and stabilization of cell-cell contacts, resulting in E-cadherin being referred to by some as one of the "caretakers of the epithelial phenotype" (187). And while EMT is beneficial in embryonic development and wound healing, upon its official recognition in 1982, researchers quickly drew parallels between it and the invasive properties of cancer. Indeed, E-cadherin was found to be altered or downregulated in many cases of invasive and dedifferentiated human cancers (188).

Transcriptional regulation of EMT is attributed to several transcription factors, notably Snail (189; 190), Slug (191), ZEB1 (192), ZEB2 (193), and Twist1 (194). These EMT transcription factors (EMT-TFs) share the ability to downregulate E-cadherin expression, among other overlapping features, and are commonly seen activated together in mesenchymal cells (195). While the identification of drivers of EMT has tremendous therapeutic implications, it also suggests that cells have numerous pathways through which they may acquire mesenchymal features. One study found that two different EMT-inducing stimuli – epidermal growth factor and hypoxia – led to similar mesenchymal states but with different sensitivities to chemical inhibitors during the transition, supporting the existence of distinct EMT pathways (196). As a result, details such as the model of EMT or metastasis or the history of a patient (e.g., exposure to potential EMT triggers) could help explain discrepancies in the literature and may be important considerations for future research.

In agreement with their properties, mesenchymal cells can be found at the periphery of primary tumors. Based on morphology and gene expression, studies have identified mesenchymal cells at the invasive front of human breast, pancreatic, lung, and colorectal primary tumors (197-199). Further along the metastatic cascade, a study in a mouse model of pancreatic ductal adenocarcinoma (PDAC) observed a greater percentage of mesenchymal cells in circulating tumor cells (CTCs) compared to in primary tumors (200). These findings were upheld in the CTCs of human breast, liver, nasopharyngeal, lung, colon, and gastric cancer patients, with correlations made between proportion of mesenchymal cells and disease severity or progression (201; 202). Mesenchymal cells have also been observed in disseminated tumor cells (DTCs) (203; 204), though it is worth noting that in these studies epithelial DTCs were more indicative of macroscopic metastasis formation and poor patient outcomes. These observations have led some to speculate

that the ability of a dormant DTC to return to an epithelial state may determine whether it is able to successfully colonize the distant site (186; 205-207).

Despite these findings, the necessity of EMT in the metastatic cascade remains controversial. Breast cancer metastases generally display E-cadherin expression comparable to or greater than the primary tumor from which they originated (208-210), including increased expression even when the primary tumors have low expression. Furthermore, there are claims that metastasis can occur in the absence of EMT. Dykxhoorn et al. observed that the spontaneously metastatic 4T1 murine breast cancer cell line expressed the EMT repressor miR-200, whereas three murine breast cancer cell lines that are poorly or non-metastatic (67NR, 168FARN, and 4TO7) had low to absent miR-200 expression (211). Correspondingly, the 4T1 cells were the most epithelial, having low expression of the EMT inducer Zeb2 and increased expression of E-cadherin. The group then overexpressed miR-200 in 4TO7 cells, increasing E-cadherin expression and shifting the cell morphology from mesenchymal-like spindles to epithelial-like cobblestones, and observed spontaneous lung metastasis formation. These exact findings were later corroborated by another group (212). Similarly, Fischer et al. designed a lineage tracing system in which cells express RFP unless Cre recombinase expression is driven by a mesenchymal promoter (FSP1 or vimentin) and permanently switches fluorescent protein expression to GFP (213). In both PyMT- and Neu-driven mouse models of breast cancer, lung metastases were found to be composed primarily of RFP-expressing cells, with GFP-expressing cells identified as mostly hematopoietic cells and confirmed to not be cancer cells using orthotopic implant of the PyMT-driven cancer cells into wild type mice. Additionally, orthotopic implant of the PyMT-driven cells with EMT blocked by miR-200 overexpression continued to yield spontaneous metastases, altogether suggesting that EMT is not

required for metastasis. Another article came to the same conclusion using a PDAC mouse model, observing metastases in KPC mice with Twist or Snail knocked out (214).

Adding to the controversy, it is becoming increasingly apparent that downregulation of E-cadherin is not the sole driver of cell dissemination. A study in normal mammary epithelial cells found that loss of E-cadherin was not sufficient to induce dissemination, however, upregulation of Twist1 and the subsequent decrease in E-cadherin protein levels was (215). Interestingly, E-cadherin RNA levels were not affected by Twist1 upregulation, and instead, E-cadherin knockdown impaired dissemination of the Twist1-overexpressing cells. While these findings support the bona fide role of Twist1 as an inducer of cancer cell dissemination, they also suggest that E-cadherin gene expression plays a critical role in this process.

Perhaps, then, the answer lies somewhere literally between the need for EMT or the lack thereof. Some researchers have speculated that epithelial and mesenchymal cells work in tandem to produce metastases, suggesting that mesenchymal cells and their mechanisms for migration and invasion (e.g., degradation of matrix) pave the way for epithelial cells to access distant sites, at which the proliferative capabilities of epithelial cells allow them to establish metastases (216; 217). This could explain the presence of both epithelial and mesenchymal cells as CTCs and DTCs but the predominance of epithelial cells in macroscopic metastases. Another explanation, which may not be mutually exclusive with the former, is that epithelial cells are undergoing EMT only partially. Cancer cells that express both epithelial and mesenchymal genes have been observed throughout the metastatic cascade in several models (201; 218), and the “hybrid” cells collected from the models are the most metastatic in experimental metastasis models. The existence of these hybrid cells and the limited degree to which they express mesenchymal markers may explain why some previous lineage tracing experiments failed to detect EMT in metastases. Indeed, a more

recent lineage tracing study in MMTV-PyMT mice reported that most lung metastases expressed a reporter induced by N-cadherin expression, a feature of mesenchymal cells. Active N-cadherin expression itself was not observed in these tumors, though, suggesting the cells had undergone EMT (at least partially) but had since reverted to a more epithelial phenotype (219).

***Cancer Stem Cells***

Closely related to EMT is the theory of cancer stem cells (CSCs). Defined by the American Association for Cancer Research (AACR) in 2006 as "a cell within a tumor that possess [sic] the capacity to self-renew and to cause the heterogeneous lineages of cancer cells that comprise the tumor" (220), CSCs were first identified in 1994 when human acute myeloid leukemia (AML) cells with the $CD34^{+}/CD38^{-}$ surface marker phenotype were found to induce AML in SCID mice, whereas cells of other phenotypes could not (130). In 2003, Al-Hajj et al. described the identification of tumorigenic breast cancer cells, the first report of cancer stem cells in solid tumors (110). Specifically, $CD44^{+}/CD24^{low}$ (and $Lineage^{-}$, to exclude normal, non-cancer cells) cells were found to have up to 50-fold greater tumor initiation capability in mice. These cells were subsequently compared to stem cells due to their apparent ability to self-renew and to produce tumors with cells expressing various surface marker phenotypes beyond $CD44^{+}/CD24^{low}$. These findings led to the cancer stem cell hypothesis, which posits that tumors are driven by a rare population of cells that display stem cell properties (in addition to considering the possibility that cancers are derived from normal tissue stem cells) (220; 221). Since then, other markers of stemness (116; 222) and stem-associated traits – increased metastatic potential (223), anchorage independent growth (224), and drug resistance (225) – have been reported and stem-associated phenotypes have been identified in different cancers (226).

A link between EMT and CSCs was described by Mani et al., who observed that mesenchymal-like cells generated by ectopic expression of Twist or Snail or exposure to TGFβ1 in human mammary epithelial cells displayed the $CD44^{high}/CD24^{low}$ stem cell-associated phenotype described by Al-Hajj et al. (126). These same cells also produced increased mammospheres in a mammosphere assay – a measure of self-renewal capability – and notably, the mammospheres included cells with basal markers as well as cells with luminal markers. Monolayer culture of the cells resulted in both $CD44^{high}/CD24^{low}$ and $CD44^{low}/CD24^{high}$ cells, whereas $CD44^{low}/CD24^{high}$ cells yielded only cells of the same phenotype, further supportive of the stem-like differentiation capabilities of the EMT-TF-overexpressing cells. The inverse relationship was also observed, wherein naturally occurring cells with stem-associated surface marker expression in cultured human cells or isolated from mice displayed increased expression of several EMT or mesenchymal cell markers and decreased expression of E-cadherin. The same connections have been made by others using similar methods (127), as well as other methods. For example, Shimono et al. reported downregulation of miR-200 in normal mammary stem cells and breast cancer stem cells, and they found that mammosphere formation was reduced following inhibition of EMT by overexpression of miR-200 (227). The authors also linked miR-200 to inhibition of BMI1, a regulator of stem cell self-renewal whose absence is known to result in defective hematopoietic, mammary, and neural stem cells in mice. These and other findings of similarities between CSCs and mesenchymal cells or cells undergoing EMT have led some to believe that the ability to undergo EMT is a property of CSCs specifically (228).

In contrast to the described studies linking EMT and cell stemness, there is also evidence that the two features are not entirely linked. There are numerous locations in mice that display regenerative properties but lack evidence of Slug expression (229), and intestinal stem cells lack

EMT-TFs altogether (230). Additionally, some studies have suggested that a complete EMT inhibits tumor initiation capabilities and that cancer cell stemness may actually be a feature conferred during EMT (i.e., the hybrid state when the cell has both epithelial and mesenchymal traits) but not in the fully mesenchymal state (231; 232), something that warrants consideration when evaluating studies on the connections between EMT and stemness.

EMT aside, it is worth mentioning that there is debate over the existence of CSCs altogether, with opposing perspectives being offered by some of the top scientists in cancer research (233). At direct odds with the cancer stem cell hypothesis is the stochastic model for both tumor growth and metastasis, which asserts that most or all cancer cells have the potential to form tumors or metastases and that randomly acquired traits (e.g., increased ability to promote angiogenesis or to change the tumor microenvironment) ultimately drive disease progression. Among the studies used by critics of the cancer stem cell hypothesis is a study by Quintana et al. which found that approximately 25% of patient melanoma cells could form tumors in mice (234). Similarities between tumor-initiating cells could not be consistently identified, contradicting claims that tumor-initiating cells are alike or rare. The authors, though, express their appreciation of the evidence toward the existence of CSCs and propose that different types of cancer may follow different models, a sentiment shared by others (233). The authors also recognize the possibility that CSCs exist but simply may not be as rare as once thought. Appropriately, the AACR definition of CSCs does not mention a requirement for rarity.

As debate lingers, data supporting the existence of CSCs continues to be generated. In recent studies, CSCs have been observed *in vivo* using intravital microscopy. Liu et al. found that the formation of CTC clusters in patient- and cell line-derived orthotopic xenograft models is mediated by $CD44^+$ cells, and that these clusters are more metastatic than single CTCs (235).

Similarly, Sharma et al. observed macrophages inducing expression of the stem-associated transcription factors Sox2 and Oct4 in orthotopically implanted breast cancer cells (236). While these cells represented only 1% of cells in the primary tumor, CTCs demonstrated 60-fold enrichment and lung metastases demonstrated 70-fold enrichment, supporting associations between stemness and metastasis.

***Clinical implications and future directions***

EMT and stemness both entail a plasticity to cancer cells, or their ability to transition between different states. This feature, which has been proposed as a new hallmark of cancer (237), is associated with chemoresistance, as plastic cancer cells would be able to change their properties as needed for survival (185; 238). Unsurprisingly, increased chemoresistance is a feature of mesenchymal cells and CSCs (239), and thus, the diagnostic, prognostic, and therapeutic implications for EMT and cancer cell stemness are the subject of ongoing research in many labs. A recent study by Papadaki et al. surveyed the phenotypes of patient CTCs and found a negative correlation between percentage of $CSC^+/EMT^+$ cells and patient response to chemotherapy (240). $CSC^+/EMT^-$ and $CSC^-/EMT^+$ were also observed, supporting the previously described studies claiming that stemness and EMT are not mutually inclusive (229-232); however, the relative abundance of double-positive and double-negative cells support a relationship between the two phenotypes. Accordingly, scientists are researching the benefits of targeting EMT and stemness (228), especially as it relates to sensitizing or re-sensitizing cells to chemotherapeutics (reviewed extensively by Dzobo et al. (226) and Hashemi et al. (241)). Included among ongoing works are studies into drug repurposing, with several drugs approved to treat non-cancer diseases being revisited with effects on EMT and stemness in mind (242; 243). Furthermore, many miRNAs

beyond miR-200 have been identified as drivers or inhibitors of EMT, providing new mechanisms for drug design (241; 243).

In conclusion, there is ample evidence that EMT and stem-like cells play important roles in the metastatic cascade. As the ability to study and monitor cancer progression at the single cell resolution continues to increase, it is expected that the mystery that surrounds what these exact roles are and how they can be used to guide new therapies for metastatic disease will become more apparent.

## Future Directions

### *Inhibition of stemness by MN-anti-miR10b*

Chapter 3 concludes with functional *in vitro* evidence indicating that MN-anti-miR10b inhibits breast cancer cell stemness. To support this as an explanation for the therapeutic effects of MN-anti-miR10b seen *in vivo*, it will be important to translate these findings to mouse models. This could be done in multiple ways, each with caveats.

The most performed *in vivo* measure for stemness is the limiting dilution tumor initiation assay (244). Specifically, this type of experiment tests for the tumor initiation capabilities (or tumorigenicity) of cancer cells, with stem-like cancer cells believed to have greater capabilities. In one proposed experiment, breast cancer cells are pre-treated with MN-anti-miR10b or controls for at least 48 hours, in line with the treatment periods used through our previous studies. Then, cells are counted, serially diluted to a range of concentrations, and orthotopically implanted into mice. If MN-anti-miR10b inhibits stemness and stemness can be assessed by tumor initiation capability, then one would expect that cells pre-treated with MN-anti-miR10b would require more cells to establish a tumor than cells pre-treated with controls. Importantly, while metastatic cells also need to have tumor initiation capabilities, this experiment design assays tumorigenicity using

a method that excludes the metastatic process. This is particularly notable given the role of miR-10b as a driver of metastasis. Indeed, we see over 7-fold increases in miR-10b expression in metastatic MDA-MB-231 cells compared to cells in culture (**Figure 4.1**), demonstrating the value of including the metastatic process in miR-10b studies. As a result, tumor initiation at the primary tumor level would be important to evaluate but may not best reveal the effects of miR-10b inhibition. To better model metastasis, this type of experiment could be performed by intravenous transplantation of cells instead of orthotopic; however, these experimental metastasis models ignore the changes cancer cells must undergo to migrate and invade into circulation and are similarly imperfect for the study of miR-10b. It is worth reiterating that MN-anti-miR10b has already been used in spontaneous metastasis models, which best capture these metastatic processes, and in the study the administration of MN-anti-miR10b could prevent onset of metastases if treatment was initiated prior to their detection by bioluminescence imaging. While these findings were not associated with an effect on stemness at the time, in hindsight, effects on the stemness of cells at the primary tumor may explain why metastases did not form.

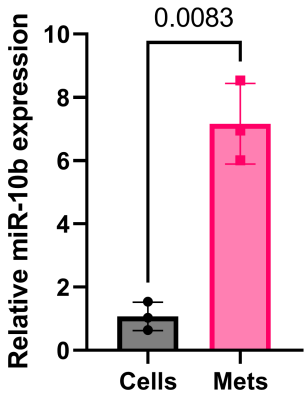


**Figure 4.1. MiR-10b expression in MDA-MB-231 cells in culture versus as metastases**. RT-qPCR results of miR-10b expression in MDA-MB-231 cells and spontaneous lymph node metastases.

***Intratumoral heterogeneity and the apoptotic effects of MN-anti-miR10b***

We previously reported on the importance of miR-10b for the viability of select cancer cell lines, including MDA-MB-231 cells, as well as the evidence of apoptosis seen in cells and lymph node metastases following treatment with MN-anti-miR10b (55; 62). Specifically, in lymph node metastases, we observed signs of apoptosis in samples collected after two once-per-week treatments. To determine the temporal relationship between MN-anti-miR10b treatment and apoptosis, with the assistance of Dr. Lorenzo Sempere, we performed TUNEL staining on MDA-MB-231-derived lymph node metastases from mice treated up to three times, once per week, with samples collected one week after last treatment (n = 2 per treatment condition). This revealed strong staining in the samples treated once compared to non-treated controls, followed by gradually diminishing signal with increasingly large acellular regions (**Figure 4.2**).

These results suggest that MN-anti-miR10b induced appreciable apoptosis in as little as one treatment, and over time and with repeated treatments, this apoptotic effect lessened as sensitive cells were cleared from the tumor. Notably, at all time points there were cells that showed no signs of apoptosis. This supports the aforementioned findings of variable cytotoxicity using MN-anti-miR10b and also explains why metastases have not been seen to regress with MN-anti-miR10b monotherapy (55; 56; 61). We speculate that inhibition of miR-10b using MN-anti-miR10b is lethal in select cells of a heterogeneous metastasis, and in the cells that it is not lethal in, it still hinders miR-10b driven processes, such as migration, invasion, and stem-like properties. And with reports that miR-10b confers drug resistance in breast cancer cells (54), it is possible that the metastasis regression observed using MN-anti-miR10b in combination with doxorubicin is the result of increased sensitization of surviving cancer cells.

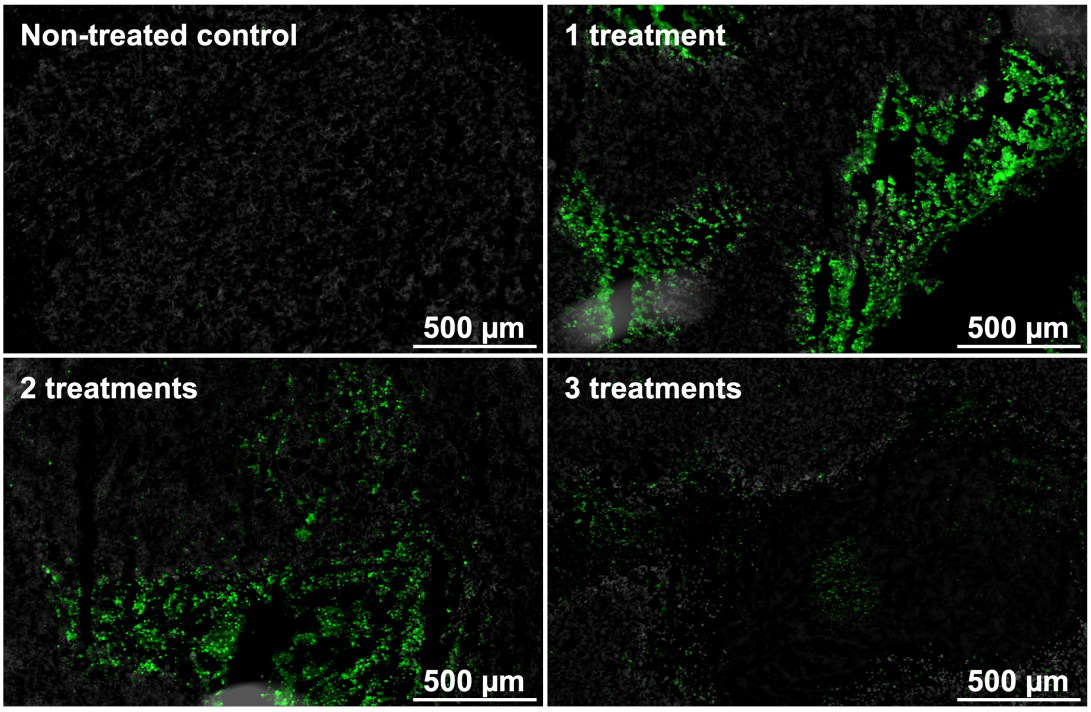


**Figure 4.2. Weekly treatment with MN-anti-miR10b induces apoptosis and cancer cell clearance in lymph node metastases.**
Terminal deoxynucleotidyl transferase dUTP nick end labeling (TUNEL) stain of lymph node metastasis sections following once-per-week treatment with MN-anti-miR10b. Samples were collected one week after last treatment.

Going forward, it will be important to further investigate the hypothesis of variable sensitivity of cells in a tumor to MN-anti-miR10b. This hypothesis would have wide-ranging implications, especially if it is found to be true *in vitro*, as well. For example, our *in vitro* studies using MN-anti-miR10b consistently utilize a 48-hour treatment period, which is sufficient to demonstrate phenotypic effects and miR-10b downregulation; however, it is plausible that we are eliminating a high-sensitivity cell population during the treatment period and that our *in vitro* experiments are not representing the full extent of the effects of MN-anti-miR10b. If true, identifying the drivers of this variable sensitivity may offer important clues into how to maximize the therapeutic potential of miR-10b inhibition.

***Translational studies using large animal models***

As mentioned previously, the use of companion cats as a model for metastatic breast cancer presents new opportunities for translational research using MN-anti-miR10b. Companion cats continue to be recruited for studies in drug safety and efficacy; however, at the stages they have been presenting in at the time of enrollment, the disease is advanced, providing little time for longitudinal evaluation of therapeutic efficacy. Indeed, in the case report of the first cat to be treated with MN-anti-miR10b, Cat 0 already had widespread metastases and was already scheduled for euthanasia prior to enrollment in the study. Future studies in companion cats could seek to enroll patients in earlier stages of breast cancer, allowing us to test whether MN-anti-miR10b can prevent onset of metastasis or, if already metastasized, delay or halt its progression, as it does in mouse models.

## WORKS CITED

1. Siegel RL, Giaquinto AN, Jemal A: Cancer statistics, 2024. CA Cancer J Clin 2024;74:12-49

2. Redig AJ, McAllister SS: Breast cancer as a systemic disease: a view of metastasis. J Intern Med 2013;274:113-126

3. American Cancer Society: Breast Cancer Facts & Figures 2022-2024. Atlanta: American Cancer Society, Inc 2022;

4. Dillekas H, Rogers MS, Straume O: Are 90% of deaths from cancer caused by metastases? Cancer Med 2019;8:5574-5576

5. Hanahan D, Weinberg RA: The hallmarks of cancer. Cell 2000;100:57-70

6. Kim T, Croce CM: MicroRNA: trends in clinical trials of cancer diagnosis and therapy strategies. Exp Mol Med 2023;55:1314-1321

7. Peng Y, Croce CM: The role of MicroRNAs in human cancer. Signal Transduct Target Ther 2016;1:15004

8. Kim VN: MicroRNA biogenesis: coordinated cropping and dicing. Nat Rev Mol Cell Biol 2005;6:376-385

9. Lam JK, Chow MY, Zhang Y, Leung SW: siRNA Versus miRNA as Therapeutics for Gene Silencing. Mol Ther Nucleic Acids 2015;4:e252

10. Selbach M, Schwanhausser B, Thierfelder N, Fang Z, Khanin R, Rajewsky N: Widespread changes in protein synthesis induced by microRNAs. Nature 2008;455:58-63

11. Lee Y, Kim M, Han J, Yeom KH, Lee S, Baek SH, Kim VN: MicroRNA genes are transcribed by RNA polymerase II. EMBO J 2004;23:4051-4060

12. Lau NC, Lim LP, Weinstein EG, Bartel DP: An abundant class of tiny RNAs with probable regulatory roles in Caenorhabditis elegans. Science 2001;294:858-862

13. Lee RC, Ambros V: An extensive class of small RNAs in Caenorhabditis elegans. Science 2001;294:862-864

14. Lagos-Quintana M, Rauhut R, Lendeckel W, Tuschl T: Identification of novel genes coding for small expressed RNAs. Science 2001;294:853-858

15. Lee Y, Ahn C, Han J, Choi H, Kim J, Yim J, Lee J, Provost P, Radmark O, Kim S, Kim VN: The nuclear RNase III Drosha initiates microRNA processing. Nature 2003;425:415-419

16. Yi R, Qin Y, Macara IG, Cullen BR: Exportin-5 mediates the nuclear export of pre-microRNAs and short hairpin RNAs. Genes Dev 2003;17:3011-3016

17. Bernstein E, Caudy AA, Hammond SM, Hannon GJ: Role for a bidentate ribonuclease in the initiation step of RNA interference. Nature 2001;409:363-366

18. Rand TA, Petersen S, Du F, Wang X: Argonaute2 cleaves the anti-guide strand of siRNA during RISC activation. Cell 2005;123:621-629

19. Fabian MR, Sonenberg N: The mechanics of miRNA-mediated gene silencing: a look under the hood of miRISC. Nat Struct Mol Biol 2012;19:586-593

20. Jonas S, Izaurralde E: Towards a molecular understanding of microRNA-mediated gene silencing. Nat Rev Genet 2015;16:421-433

21. Lewis BP, Shih IH, Jones-Rhoades MW, Bartel DP, Burge CB: Prediction of mammalian microRNA targets. Cell 2003;115:787-798

22. Agarwal V, Bell GW, Nam JW, Bartel DP: Predicting effective microRNA target sites in mammalian mRNAs. Elife 2015;4

23. Gu S, Jin L, Zhang F, Sarnow P, Kay MA: Biological basis for restriction of microRNA targets to the 3' untranslated region in mammalian mRNAs. Nat Struct Mol Biol 2009;16:144-150

24. Liu J, Carmell MA, Rivas FV, Marsden CG, Thomson JM, Song JJ, Hammond SM, Joshua-Tor L, Hannon GJ: Argonaute2 is the catalytic engine of mammalian RNAi. Science 2004;305:1437-1441

25. Matranga C, Tomari Y, Shin C, Bartel DP, Zamore PD: Passenger-strand cleavage facilitates assembly of siRNA into Ago2-containing RNAi enzyme complexes. Cell 2005;123:607-620

26. Ameres SL, Horwich MD, Hung JH, Xu J, Ghildiyal M, Weng Z, Zamore PD: Target RNA-directed trimming and tailing of small silencing RNAs. Science 2010;328:1534-1539

27. Park JH, Shin SY, Shin C: Non-canonical targets destabilize microRNAs in human Argonautes. Nucleic Acids Res 2017;45:1569-1583

28. De N, Young L, Lau PW, Meisner NC, Morrissey DV, MacRae IJ: Highly complementary target RNAs promote release of guide RNAs from human Argonaute2. Mol Cell 2013;50:344-355

29. Huse JT, Holland EC: Yin and yang: cancer-implicated miRNAs that have it both ways. Cell Cycle 2009;8:3611-3612

30. Cava C, Bertoli G, Castiglioni I: Portrait of Tissue-Specific Coexpression Networks of Noncoding RNAs (miRNA and lncRNA) and mRNAs in Normal Tissues. Comput Math Methods Med 2019;2019:9029351

31. Jouravleva K, Vega-Badillo J, Zamore PD: Principles and pitfalls of high-throughput analysis of microRNA-binding thermodynamics and kinetics by RNA Bind-n-Seq. Cell Rep Methods 2022;2:100185

32. Chipman LB, Pasquinelli AE: miRNA Targeting: Growing beyond the Seed. Trends Genet 2019;35:215-222

33. Chen Y, Wang X: miRDB: an online database for prediction of functional microRNA targets. Nucleic Acids Res 2020;48:D127-D131

34. McGeary SE, Lin KS, Shi CY, Pham TM, Bisaria N, Kelley GM, Bartel DP: The biochemical basis of microRNA targeting efficacy. Science 2019;366

35. Kumar A, Wong AK, Tizard ML, Moore RJ, Lefevre C: miRNA_Targets: a database for miRNA target predictions in coding and non-coding regions of mRNAs. Genomics 2012;100:352-356

36. Riolo G, Cantara S, Marzocchi C, Ricci C: miRNA Targets: From Prediction Tools to Experimental Validation. Methods Protoc 2020;4

37. Huang HY, Lin YC, Cui S, Huang Y, Tang Y, Xu J, Bao J, Li Y, Wen J, Zuo H, Wang W, Li J, Ni J, Ruan Y, Li L, Chen Y, Xie Y, Zhu Z, Cai X, Chen X, Yao L, Chen Y, Luo Y, LuXu S, Luo M, Chiu CM, Ma K, Zhu L, Cheng GJ, Bai C, Chiang YC, Wang L, Wei F, Lee TY, Huang HD: miRTarBase update 2022: an informative resource for experimentally validated miRNA-target interactions. Nucleic Acids Res 2022;50:D222-D230

38. Ma L, Teruya-Feldstein J, Weinberg RA: Tumour invasion and metastasis initiated by microRNA-10b in breast cancer. Nature 2007;449:682-688

39. Lee RC, Feinbaum RL, Ambros V: The C. elegans heterochronic gene lin-4 encodes small RNAs with antisense complementarity to lin-14. Cell 1993;75:843-854

40. Reinhart BJ, Slack FJ, Basson M, Pasquinelli AE, Bettinger JC, Rougvie AE, Horvitz HR, Ruvkun G: The 21-nucleotide let-7 RNA regulates developmental timing in Caenorhabditis elegans. Nature 2000;403:901-906

41. Calin GA, Dumitru CD, Shimizu M, Bichi R, Zupo S, Noch E, Aldler H, Rattan S, Keating M, Rai K, Rassenti L, Kipps T, Negrini M, Bullrich F, Croce CM: Frequent deletions and down-regulation of micro- RNA genes miR15 and miR16 at 13q14 in chronic lymphocytic leukemia. Proc Natl Acad Sci U S A 2002;99:15524-15529

42. Klein U, Lia M, Crespo M, Siegel R, Shen Q, Mo T, Ambesi-Impiombato A, Califano A, Migliazza A, Bhagat G, Dalla-Favera R: The DLEU2/miR-15a/16-1 cluster controls B cell proliferation and its deletion leads to chronic lymphocytic leukemia. Cancer Cell 2010;17:28-40

43. Iorio MV, Ferracin M, Liu CG, Veronese A, Spizzo R, Sabbioni S, Magri E, Pedriali M, Fabbri M, Campiglio M, Menard S, Palazzo JP, Rosenberg A, Musiani P, Volinia S, Nenci I, Calin GA, Querzoli P, Negrini M, Croce CM: MicroRNA gene expression deregulation in human breast cancer. Cancer Res 2005;65:7065-7070

44. Han X, Yan S, Weijie Z, Feng W, Liuxing W, Mengquan L, Qingxia F: Critical role of miR-10b in transforming growth factor-beta1-induced epithelial-mesenchymal transition in breast cancer. Cancer Gene Ther 2014;21:60-67

45. Croset M, Goehrig D, Frackowiak A, Bonnelye E, Ansieau S, Puisieux A, Clezardin P: TWIST1 expression in breast cancer cells facilitates bone metastasis formation. J Bone Miner Res 2014;29:1886-1899

46. Qin Q, Xu Y, He T, Qin C, Xu J: Normal and disease-related biological functions of Twist1 and underlying molecular mechanisms. Cell Res 2012;22:90-106

47. Figeac N, Daczewska M, Marcelle C, Jagla K: Muscle stem cells and model systems for their investigation. Dev Dyn 2007;236:3332-3342

48. Wang SM, Coljee VW, Pignolo RJ, Rotenberg MO, Cristofalo VJ, Sierra F: Cloning of the human twist gene: its expression is retained in adult mesodermally-derived tissues. Gene 1997;187:83-92

49. Sheedy P, Medarova Z: The fundamental role of miR-10b in metastatic cancer. Am J Cancer Res 2018;8:1674-1688

50. Ye X, Weinberg RA: Epithelial-Mesenchymal Plasticity: A Central Regulator of Cancer Progression. Trends Cell Biol 2015;25:675-686

51. Lo PK, Zhang Y, Yao Y, Wolfson B, Yu J, Han SY, Duru N, Zhou Q: Tumor-associated myoepithelial cells promote the invasive progression of ductal carcinoma in situ through activation of TGFbeta signaling. J Biol Chem 2017;292:11466-11484

52. Kim J, Siverly AN, Chen D, Wang M, Yuan Y, Wang Y, Lee H, Zhang J, Muller WJ, Liang H, Gan B, Yang X, Sun Y, You MJ, Ma L: Ablation of miR-10b Suppresses Oncogene-Induced Mammary Tumorigenesis and Metastasis and Reactivates Tumor-Suppressive Pathways. Cancer Res 2016;76:6424-6435

53. Bahena-Ocampo I, Espinosa M, Ceballos-Cancino G, Lizarraga F, Campos-Arroyo D, Schwarz A, Maldonado V, Melendez-Zajgla J, Garcia-Lopez P: miR-10b expression in breast cancer stem cells supports self-renewal through negative PTEN regulation and sustained AKT activation. EMBO Rep 2016;17:648-658

54. Ahmad A, Ginnebaugh KR, Yin S, Bollig-Fischer A, Reddy KB, Sarkar FH: Functional role of miR-10b in tamoxifen resistance of ER-positive breast cancer cells through down-regulation of HDAC4. BMC Cancer 2015;15:540

55. Yoo B, Kavishwar A, Ross A, Wang P, Tabassum DP, Polyak K, Barteneva N, Petkova V, Pantazopoulos P, Tena A, Moore A, Medarova Z: Combining miR-10b-Targeted Nanotherapy with Low-Dose Doxorubicin Elicits Durable Regressions of Metastatic Breast Cancer. Cancer Res 2015;75:4407-4415

56. Yoo B, Kavishwar A, Wang P, Ross A, Pantazopoulos P, Dudley M, Moore A, Medarova Z: Therapy targeted to the metastatic niche is effective in a model of stage IV breast cancer. Sci Rep 2017;7:45060

57. Gastelum-Lopez MLA, Aguilar-Medina M, Garcia Mata C, Lopez-Gutierrez J, Romero-Quintana G, Bermudez M, Avendano-Felix M, Lopez-Camarillo C, Perez-Plascencia C, Beltran AS, Ramos-Payan R: Organotypic 3D Cell-Architecture Impacts the Expression Pattern of miRNAs-mRNAs Network in Breast Cancer SKBR3 Cells. Noncoding RNA 2023;9

58. Glynn CL, Khan S, Kerin MJ, Dwyer RM: Isolation of secreted microRNAs (miRNAs) from cell-conditioned media. Microrna 2013;2:14-19

59. Singh R, Pochampally R, Watabe K, Lu Z, Mo YY: Exosome-mediated transfer of miR-10b promotes cell invasion in breast cancer. Mol Cancer 2014;13:256

60. Plummer PN, Freeman R, Taft RJ, Vider J, Sax M, Umer BA, Gao D, Johns C, Mattick JS, Wilton SD, Ferro V, McMillan NA, Swarbrick A, Mittal V, Mellick AS: MicroRNAs regulate tumor angiogenesis modulated by endothelial progenitor cells. Cancer Res 2013;73:341-352

61. Yigit MV, Ghosh SK, Kumar M, Petkova V, Kavishwar A, Moore A, Medarova Z: Context-dependent differences in miR-10b breast oncogenesis can be targeted for the prevention and arrest of lymph node metastasis. Oncogene 2013;32:1530-1538

62. Yoo B, Greninger P, Stein GT, Egan RK, McClanaghan J, Moore A, Benes CH, Medarova Z: Potent and selective effect of the mir-10b inhibitor MN-anti-mir10b in human cancer cells of diverse primary disease origin. PLoS One 2018;13:e0201046

63. Knirsh R, Ben-Dror I, Modai S, Shomron N, Vardimon L: MicroRNA 10b promotes abnormal expression of the proto-oncogene c-Jun in metastatic breast cancer cells. Oncotarget 2016;7:59932-59944

64. Liu Y, Zhao J, Zhang PY, Zhang Y, Sun SY, Yu SY, Xi QS: MicroRNA-10b targets E-cadherin and modulates breast cancer metastasis. Med Sci Monit 2012;18:BR299-308

65. Zhang J, Yang J, Zhang X, Xu J, Sun Y, Zhang P: MicroRNA-10b expression in breast cancer and its clinical association. PLoS One 2018;13:e0192509

66. Liu X, Guan Y, Wang L, Niu Y: MicroRNA-10b expression in node-negative breast cancer-correlation with metastasis and angiogenesis. Oncol Lett 2017;14:5845-5852

67. Bertoli G, Cava C, Castiglioni I: MicroRNAs: New Biomarkers for Diagnosis, Prognosis, Therapy Prediction and Therapeutic Tools for Breast Cancer. Theranostics 2015;5:1122-1143

68. Raychaudhuri M, Schuster T, Buchner T, Malinowsky K, Bronger H, Schwarz-Boeger U, Hofler H, Avril S: Intratumoral heterogeneity of microRNA expression in breast cancer. J Mol Diagn 2012;14:376-384

69. Markou A, Yousef GM, Stathopoulos E, Georgoulias V, Lianidou E: Prognostic significance of metastasis-related microRNAs in early breast cancer patients with a long follow-up. Clin Chem 2014;60:197-205

70. Gasch C, Plummer PN, Jovanovic L, McInnes LM, Wescott D, Saunders CM, Schneeweiss A, Wallwiener M, Nelson C, Spring KJ, Riethdorf S, Thompson EW, Pantel K, Mellick AS: Heterogeneity of miR-10b expression in circulating tumor cells. Sci Rep 2015;5:15980

71. Mar-Aguilar F, Mendoza-Ramirez JA, Malagon-Santiago I, Espino-Silva PK, Santuario-Facio SK, Ruiz-Flores P, Rodriguez-Padilla C, Resendez-Perez D: Serum circulating microRNA profiling for identification of potential breast cancer biomarkers. Dis Markers 2013;34:163-169

72. Khalighfard S, Alizadeh AM, Irani S, Omranipour R: Plasma miR-21, miR-155, miR-10b, and Let-7a as the potential biomarkers for the monitoring of breast cancer patients. Sci Rep 2018;8:17981

73. Xu SB, Fan RH, Qin X, Han RM: microRNA Prognostic Signature for Postoperative Success of Metastatic Orthopedic Cancers: Implications for Precision Microsurgery. Front Cell Dev Biol 2021;9:704505

74. Davey MG, Abbas R, Kerin EP, Casey MC, McGuire A, Waldron RM, Heneghan HM, Newell J, McDermott AM, Keane MM, Lowery AJ, Miller N, Kerin MJ: Circulating microRNAs can predict chemotherapy-induced toxicities in patients being treated for primary breast cancer. Breast Cancer Res Treat 2023;202:73-81

75. Garzon R, Pichiorri F, Palumbo T, Iuliano R, Cimmino A, Aqeilan R, Volinia S, Bhatt D, Alder H, Marcucci G, Calin GA, Liu CG, Bloomfield CD, Andreeff M, Croce CM: MicroRNA fingerprints during human megakaryocytopoiesis. Proc Natl Acad Sci U S A 2006;103:5078-5083

76. Eissa S, Matboli M, Shehata HH, Essawy NO: MicroRNA-10b and minichromosome maintenance complex component 5 gene as prognostic biomarkers in breast cancer. Tumour Biol 2015;36:4487-4494

77. Huang Q, Song Q, Zhong W, Chen Y, Liang L: MicroRNA-10b and the clinical outcomes of various cancers: A systematic review and meta-analysis. Clin Chim Acta 2017;474:14-22

78. Chen W, Cai F, Zhang B, Barekati Z, Zhong XY: The level of circulating miRNA-10b and miRNA-373 in detecting lymph node metastasis of breast cancer: potential biomarkers. Tumour Biol 2013;34:455-462

79. Mangolini A, Ferracin M, Zanzi MV, Saccenti E, Ebnaof SO, Poma VV, Sanz JM, Passaro A, Pedriali M, Frassoldati A, Querzoli P, Sabbioni S, Carcoforo P, Hollingsworth A, Negrini M: Diagnostic and prognostic microRNAs in the serum of breast cancer patients measured by droplet digital PCR. Biomark Res 2015;3:12

80. Baffa R, Fassan M, Volinia S, O'Hara B, Liu CG, Palazzo JP, Gardiman M, Rugge M, Gomella LG, Croce CM, Rosenberg A: MicroRNA expression profiling of human metastatic cancers identifies cancer gene targets. J Pathol 2009;219:214-221

81. Diener C, Keller A, Meese E: Emerging concepts of miRNA therapeutics: from cells to clinic. Trends Genet 2022;38:613-626

82. Rupaimoole R, Slack FJ: MicroRNA therapeutics: towards a new era for the management of cancer and other diseases. Nat Rev Drug Discov 2017;16:203-222

83. Yigit MV, Moore A, Medarova Z: Magnetic nanoparticles for cancer diagnosis and therapy. Pharm Res 2012;29:1180-1188

84. Ma L, Reinhardt F, Pan E, Soutschek J, Bhat B, Marcusson EG, Teruya-Feldstein J, Bell GW, Weinberg RA: Therapeutic silencing of miR-10b inhibits metastasis in a mouse mammary tumor model. Nat Biotechnol 2010;28:341-347

85. Jin H, Yu Y, Chrisler WB, Xiong Y, Hu D, Lei C: Delivery of MicroRNA-10b with Polylysine Nanoparticles for Inhibition of Breast Cancer Cell Wound Healing. Breast Cancer (Auckl) 2012;6:9-19

86. Savan NA, Saavedra PV, Halim A, Yuzbasiyan-Gurkan V, Wang P, Yoo B, Kiupel M, Sempere L, Medarova Z, Moore A: Case report: MicroRNA-10b as a therapeutic target in feline metastatic mammary carcinoma and its implications for human clinical trials. Front Oncol 2022;12:959630

87. An Open-Label, Single-Center, Phase 0, Microdose Study to Demonstrate Delivery of TTX-MC138-NODAGA-Cu64 to Radiographically Confirmed Metastases in Subjects With Advanced Solid Tumors. 2023

88. A Phase 1/2 Multicenter, Open-Label, Dose-escalation and Expansion Study of TTX-MC138 in Subjects With Advanced Solid Tumors. 2023

89. Devulapally R, Sekar NM, Sekar TV, Foygel K, Massoud TF, Willmann JK, Paulmurugan R: Polymer nanoparticles mediated codelivery of antimiR-10b and antimiR-21 for achieving triple negative breast cancer therapy. ACS Nano 2015;9:2290-2302

90. Ahir M, Upadhyay P, Ghosh A, Sarker S, Bhattacharya S, Gupta P, Ghosh S, Chattopadhyay S, Adhikary A: Delivery of dual miRNA through CD44-targeted mesoporous silica nanoparticles for enhanced and effective triple-negative breast cancer therapy. Biomater Sci 2020;8:2939-2954

91. Monroig-Bosque PDC, Shah MY, Fu X, Fuentes-Mattei E, Ling H, Ivan C, Nouraee N, Huang B, Chen L, Pileczki V, Redis RS, Jung EJ, Zhang X, Lehrer M, Nagvekar R, Mafra ACP, Monroig-Bosque MDM, Irimie A, Rivera C, Dan Dumitru C, Berindan-Neagoe I, Nikonowicz EP, Zhang S, Calin GA: OncomiR-10b hijacks the small molecule inhibitor linifanib in human cancers. Sci Rep 2018;8:13106

92. Chan E, Goff LW, Cardin DB, Ancell K, Smith SJ, Whisenant JG, Ye F, Berlin JD: Phase II study of the Multikinase inhibitor of angiogenesis, Linifanib, in patients with metastatic and refractory colorectal cancer expressing mutated KRAS. Invest New Drugs 2017;35:491-498

93. Ramalingam SS, Shtivelband M, Soo RA, Barrios CH, Makhson A, Segalla JG, Pittman KB, Kolman P, Pereira JR, Srkalovic G, Belani CP, Axelrod R, Owonikoko TK, Qin Q, Qian J, McKeegan EM, Devanarayan V, McKee MD, Ricker JL, Carlson DM, Gorbunova VA: Randomized phase II study of carboplatin and paclitaxel with either linifanib or placebo for advanced nonsquamous non-small-cell lung cancer. J Clin Oncol 2015;33:433-441

94. Wang ES, Yee K, Koh LP, Hogge D, Enschede S, Carlson DM, Dudley M, Glaser K, McKeegan E, Albert DH, Li X, Pradhan R, Stock W: Phase 1 trial of linifanib (ABT-869) in patients with refractory or relapsed acute myeloid leukemia. Leuk Lymphoma 2012;53:1543-1551

95. Li Y, Wu P, Zhu M, Liang M, Zhang L, Zong Y, Wan M: High-Performance Delivery of a CRISPR Interference System via Lipid-Polymer Hybrid Nanoparticles Combined with Ultrasound-Mediated Microbubble Destruction for Tumor-Specific Gene Repression. Adv Healthc Mater 2023;12:e2203082

96. Wang D, Wang L, Zheng L, Chen J, Zhang W, Zhou W, Yang X, Jiang L, Jin X, Yu X, Liu X, Chen H, Xu J: Enhancing the Management of Metastatic Tumors by Robust Co-Delivery of 5-Fluorouracil/MicroRNA-10b Inhibitor Using EGFR-Targeted Nanovehicles. Adv Healthc Mater 2023;12:e2202989

97. Teplyuk NM, Uhlmann EJ, Gabriely G, Volfovsky N, Wang Y, Teng J, Karmali P, Marcusson E, Peter M, Mohan A, Kraytsberg Y, Cialic R, Chiocca EA, Godlewski J, Tannous B, Krichevsky AM: Therapeutic potential of targeting microRNA-10b in established intracranial glioblastoma: first steps toward the clinic. EMBO Mol Med 2016;8:268-287

98. Malhotra M, Sekar TV, Ananta JS, Devulapally R, Afjei R, Babikir HA, Paulmurugan R, Massoud TF: Targeted nanoparticle delivery of therapeutic antisense microRNAs presensitizes glioblastoma cells to lower effective doses of temozolomide in vitro and in a mouse model. Oncotarget 2018;9:21478-21494

99. Ananta JS, Paulmurugan R, Massoud TF: Tailored Nanoparticle Codelivery of antimiR-21 and antimiR-10b Augments Glioblastoma Cell Kill by Temozolomide: Toward a "Personalized" Anti-microRNA Therapy. Mol Pharm 2016;13:3164-3175

100. Chen M, Kim B, Robertson N, Mondal SK, Medarova Z, Moore A: Co-administration of temozolomide (TMZ) and the experimental therapeutic targeting miR-10b, profoundly affects the tumorigenic phenotype of human glioblastoma cells. Front Mol Biosci 2023;10:1179343

101. Regulus Announces Clinical Candidate Nomination for the Treatment of Glioblastoma Multiforme [article online], 2019. Available from https://www.prnewswire.com/news-releases/regulus-announces-clinical-candidate-nomination-for-the-treatment-of-glioblastoma-multiforme-300773622.html. Accessed 2024 Aug 24

102. Houssami N, Macaskill P, Balleine RL, Bilous M, Pegram MD: HER2 discordance between primary breast cancer and its paired metastasis: tumor biology or test artefact? Insights through meta-analysis. Breast Cancer Res Treat 2011;129:659-674

103. Kumar M, Yigit M, Dai G, Moore A, Medarova Z: Image-guided breast tumor therapy using a small interfering RNA nanodrug. Cancer Res 2010;70:7553-7561

104. Sporn MB: The war on cancer. Lancet 1996;347:1377-1381

105. Ha M, Kim VN: Regulation of microRNA biogenesis. Nat Rev Mol Cell Biol 2014;15:509-524

106. Mancini R, Noto A, Pisanu ME, De Vitis C, Maugeri-Sacca M, Ciliberto G: Metabolic features of cancer stem cells: the emerging role of lipid metabolism. Oncogene 2018;37:2367-2378

107. Lin J, Teo S, Lam DH, Jeyaseelan K, Wang S: MicroRNA-10b pleiotropically regulates invasion, angiogenicity and apoptosis of tumor cells resembling mesenchymal subtype of glioblastoma multiforme. Cell Death Dis 2012;3:e398

108. Wimmer M, Zauner R, Ablinger M, Pinon-Hofbauer J, Guttmann-Gruber C, Reisenberger M, Lettner T, Niklas N, Proell J, Sajinovic M, De Souza P, Hainzl S, Kocher T, Murauer EM, Bauer JW, Strunk D, Reichelt J, Mellick AS, Wally V: A cancer stem cell-like phenotype is associated with miR-10b expression in aggressive squamous cell carcinomas. Cell Commun Signal 2020;18:61

109. Sun JG, Liao RX, Qiu J, Jin JY, Wang XX, Duan YZ, Chen FL, Hao P, Xie QC, Wang ZX, Li DZ, Chen ZT, Zhang SX: Microarray-based analysis of microRNA expression in breast cancer stem cells. J Exp Clin Cancer Res 2010;29:174

110. Al-Hajj M, Wicha MS, Benito-Hernandez A, Morrison SJ, Clarke MF: Prospective identification of tumorigenic breast cancer cells. Proc Natl Acad Sci U S A 2003;100:3983-3988

111. Sheridan C, Kishimoto H, Fuchs RK, Mehrotra S, Bhat-Nakshatri P, Turner CH, Goulet R, Jr., Badve S, Nakshatri H: CD44+/CD24- breast cancer cells exhibit enhanced invasive properties: an early step necessary for metastasis. Breast Cancer Res 2006;8:R59

112. Li W, Ma H, Zhang J, Zhu L, Wang C, Yang Y: Unraveling the roles of CD44/CD24 and ALDH1 as cancer stem cell markers in tumorigenesis and metastasis. Sci Rep 2017;7:13856

113. Feng ZM, Qiu J, Chen XW, Liao RX, Liao XY, Zhang LP, Chen X, Li Y, Chen ZT, Sun JG: Essential role of miR-200c in regulating self-renewal of breast cancer stem cells and their counterparts of mammary epithelium. BMC Cancer 2015;15:645

114. Samanta D, Semenza GL: In Vitro Assays of Breast Cancer Stem Cells. Methods Mol Biol 2018;1742:237-246

115. Zhou L, Sheng D, Wang D, Ma W, Deng Q, Deng L, Liu S: Identification of cancer-type specific expression patterns for active aldehyde dehydrogenase (ALDH) isoforms in ALDEFLUOR assay. Cell Biol Toxicol 2019;35:161-177

116. Ginestier C, Hur MH, Charafe-Jauffret E, Monville F, Dutcher J, Brown M, Jacquemier J, Viens P, Kleer CG, Liu S, Schott A, Hayes D, Birnbaum D, Wicha MS, Dontu G: ALDH1 is a marker of normal and malignant human mammary stem cells and a predictor of poor clinical outcome. Cell Stem Cell 2007;1:555-567

117. Wei Y, Li Y, Chen Y, Liu P, Huang S, Zhang Y, Sun Y, Wu Z, Hu M, Wu Q, Wu H, Liu F, She T, Ning Z: ALDH1: A potential therapeutic target for cancer stem cells in solid tumors. Front Oncol 2022;12:1026278

118. Shaw FL, Harrison H, Spence K, Ablett MP, Simoes BM, Farnie G, Clarke RB: A detailed mammosphere assay protocol for the quantification of breast stem cell activity. J Mammary Gland Biol Neoplasia 2012;17:111-117

119. Yousefnia S, Ghaedi K, Seyed Forootan F, Nasr Esfahani MH: Characterization of the stemness potency of mammospheres isolated from the breast cancer cell lines. Tumour Biol 2019;41:1010428319869101

120. Pinto B, Henriques AC, Silva PMA, Bousbaa H: Three-Dimensional Spheroids as In Vitro Preclinical Models for Cancer Research. Pharmaceutics 2020;12

121. do Amaral JB, Urabayashi MS, Machado-Santelli GM: Cell death and lumen formation in spheroids of MCF-7 cells. Cell Biol Int 2010;34:267-274

122. Nassef MZ, Melnik D, Kopp S, Sahana J, Infanger M, Lutzenberg R, Relja B, Wehland M, Grimm D, Kruger M: Breast Cancer Cells in Microgravity: New Aspects for Cancer Research. Int J Mol Sci 2020;21

123. Gayan S, Teli A, Dey T: Inherent aggressive character of invasive and non-invasive cells dictates the in vitro migration pattern of multicellular spheroid. Sci Rep 2017;7:11527

124. Ardekani AM, Naeini MM: The Role of MicroRNAs in Human Diseases. Avicenna J Med Biotechnol 2010;2:161-179

125. Biagioni F, Bossel Ben-Moshe N, Fontemaggi G, Yarden Y, Domany E, Blandino G: The locus of microRNA-10b: a critical target for breast cancer insurgence and dissemination. Cell Cycle 2013;12:2371-2375

126. Mani SA, Guo W, Liao MJ, Eaton EN, Ayyanan A, Zhou AY, Brooks M, Reinhard F, Zhang CC, Shipitsin M, Campbell LL, Polyak K, Brisken C, Yang J, Weinberg RA: The epithelial-mesenchymal transition generates cells with properties of stem cells. Cell 2008;133:704-715

127. Morel AP, Lievre M, Thomas C, Hinkal G, Ansieau S, Puisieux A: Generation of breast cancer stem cells through epithelial-mesenchymal transition. PLoS One 2008;3:e2888

128. Kuo KK, Lee KT, Chen KK, Yang YH, Lin YC, Tsai MH, Wuputra K, Lee YL, Ku CC, Miyoshi H, Nakamura Y, Saito S, Wu CC, Chai CY, Eckner R, Steve Lin CL, Wang SS, Wu DC, Lin CS, Yokoyama KK: Positive Feedback Loop of OCT4 and c-JUN Expedites Cancer Stemness in Liver Cancer. Stem Cells 2016;34:2613-2624

129. Jiao X, Katiyar S, Willmarth NE, Liu M, Ma X, Flomenberg N, Lisanti MP, Pestell RG: c-Jun induces mammary epithelial cellular invasion and breast cancer stem cell expansion. J Biol Chem 2010;285:8218-8226

130. Lapidot T, Sirard C, Vormoor J, Murdoch B, Hoang T, Caceres-Cortes J, Minden M, Paterson B, Caligiuri MA, Dick JE: A cell initiating human acute myeloid leukaemia after transplantation into SCID mice. Nature 1994;367:645-648

131. Visvader JE: Cells of origin in cancer. Nature 2011;469:314-322

132. Borah A, Raveendran S, Rochani A, Maekawa T, Kumar DS: Targeting self-renewal pathways in cancer stem cells: clinical implications for cancer therapy. Oncogenesis 2015;4:e177

133. Huang ME, Ye YC, Chen SR, Chai JR, Lu JX, Zhoa L, Gu LJ, Wang ZY: Use of all-trans retinoic acid in the treatment of acute promyelocytic leukemia. Blood 1988;72:567-572

134. Matthay KK, Reynolds CP, Seeger RC, Shimada H, Adkins ES, Haas-Kogan D, Gerbing RB, London WB, Villablanca JG: Long-term results for children with high-risk neuroblastoma treated on a randomized trial of myeloablative therapy followed by 13-cis-retinoic acid: a children's oncology group study. J Clin Oncol 2009;27:1007-1013

135. Zhu K, Xia Y, Tian X, He Y, Zhou J, Han R, Guo H, Song T, Chen L, Tian X: Characterization and therapeutic perspectives of differentiation-inducing therapy in malignant tumors. Front Genet 2023;14:1271381

136. Martinez-Illescas NG, Leal S, Gonzalez P, Grana-Castro O, Munoz-Oliveira JJ, Cortes-Pena A, Gomez-Gil M, Vega Z, Neva V, Romero A, Quintela-Fandino M, Ciruelos E, Sanz C, Aragon S, Sotolongo L, Jimenez S, Caleiras E, Mulero F, Sanchez C, Malumbres M, Salazar-Roa M: miR-203 drives breast cancer cell differentiation. Breast Cancer Res 2023;25:91

137. Bryan M, Pulte ED, Toomey KC, Pliner L, Pavlick AC, Saunders T, Wieder R: A pilot phase II trial of all-trans retinoic acid (Vesanoid) and paclitaxel (Taxol) in patients with recurrent or metastatic breast cancer. Invest New Drugs 2011;29:1482-1487

138. Butner JD, Dogra P, Chung C, Ruiz-Ramirez J, Nizzero S, Plodinec M, Li X, Pan PY, Chen SH, Cristini V, Ozpolat B, Calin GA, Wang Z: Dedifferentiation-mediated stem cell niche maintenance in early-stage ductal carcinoma in situ progression: insights from a multiscale modeling study. Cell Death Dis 2022;13:485

139. Saito S, Ku CC, Wuputra K, Pan JB, Lin CS, Lin YC, Wu DC, Yokoyama KK: Biomarkers of Cancer Stem Cells for Experimental Research and Clinical Application. J Pers Med 2022;12

140. Walcher L, Kistenmacher AK, Suo H, Kitte R, Dluczek S, Strauss A, Blaudszun AR, Yevsa T, Fricke S, Kossatz-Boehlert U: Cancer Stem Cells-Origins and Biomarkers: Perspectives for Targeted Personalized Therapies. Front Immunol 2020;11:1280

141. Abdoli Shadbad M, Hosseinkhani N, Asadzadeh Z, Derakhshani A, Karim Ahangar N, Hemmat N, Lotfinejad P, Brunetti O, Silvestris N, Baradaran B: A Systematic Review to Clarify the Prognostic Values of CD44 and CD44(+)CD24(-) Phenotype in Triple-Negative Breast Cancer Patients: Lessons Learned and The Road Ahead. Front Oncol 2021;11:689839

142. Sun H, Jia J, Wang X, Ma B, Di L, Song G, Ren J: CD44+/CD24- breast cancer cells isolated from MCF-7 cultures exhibit enhanced angiogenic properties. Clin Transl Oncol 2013;15:46-54

143. Zhang P, Hong H, Sun X, Jiang H, Ma S, Zhao S, Zhang M, Wang Z, Jiang C, Liu H: MicroRNA-10b regulates epithelial-mesenchymal transition by modulating KLF4/Notch1/E-cadherin in cisplatin-resistant nasopharyngeal carcinoma cells. Am J Cancer Res 2016;6:141-156

144. Xie Y, Wang Q, Gao N, Wu F, Lan F, Zhang F, Jin L, Huang Z, Ge J, Wang H, Wang Y: MircroRNA-10b Promotes Human Embryonic Stem Cell-Derived Cardiomyocyte Proliferation via Novel Target Gene LATS1. Mol Ther Nucleic Acids 2020;19:437-445

145. Li J, Garavaglia S, Ye Z, Moretti A, Belyaeva OV, Beiser A, Ibrahim M, Wilk A, McClellan S, Klyuyeva AV, Goggans KR, Kedishvili NY, Salter EA, Wierzbicki A, Migaud ME, Mullett SJ, Yates NA, Camacho CJ, Rizzi M, Sobol RW: A specific inhibitor of ALDH1A3 regulates retinoic acid biosynthesis in glioma stem cells. Commun Biol 2021;4:1420

146. Eyre R, Alferez DG, Spence K, Kamal M, Shaw FL, Simoes BM, Santiago-Gomez A, Sarmiento-Castro A, Bramley M, Absar M, Saad Z, Chatterjee S, Kirwan C, Gandhi A, Armstrong AC, Wardley AM, O'Brien CS, Farnie G, Howell SJ, Clarke RB: Patient-derived Mammosphere and Xenograft Tumour Initiation Correlates with Progression to Metastasis. J Mammary Gland Biol Neoplasia 2016;21:99-109

147. Guessous F, Alvarado-Velez M, Marcinkiewicz L, Zhang Y, Kim J, Heister S, Kefas B, Godlewski J, Schiff D, Purow B, Abounader R: Oncogenic effects of miR-10b in glioblastoma stem cells. J Neurooncol 2013;112:153-163

148. Moriarty CH, Pursell B, Mercurio AM: miR-10b targets Tiam1: implications for Rac activation and carcinoma migration. J Biol Chem 2010;285:20541-20546

149. Tian Y, Luo A, Cai Y, Su Q, Ding F, Chen H, Liu Z: MicroRNA-10b promotes migration and invasion through KLF4 in human esophageal cancer cell lines. J Biol Chem 2010;285:7986-7994

150. Love MI, Huber W, Anders S: Moderated estimation of fold change and dispersion for RNA-seq data with DESeq2. Genome Biol 2014;15:550

151. Wickham H: ggplot2 : Elegant Graphics for Data Analysis. In *Use R!,* 2nd ed. Cham, Springer International Publishing : Imprint: Springer,, 2016, p. 1 online resource (XVI, 260 pages 232 illustrations, 140 illustrations in color

152. Kolberg L, Raudvere U, Kuzmin I, Adler P, Vilo J, Peterson H: g:Profiler-interoperable web service for functional enrichment analysis and gene identifier mapping (2023 update). Nucleic Acids Res 2023;51:W207-W212

153. Chen H, Boutros PC: VennDiagram: a package for the generation of highly-customizable Venn and Euler diagrams in R. BMC Bioinformatics 2011;12:35

154. Ritchie ME, Phipson B, Wu D, Hu Y, Law CW, Shi W, Smyth GK: limma powers differential expression analyses for RNA-sequencing and microarray studies. Nucleic Acids Res 2015;43:e47

155. Almanaa TN, Geusz ME, Jamasbi RJ: A new method for identifying stem-like cells in esophageal cancer cell lines. J Cancer 2013;4:536-548

156. Zanoni M, Piccinini F, Arienti C, Zamagni A, Santi S, Polico R, Bevilacqua A, Tesei A: 3D tumor spheroid models for in vitro therapeutic screening: a systematic approach to enhance the biological relevance of data obtained. Sci Rep 2016;6:19103

157. O'Brien J, Hayder H, Zayed Y, Peng C: Overview of MicroRNA Biogenesis, Mechanisms of Actions, and Circulation. Front Endocrinol (Lausanne) 2018;9:402

158. Kobayashi H, Singer RH: Single-molecule imaging of microRNA-mediated gene silencing in cells. Nat Commun 2022;13:1435

159. Mootha VK, Lindgren CM, Eriksson KF, Subramanian A, Sihag S, Lehar J, Puigserver P, Carlsson E, Ridderstrale M, Laurila E, Houstis N, Daly MJ, Patterson N, Mesirov JP, Golub TR, Tamayo P, Spiegelman B, Lander ES, Hirschhorn JN, Altshuler D, Groop LC: PGC-1alpha-responsive genes involved in oxidative phosphorylation are coordinately downregulated in human diabetes. Nat Genet 2003;34:267-273

160. Subramanian A, Tamayo P, Mootha VK, Mukherjee S, Ebert BL, Gillette MA, Paulovich A, Pomeroy SL, Golub TR, Lander ES, Mesirov JP: Gene set enrichment analysis: a knowledge-

based approach for interpreting genome-wide expression profiles. Proc Natl Acad Sci U S A 2005;102:15545-15550

161. Ayaz G, Yan H, Malik N, Huang J: An Updated View of the Roles of p53 in Embryonic Stem Cells. Stem Cells 2022;40:883-891

162. Lin T, Lin Y: p53 switches off pluripotency on differentiation. Stem Cell Res Ther 2017;8:44

163. Spike BT, Wahl GM: p53, Stem Cells, and Reprogramming: Tumor Suppression beyond Guarding the Genome. Genes Cancer 2011;2:404-419

164. Loh JJ, Ma S: Hallmarks of cancer stemness. Cell Stem Cell 2024;31:617-639

165. Kaiser AM, Gatto A, Hanson KJ, Zhao RL, Raj N, Ozawa MG, Seoane JA, Bieging-Rolett KT, Wang M, Li I, Trope WL, Liou DZ, Shrager JB, Plevritis SK, Newman AM, Van Rechem C, Attardi LD: p53 governs an AT1 differentiation programme in lung cancer suppression. Nature 2023;619:851-859

166. Bisio A, De Sanctis V, Del Vescovo V, Denti MA, Jegga AG, Inga A, Ciribilli Y: Identification of new p53 target microRNAs by bioinformatics and functional analysis. BMC Cancer 2013;13:552

167. Lin CC, Liao WT, Yang TY, Lu HJ, Hsu SL, Wu CC: MicroRNA-10b modulates cisplatin tolerance by targeting p53 directly in lung cancer cells. Oncol Rep 2021;46

168. Meric-Bernstam F, Zheng X, Shariati M, Damodaran S, Wathoo C, Brusco L, Demirhan ME, Tapia C, Eterovic AK, Basho RK, Ueno NT, Janku F, Sahin A, Rodon J, Broaddus R, Kim TB, Mendelsohn J, Mills Shaw KR, Tripathy D, Mills GB, Chen K: Survival Outcomes by TP53 Mutation Status in Metastatic Breast Cancer. JCO Precis Oncol 2018;2018

169. Marvalim C, Datta A, Lee SC: Role of p53 in breast cancer progression: An insight into p53 targeted therapy. Theranostics 2023;13:1421-1442

170. Berke TP, Slight SH, Hyder SM: Role of Reactivating Mutant p53 Protein in Suppressing Growth and Metastasis of Triple-Negative Breast Cancer. Onco Targets Ther 2022;15:23-30

171. Barker N, van Es JH, Kuipers J, Kujala P, van den Born M, Cozijnsen M, Haegebarth A, Korving J, Begthel H, Peters PJ, Clevers H: Identification of stem cells in small intestine and colon by marker gene Lgr5. Nature 2007;449:1003-1007

172. Morgan RG, Mortensson E, Williams AC: Targeting LGR5 in Colorectal Cancer: therapeutic gold or too plastic? Br J Cancer 2018;118:1410-1418

173. Cao W, Li M, Liu J, Zhang S, Noordam L, Verstegen MMA, Wang L, Ma B, Li S, Wang W, Bolkestein M, Doukas M, Chen K, Ma Z, Bruno M, Sprengers D, Kwekkeboom J, van der Laan LJW, Smits R, Peppelenbosch MP, Pan Q: LGR5 marks targetable tumor-initiating cells in mouse liver cancer. Nat Commun 2020;11:1961

174. Trejo CL, Luna G, Dravis C, Spike BT, Wahl GM: Lgr5 is a marker for fetal mammary stem cells, but is not essential for stem cell activity or tumorigenesis. npj Breast Cancer 2017;3:16

175. Lee HJ, Myung JK, Kim HS, Lee DH, Go HS, Choi JH, Koh HM, Lee S-J, Jang B: Expression of LGR5 in mammary myoepithelial cells and in triple-negative breast cancers. Scientific Reports 2021;11:17750

176. Bourguignon LY, Wong G, Earle C, Krueger K, Spevak CC: Hyaluronan-CD44 interaction promotes c-Src-mediated twist signaling, microRNA-10b expression, and RhoA/RhoC up-regulation, leading to Rho-kinase-associated cytoskeleton activation and breast tumor cell invasion. J Biol Chem 2010;285:36721-36735

177. De Maria R, Olivero M, Iussich S, Nakaichi M, Murata T, Biolatti B, Di Renzo MF: Spontaneous feline mammary carcinoma is a model of HER2 overexpressing poor prognosis human breast cancer. Cancer Res 2005;65:907-912

178. Wiese DA, Thaiwong T, Yuzbasiyan-Gurkan V, Kiupel M: Feline mammary basal-like adenocarcinomas: a potential model for human triple-negative breast cancer (TNBC) with basal-like subtype. BMC Cancer 2013;13:403

179. Hahn KA, Bravo L, Avenell JS: Feline breast carcinoma as a pathologic and therapeutic model for human breast cancer. In Vivo 1994;8:825-828

180. Schmidt PL: Companion animals as sentinels for public health. Vet Clin North Am Small Anim Pract 2009;39:241-250

181. Soares M, Madeira S, Correia J, Peleteiro M, Cardoso F, Ferreira F: Molecular based subtyping of feline mammary carcinomas and clinicopathological characterization. Breast 2016;27:44-51

182. Brunetti B, Asproni P, Beha G, Muscatello LV, Millanta F, Poli A, Benazzi C, Sarli G: Molecular phenotype in mammary tumours of queens: correlation between primary tumour and lymph node metastasis. J Comp Pathol 2013;148:206-213

183. Granados-Soler JL, Junginger J, Hewicker-Trautwein M, Bornemann-Kolatzki K, Beck J, Brenig B, Betz D, Schille JT, Murua Escobar H, Nolte I: TiHo-0906: a new feline mammary cancer cell line with molecular, morphological, and immunocytological characteristics of epithelial to mesenchymal transition. Sci Rep 2018;8:13231

184. Vilhena H, Figueira AC, Schmitt F, Canadas A, Chaves R, Gama A, Dias-Pereira P: Canine and Feline Spontaneous Mammary Tumours as Models of Human Breast Cancer. 2020, p. 173-207

185. Fares J, Fares MY, Khachfe HH, Salhab HA, Fares Y: Molecular principles of metastasis: a hallmark of cancer revisited. Signal Transduct Target Ther 2020;5:28

186. Nieto MA, Huang RY, Jackson RA, Thiery JP: Emt: 2016. Cell 2016;166:21-45

187. Thiery JP: Epithelial-mesenchymal transitions in tumour progression. Nat Rev Cancer 2002;2:442-454

188. Hirohashi S: Inactivation of the E-cadherin-mediated cell adhesion system in human cancers. Am J Pathol 1998;153:333-339

189. Batlle E, Sancho E, Franci C, Dominguez D, Monfar M, Baulida J, Garcia De Herreros A: The transcription factor snail is a repressor of E-cadherin gene expression in epithelial tumour cells. Nat Cell Biol 2000;2:84-89

190. Cano A, Perez-Moreno MA, Rodrigo I, Locascio A, Blanco MJ, del Barrio MG, Portillo F, Nieto MA: The transcription factor snail controls epithelial-mesenchymal transitions by repressing E-cadherin expression. Nat Cell Biol 2000;2:76-83

191. Hajra KM, Chen DY, Fearon ER: The SLUG zinc-finger protein represses E-cadherin in breast cancer. Cancer Res 2002;62:1613-1618

192. Eger A, Aigner K, Sonderegger S, Dampier B, Oehler S, Schreiber M, Berx G, Cano A, Beug H, Foisner R: DeltaEF1 is a transcriptional repressor of E-cadherin and regulates epithelial plasticity in breast cancer cells. Oncogene 2005;24:2375-2385

193. Comijn J, Berx G, Vermassen P, Verschueren K, van Grunsven L, Bruyneel E, Mareel M, Huylebroeck D, van Roy F: The two-handed E box binding zinc finger protein SIP1 downregulates E-cadherin and induces invasion. Mol Cell 2001;7:1267-1278

194. Yang J, Mani SA, Donaher JL, Ramaswamy S, Itzykson RA, Come C, Savagner P, Gitelman I, Richardson A, Weinberg RA: Twist, a master regulator of morphogenesis, plays an essential role in tumor metastasis. Cell 2004;117:927-939

195. Yamada S, Okumura N, Wei L, Fuchs BC, Fujii T, Sugimoto H, Nomoto S, Takeda S, Tanabe KK, Kodera Y: Epithelial to mesenchymal transition is associated with shorter disease-free survival in hepatocellular carcinoma. Ann Surg Oncol 2014;21:3882-3890

196. Cursons J, Leuchowius KJ, Waltham M, Tomaskovic-Crook E, Foroutan M, Bracken CP, Redfern A, Crampin EJ, Street I, Davis MJ, Thompson EW: Stimulus-dependent differences in signalling regulate epithelial-mesenchymal plasticity and change the effects of drugs in breast cancer cell lines. Cell Commun Signal 2015;13:26

197. Brabletz T, Jung A, Hermann K, Gunther K, Hohenberger W, Kirchner T: Nuclear overexpression of the oncoprotein beta-catenin in colorectal cancer is localized predominantly at the invasion front. Pathol Res Pract 1998;194:701-704

198. Brabletz T, Jung A, Reu S, Porzner M, Hlubek F, Kunz-Schughart LA, Knuechel R, Kirchner T: Variable beta-catenin expression in colorectal cancers indicates tumor progression driven by the tumor environment. Proc Natl Acad Sci U S A 2001;98:10356-10361

199. Bronsert P, Enderle-Ammour K, Bader M, Timme S, Kuehs M, Csanadi A, Kayser G, Kohler I, Bausch D, Hoeppner J, Hopt UT, Keck T, Stickeler E, Passlick B, Schilling O, Reiss CP, Vashist Y, Brabletz T, Berger J, Lotz J, Olesch J, Werner M, Wellner UF: Cancer cell invasion and EMT marker expression: a three-dimensional study of the human cancer-host interface. J Pathol 2014;234:410-422

200. Rhim AD, Mirek ET, Aiello NM, Maitra A, Bailey JM, McAllister F, Reichert M, Beatty GL, Rustgi AK, Vonderheide RH, Leach SD, Stanger BZ: EMT and dissemination precede pancreatic tumor formation. Cell 2012;148:349-361

201. Yu M, Bardia A, Wittner BS, Stott SL, Smas ME, Ting DT, Isakoff SJ, Ciciliano JC, Wells MN, Shah AM, Concannon KF, Donaldson MC, Sequist LV, Brachtel E, Sgroi D, Baselga J, Ramaswamy S, Toner M, Haber DA, Maheswaran S: Circulating breast tumor cells exhibit dynamic changes in epithelial and mesenchymal composition. Science 2013;339:580-584

202. Wu S, Liu S, Liu Z, Huang J, Pu X, Li J, Yang D, Deng H, Yang N, Xu J: Classification of circulating tumor cells by epithelial-mesenchymal transition markers. PLoS One 2015;10:e0123976

203. Driemel C, Kremling H, Schumacher S, Will D, Wolters J, Lindenlauf N, Mack B, Baldus SA, Hoya V, Pietsch JM, Panagiotidou P, Raba K, Vay C, Vallbohmer D, Harreus U, Knoefel WT, Stoecklein NH, Gires O: Context-dependent adaption of EpCAM expression in early systemic esophageal cancer. Oncogene 2014;33:4904-4915

204. Liu X, Li J, Cadilha BL, Markota A, Voigt C, Huang Z, Lin PP, Wang DD, Dai J, Kranz G, Krandick A, Libl D, Zitzelsberger H, Zagorski I, Braselmann H, Pan M, Zhu S, Huang Y, Niedermeyer S, Reichel CA, Uhl B, Briukhovetska D, Suarez J, Kobold S, Gires O, Wang H: Epithelial-type systemic breast carcinoma cells with a restricted mesenchymal transition are a major source of metastasis. Sci Adv 2019;5:eaav4275

205. Hiraga T: Hypoxic Microenvironment and Metastatic Bone Disease. Int J Mol Sci 2018;19

206. Lambert AW, Weinberg RA: Linking EMT programmes to normal and neoplastic epithelial stem cells. Nat Rev Cancer 2021;21:325-338

207. Hosseini H, Obradovic MMS, Hoffmann M, Harper KL, Sosa MS, Werner-Klein M, Nanduri LK, Werno C, Ehrl C, Maneck M, Patwary N, Haunschild G, Guzvic M, Reimelt C, Grauvogl M, Eichner N, Weber F, Hartkopf AD, Taran FA, Brucker SY, Fehm T, Rack B, Buchholz S, Spang R, Meister G, Aguirre-Ghiso JA, Klein CA: Early dissemination seeds metastasis in breast cancer. Nature 2016;540:552-558

208. Beerling E, Seinstra D, de Wit E, Kester L, van der Velden D, Maynard C, Schafer R, van Diest P, Voest E, van Oudenaarden A, Vrisekoop N, van Rheenen J: Plasticity between Epithelial and Mesenchymal States Unlinks EMT from Metastasis-Enhancing Stem Cell Capacity. Cell Rep 2016;14:2281-2288

209. Jeschke U, Mylonas I, Kuhn C, Shabani N, Kunert-Keil C, Schindlbeck C, Gerber B, Friese K: Expression of E-cadherin in human ductal breast cancer carcinoma in situ, invasive carcinomas, their lymph node metastases, their distant metastases, carcinomas with recurrence and in recurrence. Anticancer Res 2007;27:1969-1974

210. Kowalski PJ, Rubin MA, Kleer CG: E-cadherin expression in primary carcinomas of the breast and its distant metastases. Breast Cancer Res 2003;5:R217-222

211. Dykxhoorn DM, Wu Y, Xie H, Yu F, Lal A, Petrocca F, Martinvalet D, Song E, Lim B, Lieberman J: miR-200 enhances mouse breast cancer cell colonization to form distant metastases. PLoS One 2009;4:e7181

212. Korpal M, Ell BJ, Buffa FM, Ibrahim T, Blanco MA, Celia-Terrassa T, Mercatali L, Khan Z, Goodarzi H, Hua Y, Wei Y, Hu G, Garcia BA, Ragoussis J, Amadori D, Harris AL, Kang Y: Direct targeting of Sec23a by miR-200s influences cancer cell secretome and promotes metastatic colonization. Nat Med 2011;17:1101-1108

213. Fischer KR, Durrans A, Lee S, Sheng J, Li F, Wong ST, Choi H, El Rayes T, Ryu S, Troeger J, Schwabe RF, Vahdat LT, Altorki NK, Mittal V, Gao D: Epithelial-to-mesenchymal transition is not required for lung metastasis but contributes to chemoresistance. Nature 2015;527:472-476

214. Zheng X, Carstens JL, Kim J, Scheible M, Kaye J, Sugimoto H, Wu CC, LeBleu VS, Kalluri R: Epithelial-to-mesenchymal transition is dispensable for metastasis but induces chemoresistance in pancreatic cancer. Nature 2015;527:525-530

215. Shamir ER, Pappalardo E, Jorgens DM, Coutinho K, Tsai WT, Aziz K, Auer M, Tran PT, Bader JS, Ewald AJ: Twist1-induced dissemination preserves epithelial identity and requires E-cadherin. J Cell Biol 2014;204:839-856

216. Tsuji T, Ibaragi S, Shima K, Hu MG, Katsurano M, Sasaki A, Hu GF: Epithelial-mesenchymal transition induced by growth suppressor p12CDK2-AP1 promotes tumor cell local invasion but suppresses distant colony growth. Cancer Res 2008;68:10377-10386

217. Tsuji T, Ibaragi S, Hu GF: Epithelial-mesenchymal transition and cell cooperativity in metastasis. Cancer Res 2009;69:7135-7139

218. Pastushenko I, Brisebarre A, Sifrim A, Fioramonti M, Revenco T, Boumahdi S, Van Keymeulen A, Brown D, Moers V, Lemaire S, De Clercq S, Minguijon E, Balsat C, Sokolow Y, Dubois C, De Cock F, Scozzaro S, Sopena F, Lanas A, D'Haene N, Salmon I, Marine JC, Voet T, Sotiropoulou PA, Blanpain C: Identification of the tumour transition states occurring during EMT. Nature 2018;556:463-468

219. Li Y, Lv Z, Zhang S, Wang Z, He L, Tang M, Pu W, Zhao H, Zhang Z, Shi Q, Cai D, Wu M, Hu G, Lui KO, Feng J, Nieto MA, Zhou B: Genetic Fate Mapping of Transient Cell Fate Reveals N-Cadherin Activity and Function in Tumor Metastasis. Dev Cell 2020;54:593-607 e595

220. Clarke MF, Dick JE, Dirks PB, Eaves CJ, Jamieson CH, Jones DL, Visvader J, Weissman IL, Wahl GM: Cancer stem cells--perspectives on current status and future directions: AACR Workshop on cancer stem cells. Cancer Res 2006;66:9339-9344

221. Wicha MS, Liu S, Dontu G: Cancer stem cells: an old idea--a paradigm shift. Cancer Res 2006;66:1883-1890; discussion 1895-1886

222. Wright MH, Calcagno AM, Salcido CD, Carlson MD, Ambudkar SV, Varticovski L: Brca1 breast tumors contain distinct CD44+/CD24- and CD133+ cells with cancer stem cell characteristics. Breast Cancer Res 2008;10:R10

223. Charafe-Jauffret E, Ginestier C, Iovino F, Wicinski J, Cervera N, Finetti P, Hur MH, Diebel ME, Monville F, Dutcher J, Brown M, Viens P, Xerri L, Bertucci F, Stassi G, Dontu G, Birnbaum D, Wicha MS: Breast cancer cell lines contain functional cancer stem cells with metastatic capacity and a distinct molecular signature. Cancer Res 2009;69:1302-1313

224. Dontu G, Abdallah WM, Foley JM, Jackson KW, Clarke MF, Kawamura MJ, Wicha MS: In vitro propagation and transcriptional profiling of human mammary stem/progenitor cells. Genes Dev 2003;17:1253-1270

225. Liu S, Wicha MS: Targeting breast cancer stem cells. J Clin Oncol 2010;28:4006-4012

226. Dzobo K, Senthebane DA, Ganz C, Thomford NE, Wonkam A, Dandara C: Advances in Therapeutic Targeting of Cancer Stem Cells within the Tumor Microenvironment: An Updated Review. Cells 2020;9

227. Shimono Y, Zabala M, Cho RW, Lobo N, Dalerba P, Qian D, Diehn M, Liu H, Panula SP, Chiao E, Dirbas FM, Somlo G, Pera RA, Lao K, Clarke MF: Downregulation of miRNA-200c links breast cancer stem cells with normal stem cells. Cell 2009;138:592-603

228. de The H: Differentiation therapy revisited. Nat Rev Cancer 2018;18:117-127

229. Parent AE, Choi C, Caudy K, Gridley T, Kusewitt DF: The developmental transcription factor slug is widely expressed in tissues of adult mice. J Histochem Cytochem 2004;52:959-965

230. Munoz J, Stange DE, Schepers AG, van de Wetering M, Koo BK, Itzkovitz S, Volckmann R, Kung KS, Koster J, Radulescu S, Myant K, Versteeg R, Sansom OJ, van Es JH, Barker N, van Oudenaarden A, Mohammed S, Heck AJ, Clevers H: The Lgr5 intestinal stem cell signature: robust expression of proposed quiescent '+4' cell markers. EMBO J 2012;31:3079-3091

231. Celia-Terrassa T, Meca-Cortes O, Mateo F, Martinez de Paz A, Rubio N, Arnal-Estape A, Ell BJ, Bermudo R, Diaz A, Guerra-Rebollo M, Lozano JJ, Estaras C, Ulloa C, Alvarez-Simon D, Mila J, Vilella R, Paciucci R, Martinez-Balbas M, de Herreros AG, Gomis RR, Kang Y, Blanco J, Fernandez PL, Thomson TM: Epithelial-mesenchymal transition can suppress major attributes of human epithelial tumor-initiating cells. J Clin Invest 2012;122:1849-1868

232. Schmidt JM, Panzilius E, Bartsch HS, Irmler M, Beckers J, Kari V, Linnemann JR, Dragoi D, Hirschi B, Kloos UJ, Sass S, Theis F, Kahlert S, Johnsen SA, Sotlar K, Scheel CH: Stem-cell-like properties and epithelial plasticity arise as stable traits after transient Twist1 activation. Cell Rep 2015;10:131-139

233. Rowan K: Are cancer stem cells real? After four decades, debate still simmers. J Natl Cancer Inst 2009;101:546-547

234. Quintana E, Shackleton M, Sabel MS, Fullen DR, Johnson TM, Morrison SJ: Efficient tumour formation by single human melanoma cells. Nature 2008;456:593-598

235. Liu X, Taftaf R, Kawaguchi M, Chang YF, Chen W, Entenberg D, Zhang Y, Gerratana L, Huang S, Patel DB, Tsui E, Adorno-Cruz V, Chirieleison SM, Cao Y, Harney AS, Patel S, Patsialou A, Shen Y, Avril S, Gilmore HL, Lathia JD, Abbott DW, Cristofanilli M, Condeelis JS, Liu H: Homophilic CD44 Interactions Mediate Tumor Cell Aggregation and Polyclonal Metastasis in Patient-Derived Breast Cancer Models. Cancer Discov 2019;9:96-113

236. Sharma VP, Tang B, Wang Y, Duran CL, Karagiannis GS, Xue EA, Entenberg D, Borriello L, Coste A, Eddy RJ, Kim G, Ye X, Jones JG, Grunblatt E, Agi N, Roy S, Bandyopadhyaya G, Adler E, Surve CR, Esposito D, Goswami S, Segall JE, Guo W, Condeelis JS, Wakefield LM, Oktay MH: Live tumor imaging shows macrophage induction and TMEM-mediated enrichment of cancer stem cells during metastatic dissemination. Nat Commun 2021;12:7300

237. Hanahan D: Hallmarks of Cancer: New Dimensions. Cancer Discov 2022;12:31-46

238. Hanahan D, Weinberg RA: Hallmarks of cancer: the next generation. Cell 2011;144:646-674

239. Liang L, Kaufmann AM: The Significance of Cancer Stem Cells and Epithelial-Mesenchymal Transition in Metastasis and Anti-Cancer Therapy. Int J Mol Sci 2023;24

240. Papadaki MA, Stoupis G, Theodoropoulos PA, Mavroudis D, Georgoulias V, Agelaki S: Circulating Tumor Cells with Stemness and Epithelial-to-Mesenchymal Transition Features Are Chemoresistant and Predictive of Poor Outcome in Metastatic Breast Cancer. Mol Cancer Ther 2019;18:437-447

241. Hashemi M, Arani HZ, Orouei S, Fallah S, Ghorbani A, Khaledabadi M, Kakavand A, Tavakolpournegari A, Saebfar H, Heidari H, Salimimoghadam S, Entezari M, Taheriazam A, Hushmandi K: EMT mechanism in breast cancer metastasis and drug resistance: Revisiting molecular interactions and biological functions. Biomed Pharmacother 2022;155:113774

242. Ramesh V, Brabletz T, Ceppi P: Targeting EMT in Cancer with Repurposed Metabolic Inhibitors. Trends Cancer 2020;6:942-950

243. Du B, Shim JS: Targeting Epithelial-Mesenchymal Transition (EMT) to Overcome Drug Resistance in Cancer. Molecules 2016;21

244. den Hollander P, Joseph R, Vasaikar S, Kuburich NA, Deshmukh AP, Mani SA: Limiting Dilution Tumor Initiation Assay: An In Vivo Approach for the Study of Cancer Stem Cells. Methods Mol Biol 2022;2429:547-554